Interaction between groundwater and TBM (Tunnel Boring Machine) excavated tunnels

PhD Thesis

Hydrogeology Group (GHS)

Institute of Environmental Assessment and Water Research (IDAEA), Spanish Research Council (CSIC)

Dept Geotechnical Engineering and Geosciences, Universitat Politecnica de Catalunya, UPC-BarcelonaTech

Author:

Jordi Font-Capó

Advisors:

Dr. Enric Vázquez Suñé

Dr. Jesús Carrera

July, 2012

This thesis was co-funded by the Technical University of Catalonia (UPC) and the Generalitat de Catalunya (Grup Consolidat de Recerca: Grup d'Hidrologia Subterrània, 2009-SGR-1057). Additional funding was provided by GISA Gestió d'Infrastructures S.A. (Generalitat de Catalunya). Other financial support was provided by Spanish Ministry of Science and Innovation (HEROS project: CGL2007-66748 and MEPONE project: BIA2010-20244); Spanish Ministry of Industry (GEO-3D Project: PROFIT 2007-2009; and UTELinia9 (FCC, Ferrovial-Agroman, OHL, COPISA y COPCIS.

I. Abstract

A number of problems, e.g. sudden inflows are encountered during tunneling under the piezometric level, especially when the excavation crosses high transmissivity areas. These inflows may drag materials when the tunnel crosses low competent layers, resulting in subsidence, chimney formation and collapses. Moreover, inflows can lead to a decrease in head level because of aquifer drainage. Tunnels can be drilled by a tunnel boring machine (TBM) to minimize inflows and groundwater impacts, restricting the effect on the tunnel face. This method is especially suitable for urban tunneling where the works are usually undertaken near the ground surface. The aim of the thesis is to elucidate the tunneling difficulties arising from hydrogeology, and to determine groundwater impacts. The following approaches were adopted to achieve these objectives.

First, a methodology that characterizes hydrogeologically the medium crossed by the TBM is proposed. TBM is very sensitive to the sudden changes of the geological media. Two important aspects that are often overlooked are: variable groundwater behavior of faults (conduit, barrier, conduit-barrier), and role of groundwater connectivity between fractures that cross the tunnel and the rest of the rock massif. These two aspects should be taken into account in the geological and groundwater characterization to correct the tunnel design and minimize hazards. A geological study and a preliminary hydrogeological characterization (including a prior steady state investigation and cross bore-hole tests) were carried out in a granitic sector during the construction of Line 9 of the Barcelona subway (B-20 area). The hydrogeological conceptual model was constructed using a quasi-3D numerical model, and different scenarios were calibrated. Faults and dikes show a conduit-barrier behavior, which partially compartmentalized the groundwater flow. The barrier behavior, which is the most marked effect, is more prominent in faults, whereas conduit behavior is more notable in dikes. The characterization of groundwater media entailed a dewatering plan and changes in the tunnel course. This enabled us to construct the tunnel without any problems.

Second, a methodology to locate and quantify the inflows in the tunnel face of the TBM was adopted. Unexpected high water inflows constitute a major problem because they may result in the collapse of the tunnel face and affect surface structures. Such collapses interrupted boring tasks and led to costly delays during the construction of the Santa Coloma Sector of L9 (Line 9) of the Barcelona Subway. A method for predicting groundwater inflows at tunnel face scale was

implemented. A detailed 3D geological and geophysical characterization of the area was performed and a quasi-3D numerical model with a moving tunnel face boundary condition was built to simulate tunnel aquifer interaction. The model correctly predicts groundwater head variations and the magnitude of tunnel inflows concentrated at the crossing of faults and some dikes. Adaptation of the model scale to that of the tunnel and proper accounting for connectivity with the rest of the rock massif was crucial for quantifying the inflows. This method enables us to locate the hazardous areas where dewatering could be implemented.

Third, the hydrogeological impacts caused by tunneling with TBM were characterized. The lining in tunnels reduces water seepage but could cause a barrier effect because of aquifer obstruction. Analytical methods were employed to calculate the gradient and permeability variation after tunnelling. The uses of pumping tests allow determinate the barrier effect and the changes in groundwater connectivity due to tunnelling.

These approaches were adopted to help overcome the main hydrogeological problems encountered during the construction of tunnels with the TBM. Numerical models proved useful in quantifying and forecasting tunnel water inflows and head variations caused by tunnelling. A better understanding of these scenarios enabled us to find the correct solutions and to minimize the consequences of tunnel-groundwater interaction.

II. Resumen

La construcción de túneles bajo el nivel piezométrico puede comportar problemas constructivos cuando la excavación atraviese zonas muy transmisivas donde puede haber entradas repentinas de agua. Estas entradas pueden generar arrastres cuando se crucen capas muy poco competentes, llegando a provocar hundimientos, creación de chimeneas subsidencia del terreno. Además estas entradas de agua pueden provocar el descenso del nivel freático por drenaje del acuífero. Para minimizar las entradas de agua y los impactos asociados a la excavación se realizan perforaciones con tuneladoras (TBM) que restringen las afectaciones por drenaje al frente de perforación. Este método es especialmente adecuado en medios urbanos donde el túnel se sitúa cerca de la superficie. El objetivo de esta tesis será abordar las dificultades constructivas relacionadas con la hidrogeología que existen al construir túneles con tuneladora así como determinar los impactos que estas pueden producir.

En primer lugar, se busca una metodología que permita caracterizar hidrogeológicamente el terreno que será atravesado por la tuneladora ya que esta maquinaria es sensible a los cambios repentinos de medio y condiciones de terreno. Hay dos aspectos que normalmente no se tienen en cuenta: el comportamiento hidrogeológico de las fallas (conducto, barrera, conducto-barrera) y la importancia de la conectividad hidrogeológica entre las fracturas que cruzadas por el túnel y el resto del macizo rocoso. Estos dos aspectos han sido tenidos en cuenta en la caracterización geológica e hidrogeológica con el fin de corregir el diseño del túnel y minimizar riesgos geológicos. Una investigación geológica con caracterización hidrogeológica preliminar (que incluyó la revisión del estado hidrogeológico previo y ensayos de bombeo de interferencia) fue realizada en una zona granítica de la Línea 9 del metro de Barcelona (zona de la B-20). El modelo hidrogeológico conceptual fue construido usando un modelo numérico quasi-3D, donde fueron calibrados diverso escenarios. Las fallas y diques mostraron un comportamiento de conducto-barrera que compartimentaliza parcialmente el flujo. El comportamiento de barrera es el efecto mas marcado, aunque en los diques aparece comportamiento de conducto. La caracterización del medio hidrogeológico ha permitido realizar un plan de drenaje y los cambios necesarios en el diseño del túnel.

En segundo lugar, se busca una metodología que permita localizar y cuantificar las entradas de agua que pueda haber en el frente de excavación de un túnel construido con tuneladora. Entradas de agua repentinas constituyen un problema importante porque pueden provocar un

colapso del túnel que afecte estructuras superficiales. Un método para predecir las entradas de agua en el frente de túnel fue implementado en el sector de Santa Coloma de la Línea 9 del metro de Barcelona. Una caracterización geológica y geofísica 3D del área fue realizada y los resultados fueron implementados en un modelo numérico quasi-3D, donde una condición de contorno de frente de túnel móvil se ha insertado para simular la interacción con el acuífero. El modelo predice correctamente la variación de los niveles piezométricos y la magnitud de las entradas de agua concentrados en las zonas de falla y diques. La adaptación de la escala del modelo al túnel y a la conectividad con el resto del macizo ha sido crucial para cuantificar las entradas de agua. Este método permite localizar las zonas peligrosas donde el *dewatering* debería ser implementado.

En tercer lugar, se caracterizan los impactos que provoca la construcción de un túnel construido con tuneladora. Aunque el efecto dren que suelen producir la mayoría de túneles es minimizado en los túneles perforados con tuneladora con el sostenimiento que se instala después de la acción perforadora de la maquina, la construcción de esta estructura lineal impermeable puede producir una obstrucción del acuífero o efecto barrera. Se cuantifica la variación de gradientes piezométricos antes y después de la construcción de un túnel, esto se realizará con el uso de métodos analíticos que comparen los cambios reales observados. Además se cuantificaran los cambios de conectividad que provoca la construcción de un túnel comparando la variación de comportamiento observada en una serie de ensayos de bombeo realzados antes y después de la construcción de l túnel.

Todos estos enfoques permiten abordar los principales problemas hidrogeológicos que se encontraran los túneles construidos con tuneladora así como los impactos que provocan. El uso de modelos numéricos se convierte en una herramienta robusta para cuantificar y predecir las entradas de agua en el frente de túnel y las variaciones de nivel provocadas por el mismo túnel. El conocimiento de estos escenarios permitirá encontrar las mejores soluciones para minimizar las consecuencias de la acción del medio hidrogeológico sobre el túnel o viceversa.

III. Resum

La construcció de túnels sota el nivell piezomètric pot comportar problemes constructius quan l'excavació travessi zones molt transmissives on pot haver-hi entrades sobtades d'aigua . Aquestes entrades poden arrossegar materials quan es creuin capes poc competents, arribant a provocar enfonsaments, xemeneies I subsidència del terreny. D'altra banda aquestes entrades d'aigua poden provocar el descens del nivell d'aigua per drenatge de l'aqüífer. Per minimitzar les entrades d'aigua I els impactes associats a la excavació es perforen túnels amb tuneladores (TBM) que restringeixen les afeccions per drenatge al front de perforació. Aquest mètode es especialment adequat en medis urbans on el túnel es proper a la superfície. L'objectiu d'aquesta tesi serà abordar les dificultats constructives relacionades amb la hidrogeologia que existeixen al construir túnels amb tuneladora així com determinar els impactes que aquestes poden produir.

En primer lloc, es busca una metodologia que permeti caracteritzar hidrogeològicament el terreny que ha de travessar la tuneladora ja que aquestes són sensibles als canvis sobtats de medi i condicions de terreny. Hi ha dos aspectes important que normalment no son tinguts en compte: El comportament hidrogeològic de les falles (conducte, barrera, conducte-barrera) i la importància de la connectivitat hidrogeològica entre les fractures que son creuades pel túnel y la resta del massís rocós. Aquests dos aspectes han estat tinguda en compte en la caracterització geològica i hidrogeològica amb el fi de corregir el disseny del túnel i minimitzar riscos geològics. Una investigació geològica amb caracterització hidrogeològica preliminar (que va incloure la revisió de l'estat hidrogeològic previ i assaigs de bombeig d'interferència) va ser realitzada en una zona granítica de la Línia 9 del metro de Barcelona (zona de la B-20). El model hidrogeològic conceptual va ser construït fent servir un model numèric quasi-3D, on van ser calibrats diferents escenaris. Les falles i els dics van mostrar un comportament de conducte barrera que compartimentalitza el flux parcialment. El comportament de barrera es l'efecte mes marcat i es mentre que en els dics apareix el comportament de conducte. La caracterització del medi hidrogeològic ha permès realitzar un pla de drenatge i els canvis necessaris en el disseny del túnel.

En segon lloc, es troba una metodologia que permeti trobar el lloc i quantificar les entrades d'aigua que hi pot haver en el front d'excavació d'un túnel construït amb tuneladora. Les

entrades d'aigua sobtades en el túnel constitueixen un problema important perquè poden provocar un col·lapse del túnel que afecti a les estructures superficials. Un mètode per predir les entrades d'aigua en el front de túnel ha estat implementat en el sector de Santa Coloma de la Línia 9 del metro de Barcelona. Per aconseguir-ho es va realitzar una caracterització geològica i geofísica 3D, aquests resultats van ser implementats en un model numèric quasi-3D, on una condició de contorn de front de túnel mòbil ha estat inserida per simular la iteració amb l'aqüífer. El model prediu correctament la variació de nivells piezomètrics i la magnitud de les entrades d'aigua concentrades en les zones de falla i dics. L'adaptació de l'escala del model al túnel i a la connectivitat amb la resta del massís han estat clau per poder quantificar les entrades d'aigua. Aquest mètode permet localitzar les zones perilloses on el *dewatering* hauria de ser implementat.

En tercer lloc, es caracteritzen els impactes hidrogeològics que provoca la construcció d'un túnel construït amb tuneladora. Malgrat que l'efecte dren que acostumen a originar la majoria de túnels es minimitza per l'acció del sosteniment que s'instal·la just després de la maquina, la construcció d'aquesta estructura lineal impermeable pot produir una obstrucció de l'aqüífer o efecte barrera. Es quantifica la variació de gradient abans i després de la construcció d'un túnel, això es farà amb mètodes analítics que es comparen amb el canvi de gradient observat. A mes a mes es quantifiquen els canvis de connectivitat que provoca la construcció del túnel comparant la variació de comportament observada en una sèrie d'assaigs de bombeigs realitzats abans i després de la construcció del túnel.

Tots aquests enfocaments permeten abordar els principals problemes hidrogeològics que es trobaran els túnels construïts amb tuneladora així com els impactes que provoquen. L'ús de models numèrics esdevé una eina robusta per poder quantificar i predir les entrades d'aigua en el front del túnel i les variacions de nivell provocades pel mateix túnel. El coneixement d'aquests escenaris permetrà trobar les solucions adients o minimitzar les conseqüències de l'acció de medi hidrogeològic sobre el túnel o a l'inrevés.

IV. Agraïments

En primer lloc voldria agrair als meus directors de tesi, Enric Vázquez i Jesús Carrera la confiança que van dipositar en mi a l'hora de realitzar aquesta tesi i poder participar en projectes d'investigació del grup d'Hidrologia subterrània, pel seu suport, orientació i ajuda en el desenvolupament d'aquesta tasca.

Gràcies a tots els companys del grup de Hidrologia subterrània, començant pels professors i investigadors Xavier-Sànchez-Vila, Lurdes Martínez-Landa, Marteen Saaltink, Marco Denz, Carles Ayora, Jordi Cama i Daniel Fernández per la seva ajuda tan acadèmica com logística. Tasca aquesta darrera que ha comptat amb la valuosa ajuda de Teresa Garcia i Sílvia Aranda. I de la resta de doctorands amb qui he compartit feina i vivències, es impossible anomenar-los a tots, però dels mes antics podria destacar a Bernardo, Desi, Esteban, Maria, Meritxell, Manuela, Isabel, Paolo, Edu i dels mes recents a Pablo, Estanis, Anna, Violeta, Ester, Albert N., Marco B., ... la llista es interminable i per això només puc expressar la meva gratitud a tots ells.

També voldria expressar el meu agraïment Andrés Pérez-Estaún, David Martí i Ramón Carbonell de l'Institut Jaume Almera pel seu ajut i col·laboració en les tasques realitzades a l'inici de la Línia 9 a Santa Coloma de Gramanet.

A la meva família per haver-me inculcat el valor del treball i l'estudi sense el qual no s'hagués pogut dur a terme aquesta tesi. Eta Oihane nire politxe per tot el que has aguantat i ajudat i el poc que has rebut a canvi, mil esker nire maitia.

V. Table of Contents

VI. List of figures

VII. List of Tables

1. Introduction

1.1. Motivation and objectives

Shallow tunneling may give rise to a number of problems from the hydrogeological point of view, i.e. high water inflows in transmissive areas that are often associated with fractures (Deva et al., 1994; Tseng et al., 2001; Shang et al., 2004; Dalgiç, 2003) and the drawdown caused by tunnel excavation (Cesano and Olofson, 1997; Marechal et al., 1999; Marechal and Etxeberri, 2003; Gargini et al., 2008; Vincenzi et al., 2008; Gisbert et al., 2009; Yang et al., 2009; Kvaerner and Snilsberg, 2008; Raposo et al., 2010). A Tunnel Boring machine (TBM) is used to restrict the inflows to the tunnel face and to minimize groundwater impacts.

Groundwater studies in shallow tunneling are often focused on the need to locate conductive areas that may cause inflows. These studies are usually undertaken by defining the major fractures or the ones that are most likely to produce tunnel inflows (Banks et al., 1992; Mabee et al., 2002; Cesano et al., 2000, 2003; Lipponen and Airo, 2006; Lipponen, 2007). Some authors consider that fractures and faults are areas with high permeability, preferential flow and conduit behavior (e.g., Mayer and Sharp, 1998; Mabee, 1999; Cesano et al., 2000, 2003; Krisnamurthy et al., 2000; Flint et al., 2001; Mabee et al., 2002; Martínez-Landa and Carrera, 2005, 2006; Sener et al., 2005; Denny et al., 2007; Shaban et al., 2007; Folch and Mas-Pla, 2008). However, if the fractures are fault-zones, they may act as localized conduits, barriers or conduit-barriers, which are often governed by complex fault zone architecture and flow direction (Forster and Evans, 1991; Caine et al., 1996; Caine and Forster, 1999; Caine and Tomusiak, 2003; Berg and Skan, 2005; Bense and Person, 2006). The water availability of the rocks and faults crossed by the tunnel is not only determined by their hydraulic characteristics but also by the connectivity with the boundary conditions and sources of water (Moon et al., 2011). The first aim of this thesis is to define a groundwater characterization of fractured massifs where shallow tunnels must be excavated. Characterization must be carried out at a scale that allows us to resolve tunneling problems (design of the tunnel works, dewatering, inflows). The complex behavior of the faults and dikes, and the groundwater connectivity with the surrounding massif must be taken into account. Inflows can be calculated after characterizing the groundwater of the massif and fractures.

A number of analytical formulae have been developed to predict tunnel inflows under different hydraulic conditions. Most of these assume a homogeneous medium and also steady state (Goodman et al., 1965; Chisyaki, 1984; Lei, 1999; El Tani, 2003; Kolymbas and Wagner, 2007; Park et al., 2008) or transient conditions (Marechal and Perrochet, 2003; Perrochet, 2005a, 2005b; Renard, 2005). Some analytical solutions have also been developed for heterogeneous formations (Perrochet and Dematteis, 2007; Yang and Yeh, 2007) and are suitable for systems with layers that are perpendicular to the tunnel so that flow is generally radial. Moreover, they can only be used when the system is relatively unaffected by inflows. They cannot therefore be used for assessing large inflows to relatively shallow tunnels because the boundary conditions evolve with time and flow takes place primarily in the aquifer plane rather than radially in the vertical plane perpendicular to the tunnel. Moreover, tunnels excavated with a TBM are lined, the radial flow towards the tunnel is very small, and most inflows appear at the tunnel face (or in machine-rock contact). The presence of high conductivity fractures that are well connected to permeable boundaries further hinders the use of analytical formulae to compute water inflows. Numerical modeling is necessary under these conditions (Molinero et al., 2002; Witkke et al., 2006; Yang et al., 2009). The second aim of this thesis is to determine the water inflows in a tunnel excavated with a TBM.

Excavation of tunnels can have adverse consequences for the aquifers because of the changes produced in the natural regime. One of the most important effects is the piezometric drawdown caused by tunnel drainage (Cesano and Olofson, 1997; Marechal et al., 1999; Marechal and Etxeberri, 2003; Gargini et al., 2008; Vincenzi et al., 2008; Kvaerner and Snilsberg, 2008; Gisbert et al., 2009; Yang et al., 2009; Raposo et al., 2010). This effect can be considerably minimized by using a TBM to excavate the tunnel. In this case, the drawdown impact is restricted at the transient state of the tunnel face machine because of the impermeable lining employed to prevent water inflows and aquifer drainage. The use of impermeable linings results in aquifer obstruction, giving rise to the barrier effect (Marinos and Kavvadas, 1997; Vázquez-Suñé et al., 2005, Carrera and Vazquez-Suñe, 2008). Barrier effect can cause an increase in groundwater head on the upgradient side, and a decrease on the downgradient side of the tunnel (Ricci et al., 2007). The third aim of this thesis is to evaluate the barrier effect created by an impervious tunnel.

1.2. Thesis outline

This thesis consists of four chapters in addition to the introduction. With the exception of the last chapter, each chapter focuses on one of the aforementioned objectives. The chapters are based on papers that have been published, accepted or submitted to international journals. The references to the papers are contained in a footnote at the beginning of each chapter.

Chapter 2 proposes a methodology to characterize a fractured medium that must be tunneled. The construction of a conceptual geological model was followed by a hydrogeological characterization. This model was validated by a quasi-3D numerical model that incorporated different scenarios of increasing complexity. Because of the time constraints of the project, only the conceptual model based on the geological and hydrogeological data was considered when implementing changes into the tunnel design and dewatering plan. The numerical model and simulations using different scenarios were carried out after tunneling. This characterization was implemented in the B-20 sector of Line 9 of the subway of Barcelona.

Chapter 3 presents a methodology for predicting the location and magnitude of tunnel inflows using a numerical groundwater flow model. A detailed 3D geological and geophysical characterization of the area was performed and a quasi-3D numerical model with a moving tunnel face boundary condition was built to simulate tunnel aquifer interaction. The model correctly predicts groundwater head variations and the magnitude of tunnel inflows concentrated at the intersection of faults and some dikes. Adaptation of the model scale to the tunnel and accommodation of the connectivity to the rest of the rock massif was crucial for quantifying inflows. This method enabled us to locate the hazardous areas where dewatering could be implemented. The method was applied to the last 700 m of the Santa Coloma sector of Line 9 of the subway of Barcelona.

Chapter 4 is concerned with the most recent research into the impact of lined tunnels. The main impact considered was the barrier effect due to aquifer interruption as a result of tunnel excavation. The gradient variation was calculated by analytical formulae and compared with the real results. Barrier effect and connectivity variations due to the tunnel can be also calculated with pumping tests. This analysis was undertaken by comparing the differential pumping response before and after tunneling. Quantification was also undertaken using a numerical model, where tunnel geometry could be introduced, allowing us to compare the real heads after

tunneling with the calculated heads (with and without the introduction of the tunnel into the model). This quantification was implemented into a section of Line 9 of the subway of Barcelona at El Prat del Llobregat.

Chapter 5 provides a summary of the main conclusions of the thesis.

2. Groundwater characterization of a heterogeneous granitic rock massif for shallow tunneling

2.1. Introduction

Shallow tunneling may encounter a number of problems, the most important of which is high water inflows in transmissive areas that are often associated with fractures (Deva et al., 1994; Tseng et al., 2001; Shang et al., 2004; Dalgiç, 2003). A groundwater characterization is essential given that the association of soft materials and high water inflows may drag large amounts of material (Barton, 2000).

Groundwater in shallow tunneling is often approached in three steps. In the first step, attention is focused on conductive areas that may represent groundwater inflows into the tunnel. These studies are usually undertaken by defining the major fractures or the most susceptible ones to produce tunnel inflows. In this regard, considerable research has been undertaken on a regional scale, i.e. geological and geophysical studies, remote sensing and statistics have been employed to provide a rough idea of the most probable inflow areas (Banks et al., 1992; Mabee et al., 2002; Cesano et al., 2000, 2003; Lipponen and Airo, 2006; Lipponen, 2007). In the second step, fractures are considered as transmissive inflow areas in order to locate and quantify tunnel inflows. This is calculated by analytical methods (Perrochet and Dematteis, 2007; Yang and Yeh, 2007) or by numerical methods (Molinero et al., 2002; Yang et al., 2009; Font-Capo et al., 2011). The third step incorporates updated information into shallow tunneling, which enables us to predict future water inflows. However, these studies are often based on geomechanical and geological data of the civil engineering works, which rarely take into account the hydraulic relationships with the rest of the rock massif (geological information is concentrated along the tunnel length, with little attention paid to).

This chapter is based on the paper: Font-Capo, J., Vazquez-Suñe, E., Carrera., Herms, I., 2012, Groundwater characterization of a heteorogeneous granitic rock massif for shallow tunnelling, Geologica Acta, published online. DOI: 10.1344/105.000001773

From the standpoint of hydrogeology and tunneling, many authors consider that fractures and faults are areas with high permeability, preferential flow and conduit behavior (e.g., Mayer and Sharp, 1998; Mabee, 1999; Cesano et al., 2000, 2003; Krisnamurthy et al., 2000; Flint et al., 2001; Mabee et al., 2002; Sener et al., 2005; Martínez-Landa and Carrera, 2005, 2006; Shaban et al., 2007; Denny et al., 2007; Folch and Mas-Pla, 2008).

However, if the fractures are fault-zones, they may act as localized conduits, barriers or conduit-barriers, which are governed by commonly complex fault zone architecture and flow direction (Forster and Evans, 1991; Caine et al., 1996; Caine and Forster, 1999; Caine and Tomusiak, 2003; Berg and Skan, 2005; Bense and Person, 2006). Fault-zones are conceptualized as fault cores surrounded by a damage zone, which differs structurally, mechanically and petrophysically from the undeformed host rock (protolith). The damage zone is usually considered as a higher permeability zone, whereas the core zone is regarded as a lower permeability zone. (Smith and Schwartz, 1984; Chester and Logan, 1986; Forster and Evans, 1991; Chester et al., 1993; Bruhn et al., 1994; Evans and Chester, 1995; Caine et al., 1996; Evans et al., 1997). Recent research has questioned the general applicability of this simple model (Faulkner et al., 2010) for the following reason. Fault zones may contain a single fault core (sometimes with branching subsidiary faults) or a fault core that may branch, anatomize and link, entraining blocks or lenses of fractures and protolith between the layers, giving rise to asymmetric fault-zone areas (McGrath and Davison, 1995; Faulkner et al., 2003; Kim et al., 2004; Berg and Skar, 2005; Cembrano et al., 2005; Cook et al., 2006).

The structure of low and high permeability features can lead to extreme permeability heterogeneity and anisotropy (Faulkner et al., 2010). The permeability of a fault zone in the plane and perpendicular to the plane (across-fault) is governed by the permeability of the individual fault rocks/fractures and more critically by their geometric architecture in three dimensions (Lunn et al., 2008; Faulkner et al., 2010). The capacity to form barriers to flow depends on the continuity of the low permeability layers (Faulkner and Rutter, 2001). The connectivity of the most permeable areas governs the permeability along and across the fault-zones (Faulkner et al., 2010). The tunnel can cross fractures with a conduit, barrier or conduit-barrier behavior. The characteristics of crossed fractures determine the inflow volume that enters the tunnel.

Groundwater flow at massif rock scale differs from that at fracture or fault scale. This factor is useful in tunneling. Several researchers have demonstrated that fluid-flow passes through few fractures in fractured massifs (Shapiro and Hsieh, 1991; Day-Lewis et al., 2000; Knudby and

Carrera, 2005; Martínez-Landa and Carrera, 2006). Increases in the volume of water flow depend on the continuity of well connected fractures (Knudby and Carrera, 2006). The effective transmissivity related to these fractures increases with scale (Illman and Neuman, 2001, 2003; Martínez-Landa and Carrera, 2005; Le Borgne et al., 2006; Illman and Tartakowsky, 2006) or only in some particular directions (Illman, 2006). However, large scale permeability may decrease in massifs with a low permeability lineament network (Hsieh, 1998; Shapiro, 2003) where the fractures act as barriers that hinder connectivity and compartmentalize the flow (Bredehoeftt el., 1992, Bense et al., 2003, Bense and Person, 2006, Benedek et al., 2009; Gleeson and Novakowski, 2009). The conduit-barrier behavior may also be expressed at regional scale (Bredehoeft et al., 1992; Bense and Balen, 2004; Bense and Person, 2006; Mayer et al., 2007; Anderson and Bakker, 2008). The behavior of the fractures at large scale plays a major role in tunneling. The water availability of the rocks and faults crossed by the tunnel is not only determined by their hydraulic characteristics but also by the connectivity with the boundary conditions and sources of water (Moon et al., 2011).

The present paper addresses groundwater characterization of a fractured massif where shallow tunnels must be excavated. Characterization must be carried out at a scale that allows us to respond to the tunneling problems (design of the tunnel works, dewatering, inflows). The complex behavior of the faults and dikes, and the groundwater connectivity with the surrounding massif must be taken into account.

This characterization was implemented in the B-20 sector of Line 9 of the subway in Barcelona (Figure 2– 1a). In this area, the combination of intense fracturing and the presence of soft materials could give rise to problems in the tunneling works. A geological conceptual model was constructed, followed by a hydrogeological characterization. This model was validated by a quasi-3D numerical model that incorporated different scenarios of increasing complexity. Because of the time constraints of the project, only the conceptual model based on the geological and hydrogeological data was considered when implementing changes into the tunnel design and the dewatering plan. The numerical model and the simulations using different scenarios were carried out after the tunneling process.

2.2. Geological conceptual model

An accurate description of the structural geology at large scale was first carried out. The main structures, lineaments, and geological changes that could constitute the major flow conduits/pathways or barriers that may affect the groundwater were identified. A detailed geological study was undertaken after research at large scale. Where direct geological observation; (boreholes, outcrops…) were available, we could confirm the location of faults and dikes. In the B-20 area, the investigation was broadened to include (1) a general characterization or large scale investigation (photogrammetry and geological interpretation of old aerial photographs) and (2) detailed scale investigation; outcrop and borehole interpretation.

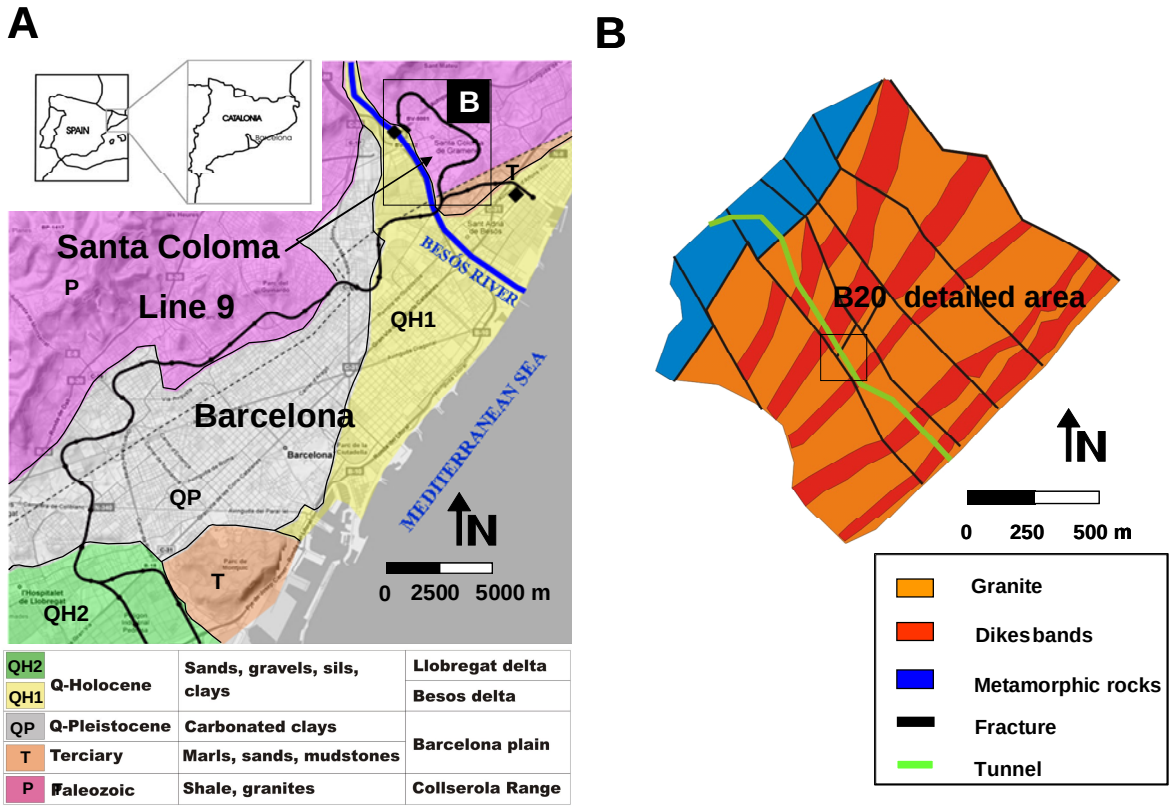

Figure 2– 1.a) Map of Barcelona conurbation and Line 9 subway. b) Large scale geological map of the Santa Coloma sector of Line 9 subway, B20 area.

Accordingly, a large scale map showing the existence of granodiorite with numerous porphyritic dikes was made (Figure 2– 1b). Granodiorite is petrographically homogeneous. The porphyritic dikes, which are kilometers in length and meters wide, have a NE-SW trend and a sub-vertical dip, occurring in sub-parallel families. They can be observed and mapped only in outcrops outside the city centre. The dikes are more resistant to erosion than granodiorite, which facilitates

identification. Subvertical strike-slip faults, trending NNW-SSE, separated by hundreds of meters displace the porphyritic dikes. These faults are late Carboniferous in age and affect Miocene sedimentary rocks south of the B-20 area, but they are absent in the B-20 area. This strongly suggests that they were reactivated in post-Miocene times (Martí et al., 2008). In fact, the contact between granodiorites and Miocene sedimentary rocks is a normal fault zone similar to other normal faults that regionally generated the Miocene extensional basins related to the formation of the Catalan margin (Cabrera et al., 2004). Cataclastic fault rocks (breccias and fault gauges) are usually associated with these normal faults.

A detailed geological investigation of the B-20 area was carried out using the bore hole core interpretation in an attempt to improve the characterization of the granodiorite, granitic dikes, and fault-zones in this area (Figure 2– 2). The granodiorite rock unit may be divided into unaltered granite and weathered granite at a depth of 25-30 meters. Differences in the elevation of the unaltered granite-weathered granite contact on the two sides of structures 1 and 2 (Figure 2– 2) probably indicate that these lineaments are faults that separate two structural blocks. The dike area was divided into two NW-SE direction dikes on the basis of the information from the drilling cores.

2.3. Hydrogeological Research

Hydrogeological research was undertaken to define the fracture connectivity and hydraulic parameters of the rock massif units. This was carried out by studying hydrogeological features and by evaluating the hydraulic tests.

The piezometric level yielded indirect information about the relative relationships of the hydraulic parameters of the different formations. The piezometric heads can provide information about the contrast of hydraulic parameters between geological rock units and the lineament geometry. The presence of high hydraulic gradients may be associated with areas with groundwater flow obstacles (Bense and Person, 2006; Yechieli et al., 2007; Benedek et al., 2009; Gleeson and Novakoski, 2009).

A piezometric map of the area (Figure 2– 2) was made with the heads obtained in the drilling program. Heads display a high gradient along Fault 1 and Fault 2. The increase in gradient was attributed to a reduction in the transmissivity in the affected area. The presence of such areas in

fractured massifs may be associated with low permeability fault zones that compartmentalize the flow. This barrier behavior may be ascribed at fracture scale to a reduction of the permeability in the central area of fault-zones (Evans, 1988; Goddart and Evans, 1995; Caine and Forster, 1999) or to the juxtaposition of different permeable layers due to fault movement (Bense et al., 2003; Bense and Person, 2006).

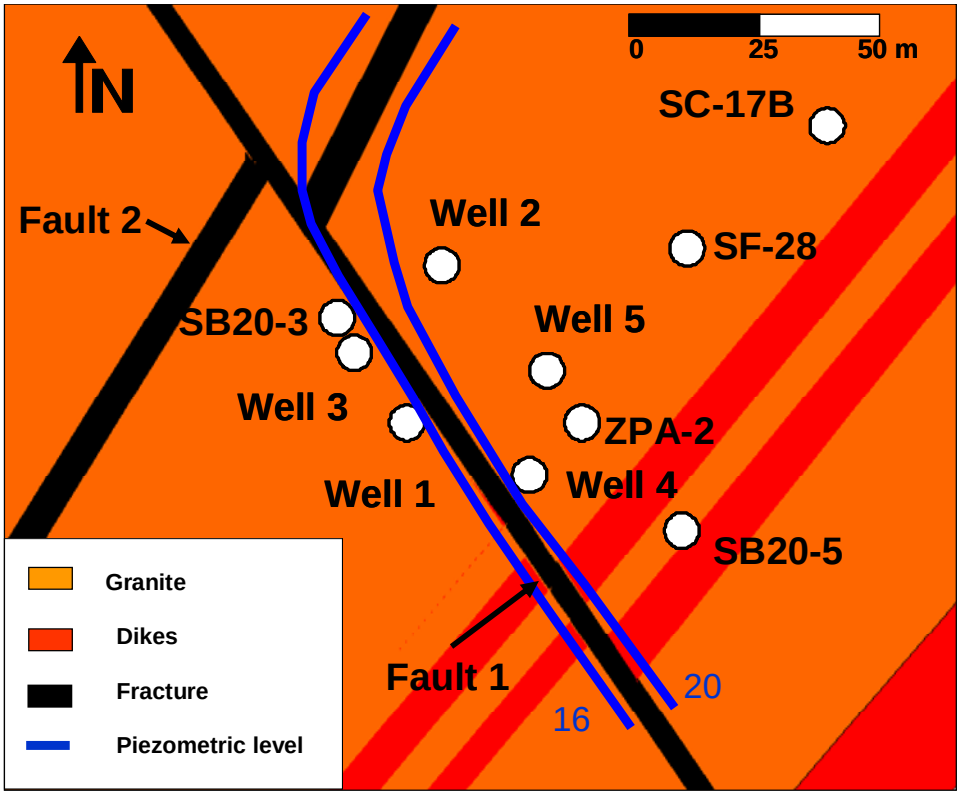

Figure 2– 2. Detailed scale geological map of the detailed area of B20, location of pumping wells and piezometers, and steady state piezometric surface.

The fractures or lineaments that play a significant role from a hydraulic point of view were identified. Hydraulic properties of these structures (conduit, barrier or conduit-barrier) must be characterized, which may be accomplished by hydraulic tests (Martínez-Landa and Carrera, 2006). Cross hole tests, which have been used to characterize groundwater flow in fractured media, are instrumental in identifying connectivity and fracture extension (Guimera et al., 1995; Day-Lewis et al., 2000; Martínez-Landa and Carrera, 2006; Illman and Tartakowsky, 2006; le Borgne et al., 2006; Benedek et al., 2009; Illman et al., 2009).

Six cross hole tests were performed in the area (RSE, 2003). Five pumping wells and five piezometers were used. The wells and piezometers were screened in the two granite levels with the exception of Well 5 and the SC-17B piezometer, which were only screened in the shallow

granite (Well 5 initially included the two granite layers but it was filled with concrete in order to test the shallow granite). All pumping tests were undertaken at a constant rate except pumping test 5, which was a step-drawdown test. Wells 1, 2, 3, 4 and 5 were used sequentially as pumping wells in the first five tests. Test number six was carried out by pumping simultaneously in three wells (Wells 1, 2, 3). Unfortunately, the drawdown responses were not measured in all the piezometers. Drawdown was measured in the following piezometers each of which corresponds to a pumping test: pumping test 1 (Wells 1, 2,3,4,5, and piezometers SC-17B, SB20-3, SB20-5), pumping test 2 (Well 2 and piezometers SF28, SC-17B, and SB20-3), pumping test 3 (Wells 3, 4 and piezometers SF-28, SC17-B, and SB20-3), pumping test 4 (Wells 2, 4 and piezometers SF-28, and SC-17B), pumping test 5 (Wells 1, 4,5 and piezometers SF-28, ZPA-2, SC-17B, and SB20-5) and finally the triple pumping test (Wells 1,2,3,4,5 and SF-28, SC-17B and SB20-3). The wells and piezometers are shown in Figure 2– 2.

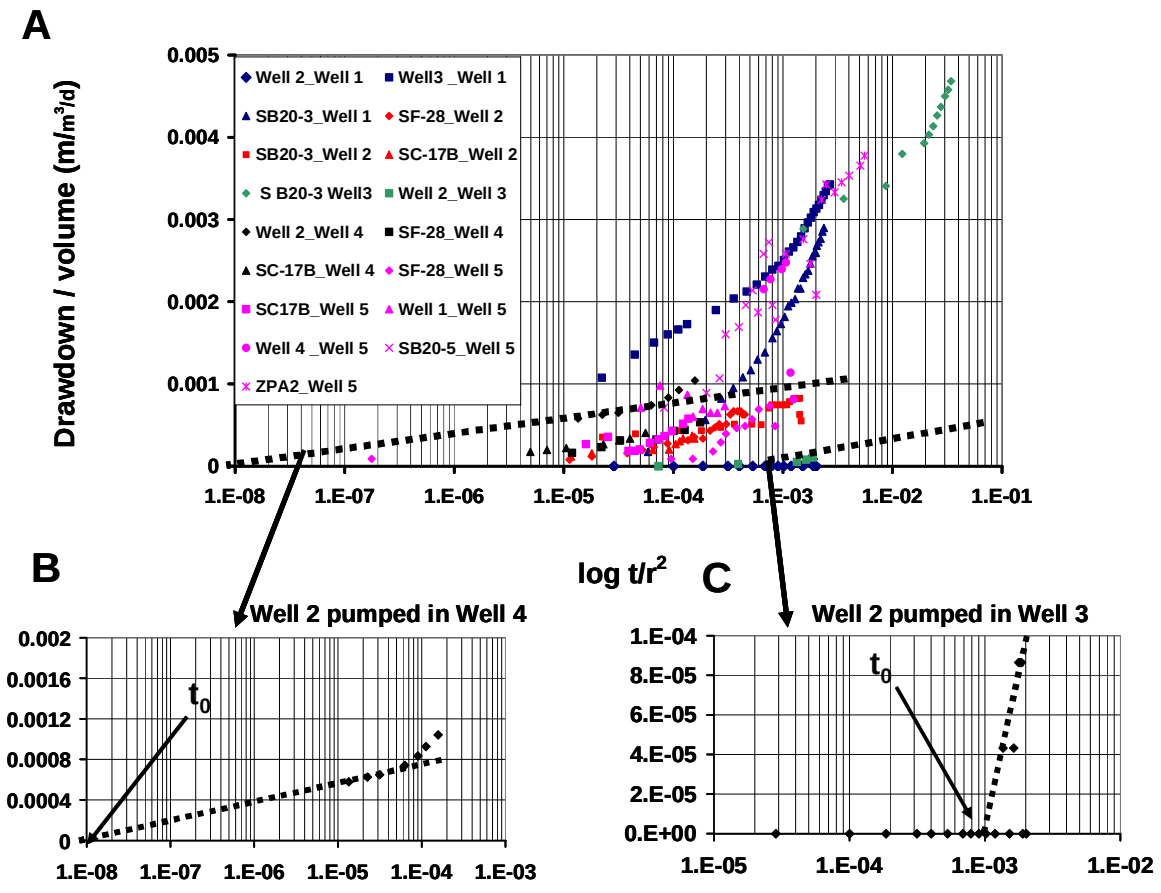

Figure 2– 3.a) Drawdown observed in the piezometers in response to the cross hole tests. The time was divided by the squared distance between the pumping well and the piezometer, and the drawdown was divided by the pumped volume rate. b) The fastest (Well 2 pumped in Well 4) and the c) slowest (Well 4 pumped in Well 1) responses are plotted separately in order to show the detail of the methodology for each piezometer response.

A preliminary interpretation using analytical methods was made to analyze drawdowns, assuming that the medium is homogeneous and infinite extent. In these cross-hole tests, the drawdown curves were analyzed individually for each observation well in each pumping test. The transmissivity varied more than one order of magnitude, the pumping wells yielding lower transmissivities (50-250 m^2/d) than the piezometers (140 to 1800 m^2/d). The distribution of transmissivity values obtained form pumping wells does not allow distinguishing between the separate hydraulic formations and the better connected fractures. This can be achieved by storativity.

Table 2– 1. Connectivity values of the observation wells (wells and piezometers) for the five pumping events.

Observation well	Pumping well	t/r^2
Well 3	Well 1	1.0E-06
S20-03	Well 1	1.0E-04
Well 2	Well 1	1.0E-03
Well 4	Well 1	7.5E-03
Well 5	Well 1	no
S20-05	Well 1	1.0E-03
SC-17C	Well 1	no
SB20-03	Well 2	2.0E-09
SF-28	Well 2	7.0E-06
SC-17C	Well 2	7.0E-07
SB20-03	Well 3	1.0E-07
Well 2	Well 3	7.0E-05
SC-17C	Well 3	no
Well 2	Well 4	1.0E-08
SC-17C	Well 4	1.0E-07
S20-03	Well 4	no
SF-28	Well 4	4.0E-02
SC-17C	Well 5	5.0E-02
SF-28	Well 5	4.0E-02
S20-05	Well 5	1.0E-05
ZPA-2	Well 5	2.0E-04
Well 4	Well 5	2.0E-04
Well 1	Well 5	6.0E-03

Storativity contains information of the connectivity relationships. The estimated storativity is apparent and provides more information than the effective transmissivity values about the degree of connectivity between pumping and observation wells (Meier et al., 1998; Sanchez Vila et al., 1999). Well connected points imply a rapid response to pumping. Rapid response can be estimated graphically by plotting drawdown versus the logarithm of time divided by the squared distance (log (t/r^2). If the medium was homogenous and isotropic, all the curves would be superimposed. A rapid response (in terms of t/r^2) implies good connectivity. The value of t/r^2 used

to determine the velocity of the response is the point t_0 where the line that joins the first drawdown points intersects the t/r^2 axis. The response of the different piezometers to pumping is plotted on the same graph (Figure 2– 3a). Drawdown was divided by the volume rate (s/Q) to eliminate the volume effect of each well in each pumping test. The results show differences of t_0 of five orders of magnitude, indicating a wide range of responses (Table 2– 1). The most extreme piezometer responses are plotted in Figure 2– 3b and Figure 2– 3c.

The values of t/r^2 between pumping boreholes are plotted on the map (Figure 2– 4). The most prominent feature is the poor (or absence of) response between Wells 1 and 3 and the SB20-3 piezometer with respect to the rest of the modeled domain. The response between pumping Well 5 (weathered granite) and the rest of the piezometers shows medium-low values which could be due to the moderate connectivity value of the weathered granite. Well 2 has a moderate or high connectivity with Well 4 and piezometer SB20-3, respectively, which are located on the other side of the possible barrier structure that divides the domain. Lines of rapid response may be observed along the SC-17B - Well 4 axis and also between Wells 4 and 2.

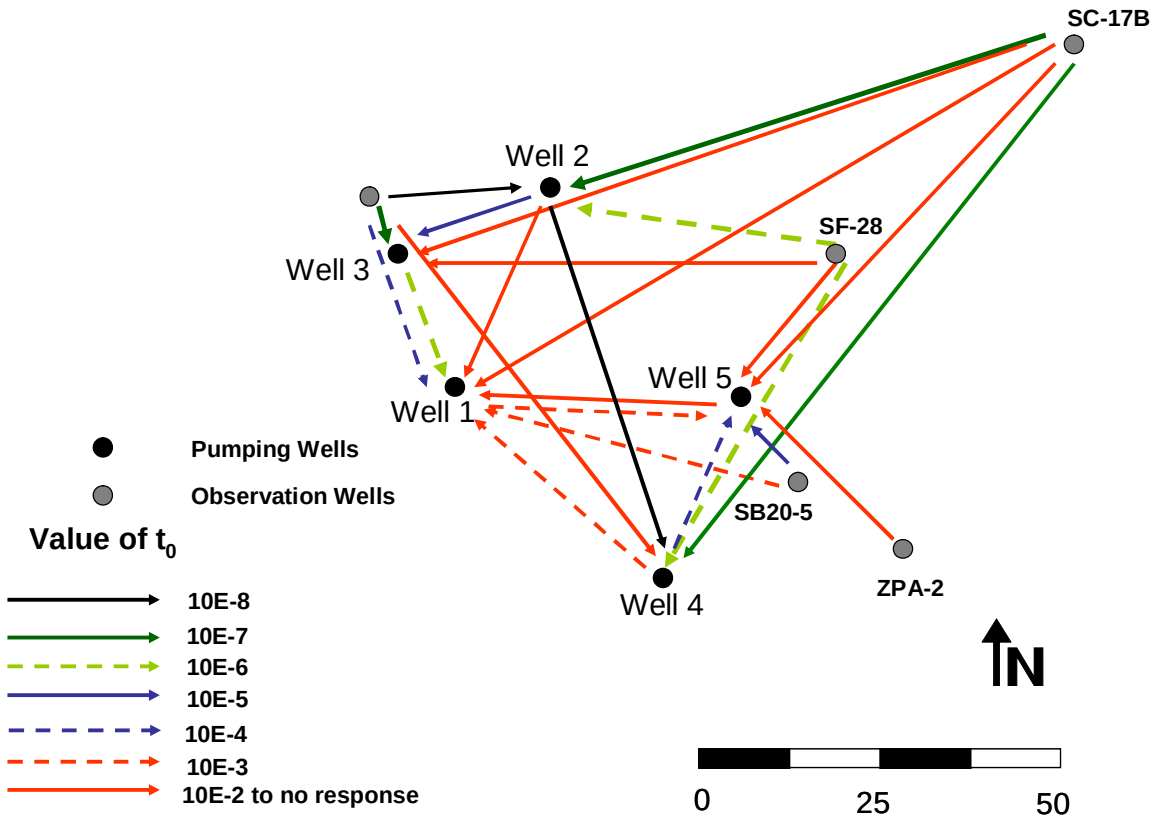

Figure 2– 4. Connectivity relationships between wells and piezometers in figure 2–3 are represented geographically. Each order of magnitude of t/r^2 is plotted in a different color.

2.4. Definition of the geometrical model

The geometrical model was constructed using the above geological and hydrogeological results. The geological structures observed at large scale, basically the NNW-SSE trending faults and the SW-NE dike zones and faults) constitute the main discontinuities of the geometrical model. Only at detailed scale was it possible to combine the results of the geological and hydrogeological research. Fault 1 presented four important characteristics: 1) a fault-zone detected in large scale geological studies, 2) a jump in depth of the contact between weathered-unaltered granite granodiorite across the fault, 3) a high hydraulic gradient, and 4) a poor cross-hole test response between the wells on the two sides of the surface of the discontinuity. Despite the fact that fault 2 had similar geometrical characteristics, the hydraulic gradient was less marked and the bore hole test did not include information about this structure. These two faults were included as fractures in the conceptual model. In the case of dikes, a preferential connectivity direction was observed along the dike axis between piezometers SC-17B and Well 4. Furthermore, the contact between the dike and granite usually involves an increase in water volume extraction in the drilling process of the boreholes. This prompted us to include a longitudinal band of fractured zones along the less permeable dike axis. Double banded structures with conduit-barrier behavior exist in some dike-granitic areas (Gudmunson, 2000; Babiker and Gudmundson, 2004; Sultan, 2008). Intermediate connectivity between Well 5 (weathered granite) and the piezometers located in dike areas suggest a medium connectivity in the upper layer. Good connectivity between Wells 2 and 4 would imply the existence of a transmissive band of fractured rocks along the low permeable fault core in Fault 1. Faults 1 and 2 were therefore transformed into a conduit-barrier system. All these geological and hydrogeological constraints were incorporated into the different models in order to test their validity.

2.5. Numerical model

The aim of the numerical model is twofold: 1) quantify the hydraulic parameters of the different lithologies of the rock massif taking into account the main hydraulic geological features and 2) calibrate the geometrical model verifying the hydraulic effect of the incorporated geological structures.

The numerical model was built after determining the main geological structures and defining the geometrical conceptual model. The model was constructed using a mixed discrete-continuum

approach in line with the methodology of Martínez-Landa and Carrera (2006). The model treated the main geological structures (faults and dikes) separately from the rest of the rock matrix (granodiorite). A quasi-3D model (two layers) was constructed to differentiate the lower layer of unaltered granite from the surface layer of weathered granite.

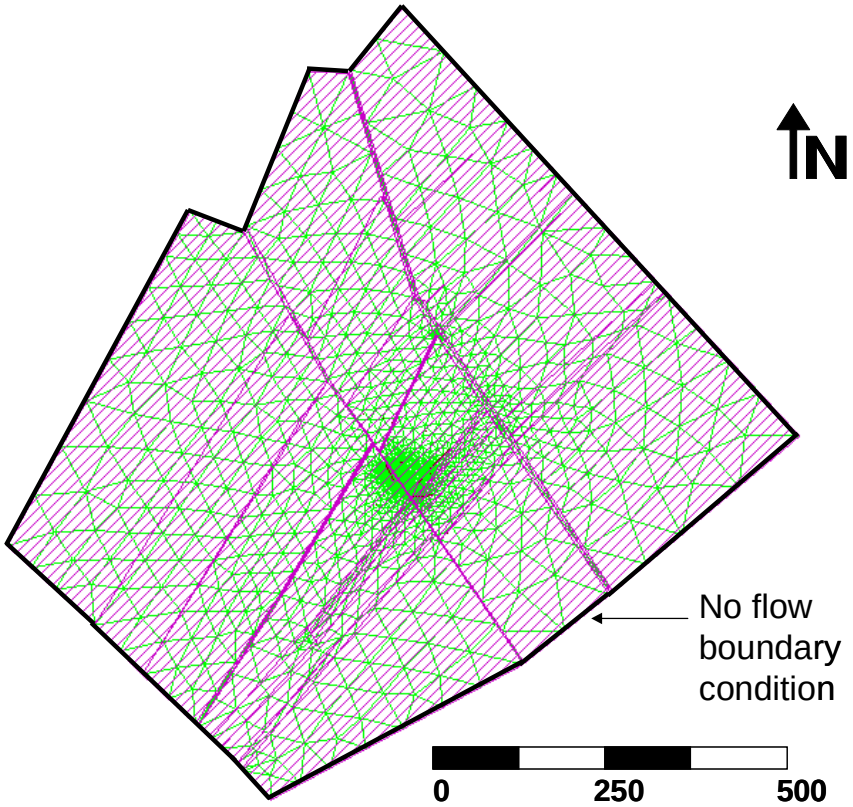

Figure 2– 5. Boundaries in the geometrical model used in the numerical model. Finite elements mesh of the numerical model, detailed B20 area and faults and dikes have finer discretization.

The numerical model was performed with the finite element code VisualTRANSIN (GHS, 2003; Medina and Carrera, 1996). The model was limited by no flow boundaries (Figure 2– 5), that were chosen to lie on structure zones along the NW and SE margins and fault-zones along the SW and NE margins. Faults and dikes were detected in the two layers and were simulated as vertical structures for the sake of simplicity. The six pumping tests were calibrated in drawdown mode simultaneously, by simulating them on one run where the beginning of each test is marked by setting a zero drawdown at all model nodes activating the flow rate at the pumping well. The method required specifying standard deviations for model and measurement errors. These were higher in pumping wells (4-10 m) than in piezometers (0.01-0.2 m) because part of the pumping well drawdown was attributed to well loss and skin effects that were not modeled. Figure 2– 7 and Figure 2– 8 do not show the drawdown of all the wells and piezometers since it was not

possible to measure drawdowns at all observation wells. Drawdowns of the pumping wells are not illustrated in these figures because their weight was negligible in the calibration process.

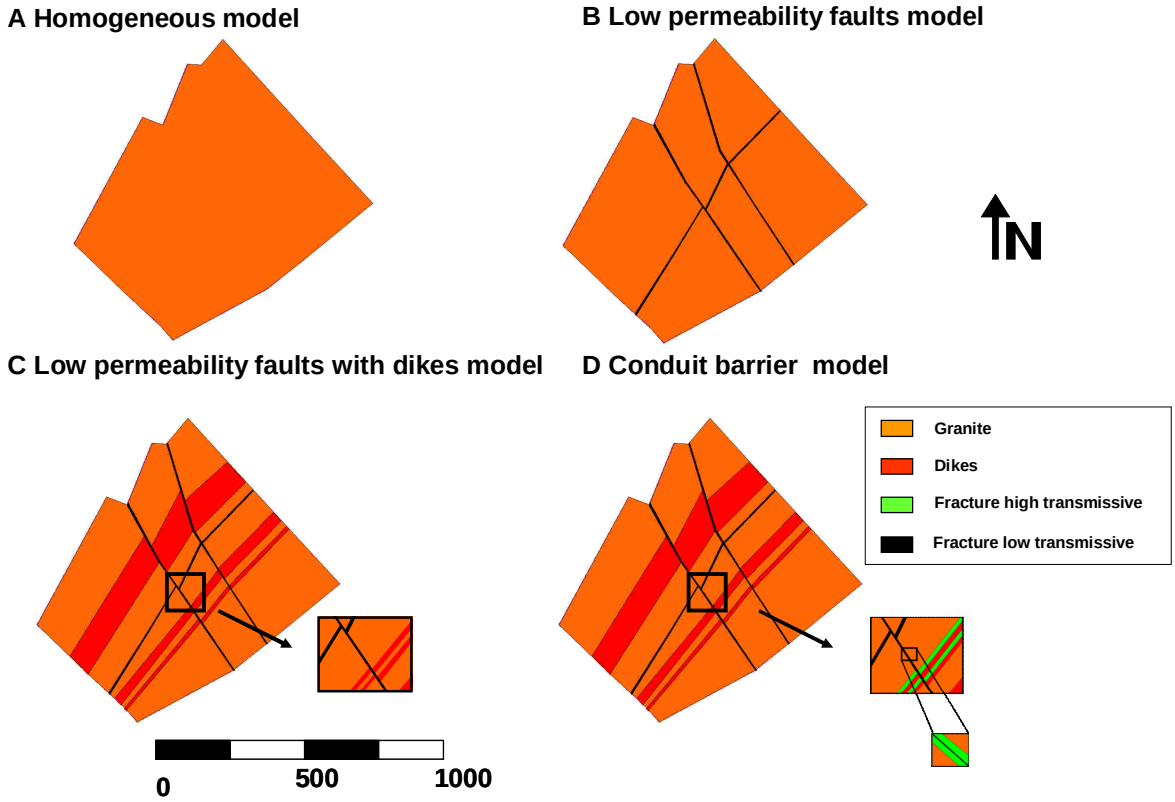

Figure 2– 6. Four scenarios calibrated in the numerical model. a) Homogeneous model b) Low permeability faults model c) Low permeability faults with dikes model d) Conduit-barrier model.

Four scenarios, which increased in complexity from the homogeneous model to the geometrical model defined above (Figure 2– 6), were calibrated in order to obtain the most suitable solution: a) a homogeneous model; b) a barrier fault model (differentiating the characteristics of granite on both sides of fault 1; c) a barrier model for faults and dikes; and d) a conduit-barrier model constructed with the damage zones surrounding the faults and the transmissive areas along the dike axes.

2.6. Results

The first scenario (homogeneous medium) yielded a poor fit at all piezometers (Figure 2– 7 and Figure 2– 8). The poor fit was especially noticeable when it corresponded to the pumping wells located on the other side of the axis of fault 1 (not active in this scenario). That is, the SB20-03

piezometer and Wells 1 and 3 produced a poor response to the pumping of wells 2, 4 and 5, as did the SC-17B, ZPA-2, SF-28 piezometers to Wells 1 and 3 (piezometer SB20-3 in the Figure 2– 8).

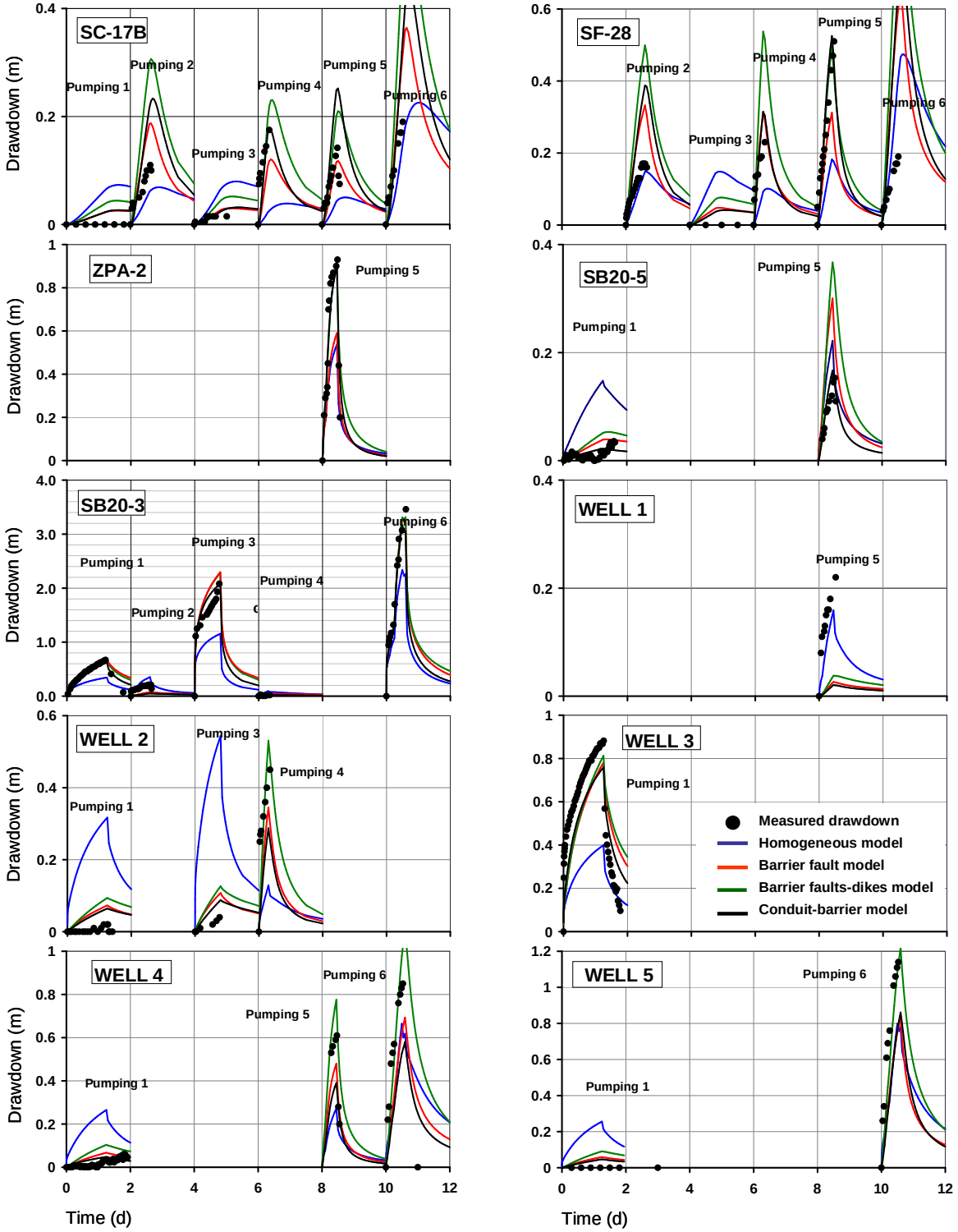

Figure 2– 7. Drawdown fits of the four calibrated scenarios for the five piezometers and pumping wells. The six pumping tests are calibrated consecutively with intervals of five days, returning to the 0 level of drawdown five days after to start the pumping test.

The second scenario incorporated the faults (barrier effect) and the differences in the transmissivity of the granites on both sides of Fault 1 (Figure 2– 7). This scenario simulated the barrier effect better because of Fault 1, which entailed a reduction in calculated drawdown of the piezometers that responded to the pumping wells located on the other side of Fault 1. The piezometers located on the south-western side of Fault 1 (Wells 1 and 3, and the SB20-3 piezometer) yielded a good fit with respect to the pumping on the same side of the fault.

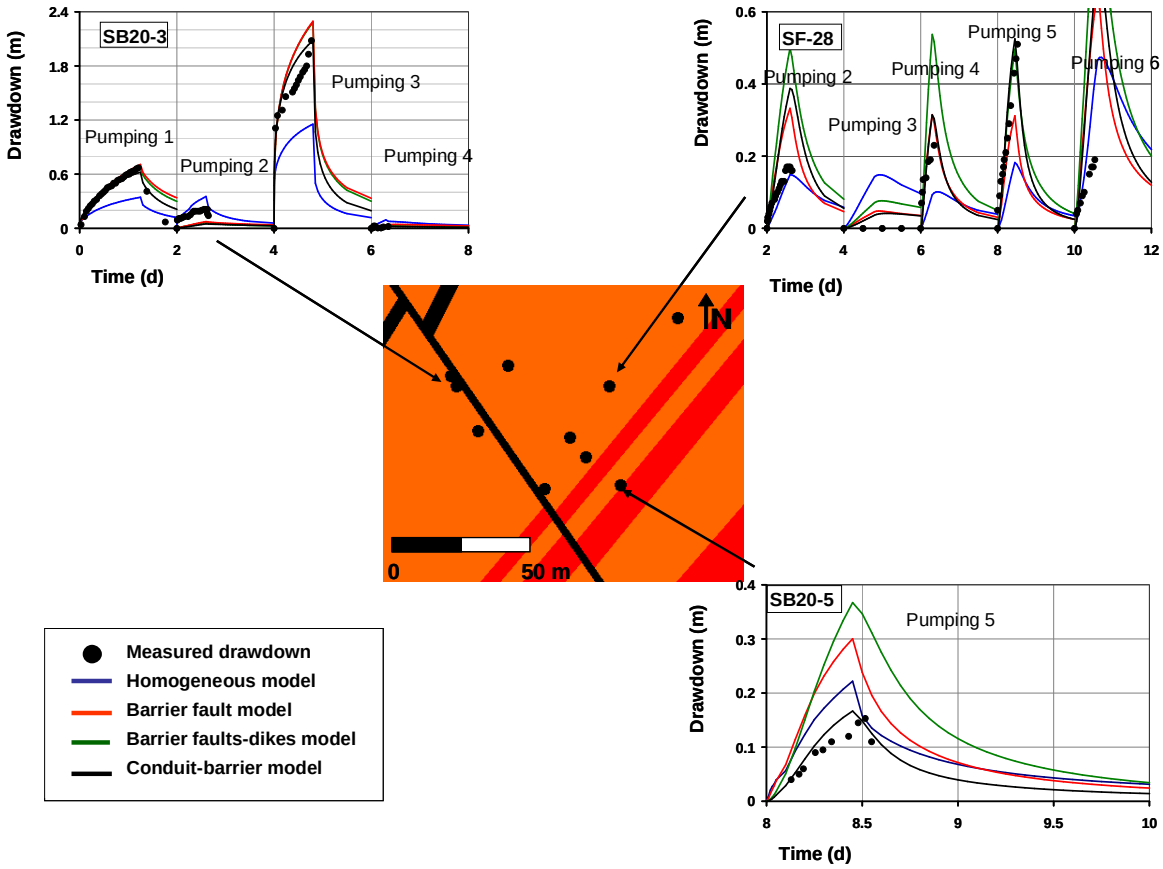

Figure 2– 8. Drawdown fits of the four calibrated scenarios for the three most representative piezometers: SF-28, SB20-3 and SB20-5.

The third scenario introduced the SW-NE trending dikes into the model geometry. There was a notable improvement in some piezometers (ZPA-2). However, the fit was equal to, or worse than, that of the second scenario in the other piezometers. Calculated drawdown was higher than observed in the majority of the piezometers (Figure 2– 7). This problem was resolved and tested in the fourth scenario by implementing high transmissivity bands surrounding the faults and the dikes (conduit-barrier model). This yielded a better fit, resulting in a decrease in calculated

drawdown. The transmissive bands dikes and faults between the SB20-5 piezometer and the pumping wells gave rise to flow paths, yielding a good fit (Figure 2– 8).

The fit in the SF-28 (Figure 2– 8) and SC-17B piezometers was always poor for pumping Well 2. Good connectivity between SB20-3 and Well 3 with Well 2 could be ascribed to the influence of Fault 2 (there is less hydrogeological information about Fault 2 than about Fault 1), which enhances the flow across Fault 1 in this area (Figure 2– 4, Figure 2– 7and Figure 2– 8). And finally there is non-symmetric behavior between Wells 1 and 5. Well 1 yields a better response to the pumping of Well 5 than Well 5 to the pumping of Well 1. This behavior could be attributed to the differential drawdown caused by each well depending on the transmissivity of the affected area. When a well is located in a high transmissivity area or when it has well connected pathways, drawdown may be transmitted a considerable distance, possibly lowering heads below some transmissive fractures. By contrast, if the area surrounding the well has less transmissivity, the well will not be able to transmit drawdown very far. In consequence, the behavior between two boreholes does not have to be symmetrical. Our model was not able to simulate this behavior probably because of the addition of concrete in Well 5 to seal the lower granite.

In summary, the model was very sensitive to the barrier structures, especially the fault-zones. The definition of Fault 1 as a barrier was crucial for explaining the response to the pumping on the other side of the fault. The presence of the dike fractured bands (high and low permeability) and the high transmissivity areas surrounding the faults enabled us to reduce drawdown and to obtain the best fit in the northern block. The hydraulic parameters of the geological rock units are shown in Table 2– 2. The transmissivity values of the weathered granite are very similar to those of the unaltered granite despite the fact that we expected them to be higher. We attribute this apparent contradiction to the intense fracturing of the upper portion of the unaltered granite. Furthermore, the fact that the wells and piezometers were mainly screened in the two granite layers hampered the separation of the parameters of the two layers.

Table 2– 2. Transmissivity values of the geological formations calibrated in the conduit-barrier model.

Rock unit	Transmissivity m^2/d
Weathered granite	20-30
Granite	20-50
Damage bands	600-5000
Core fault	0.1-0.2
Core dike	0.1-1

2.7. Discussion and Conclusions

Groundwater characterization of a fractured massif of shallow tunneling was undertaken successfully. Geological characterization and groundwater research played a major role in building a conceptual model that reflected the groundwater flow in a fractured rock massif. Numerical modeling enabled us to test the reliability of the original hypotheses.

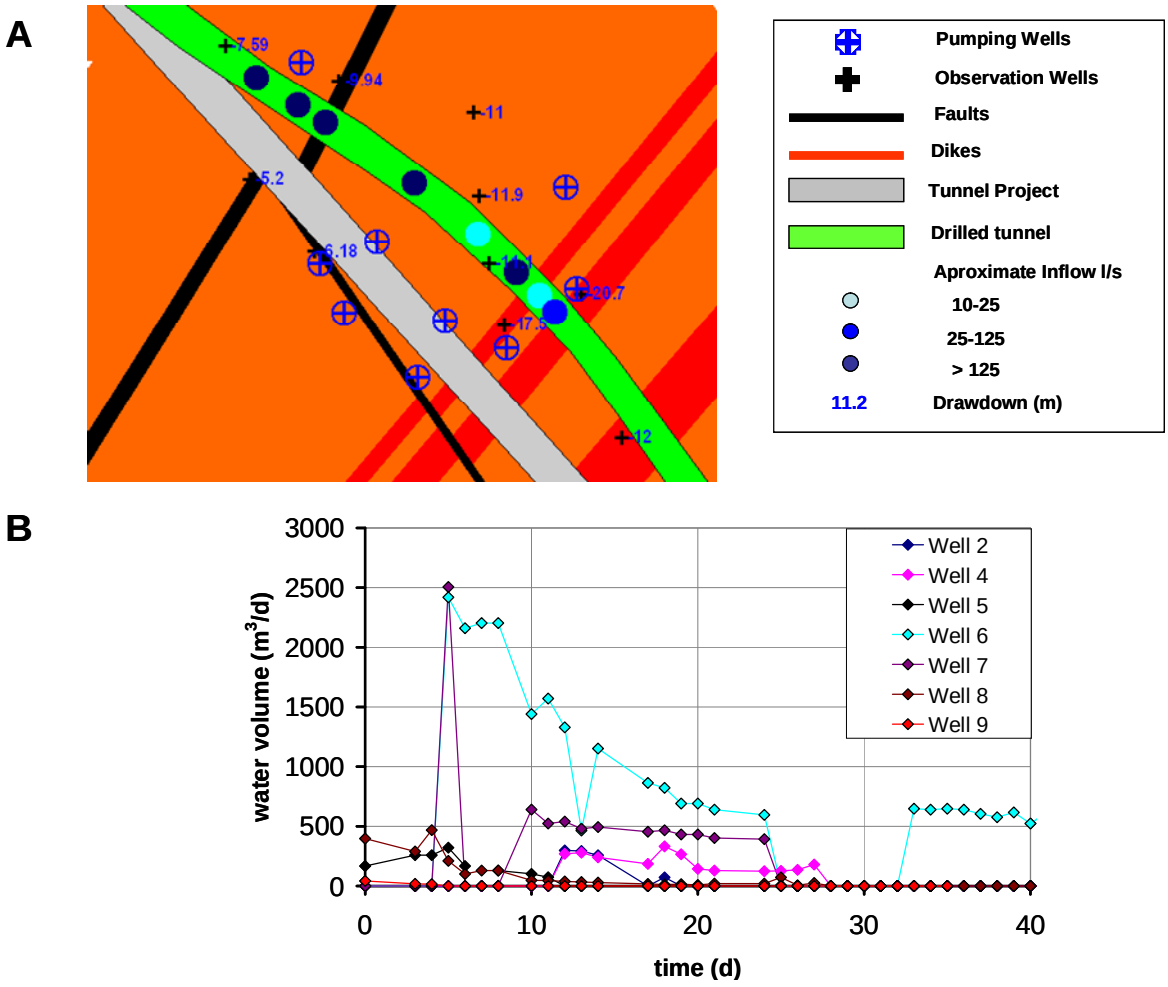

Figure 2– 9. a) Detailed area map with the location of the dewatering wells, piezometers (with their medium drawdown during the dewatering), and approximate tunnel inflow. b) Volume rate of the pumping wells during the dewatering event.

The complex groundwater behavior of the fractures was characterized in the B-20 area. Cross-hole tests proved crucial for characterizing the connectivity between the faults and dikes and granodiorite. The fault-zones provided evidence of a conduit-barrier behavior. The barrier effect was more marked than the conduit effect in faults, resulting in a groundwater behavior in blocks. The conduit effect was more prominent than the barrier effect in dikes. The most transmissible areas were those located along the contact of dikes and granite. The area that was not covered by

the cross hole test mesh presented some problems of definition. Connectivity between Well 2 and the other side of Fault 1 is not well represented in the model since Fault 2 is very close to this lineament. The absence of piezometers on the other side of this fault made its characterization difficult. The fact that the research was not restricted to the tunnel pathway enabled us to characterize the flow connectivity between the tunnel area and the rest of the rock massif. The extension of the barrier and the conduit structures determined the flow in the tunnel area.

The barrier behavior was instrumental in dewatering because it compartmentalized the flow and reduced the pumped volume and water inflows. The general drawdown of the area (tunnel inflow + dewatering) is illustrated in Figure 2– 9a, which shows that groundwater is compartmentalized and that the piezometers on the south side of Fault 1 have a lower drawdown. The most volumetric dewatering boreholes (Wells 6 and 7, Figure 2– 9b) were located in the dike areas, especially in the more transmissive bands (Figure 2– 9a). Higher tunnel inflows (qualitative information) were located before Fault 2 and in the dike area (Figure 2– 9a). A point of high water inflow was located near Well 2, which could be due to the fact that Fault 2 was imperfectly defined.

3. Groundwater inflow prediction in urban tunneling with a Tunnel Boring Machine (TBM).

3.1. Introduction

The unexpected encounter of high water inflows and soft ground is a major concern in tunnel excavation. Water inflows may drag large amounts of material and cause face instabilities, collapses, chimney formations and surface subsidence. When using tunnel boring machines (TBM) the problems caused by these inflows are often ascribed to the presence of hydraulically conductive fractures or faults (Deva et al., 1994; Tseng et al., 2001; Shang et al., 2004; Dalgiç, 2006). The simultaneous occurrence of soft geological formations and high water inflows can create a "snow ball effect" (Barton, 2000), i.e. high inflows drag soft materials that increase permeability and connectivity with the rest of the aquifer, producing further water inflows and sediment drag in a process that grows in intensity. These scenarios lead to stoppages requiring corrective measures, and higher construction costs, not to mention the risk to life and damage to property (Cesano et al., 2000; Day, 2004; Schwarz et al., 2006; Varol and Dalgiç, 2006).

This study was prompted by the difficulties encountered during the construction of the Barcelona Subway L9 (Line 9). Forty kilometers of tunnels are currently being excavated in the metropolitan area of Barcelona (Figure 3– 1a). The first tunnel sector was drilled under the town of Santa Coloma (Figure 3– 1b). A dual Tunnel Boring Machine (TBM) with a capacity to work in open mode when excavating hard rocks or closed mode when crossing unstable materials was used. The combination of unexpected weathered granite and water inflows in a small area of the Santa Coloma sector (Fondo zone) caused tunnel face instability and machine stoppage. Similar conditions had been forecasted when crossing another area of the Santa Coloma sector (B-20 zone, Figure 3– 1b). Both areas shared difficulties due to mixed face conditions (hard rock bottom-half section and weak rock top-half section) since each type of rock requires different excavation modes that are hard to handle simultaneously (Barton, 2000; Babenderende et al., 2004). Tunneling had been uneventful in the B-20 zone, because it had been well characterized (Font-Capo et al., 2011). This enabled us to modify the tunnel trajectory and to implement a

This chapter is based on the paper Font-Capo, J., Vazquez-Sune, E., Carrera, J., Marti, D.; Carbonell, R., Perez-Estaun, A., 2011, Groundwater inflow prediction in urban tunneling with a tunnel boring machine (TBM), Engineering Geology, 121, 46-54. DOI: 10.1016/j.enggeo.2011.04.012.

groundwater pumping that lowered heads and reduced water inflows into the tunnel. The problems encountered in the Fondo zone were attributed to the lack of adequate forecasting. Geological data, which were mainly derived from surface mapping, were insufficient to provide a detailed characterization. Although surface research can detect most fractures and possible inflow areas, it cannot precisely locate and determine the volume of tunnel inflows (Banks et al., 1994; Mabee, 1999, Mabee et al., 2002; Cesano et al., 2000, 2003; Lipponen, 2007). In contrast to the Fondo zone, a prediction was carried out in the B-20 zone, and this required accurate characterization, including deep borehole drilling, and the assessment of inflow rates. Given that the problem of the Fondo zone had not been anticipated, it became apparent that more effective solutions were needed to assess potentially problematic areas, characterize them and compute tunnel inflows.

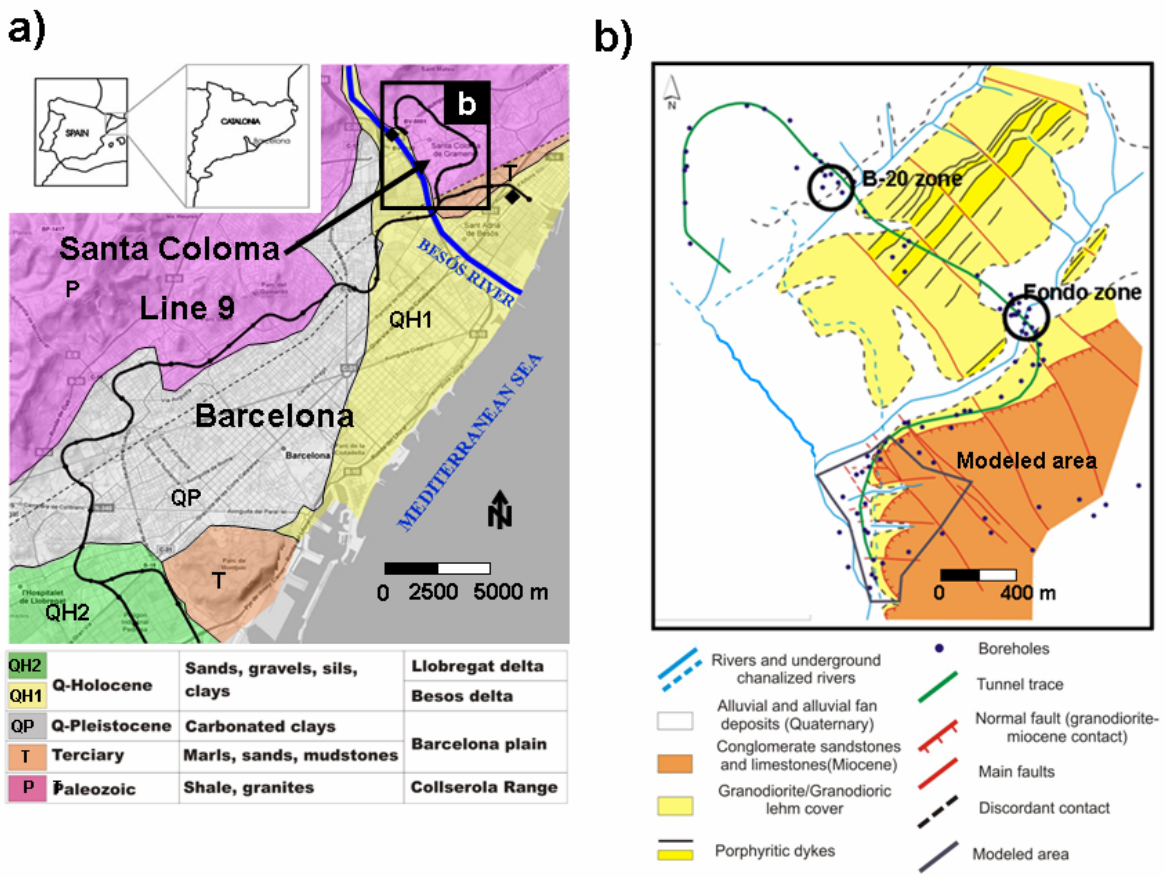

Figure 3– 1.a) Map of Barcelona conurbation and Line 9 subway, b) Geological map of the Santa Coloma sector of Line 9 subway, B20 and Fondo zones.

Inflows can be calculated by means of numerical or analytical solutions. A number of analytical formulas have been developed to predict tunnel inflows under different hydraulic conditions. Most of these assume homogeneous media and either steady state (Goodman et al., 1965;

Chisyaki, 1984; Lei, 1999; El Tani, 2003; Kolymbas and Wagner, 2007; Park et al., 2008) or transient conditions (Marechal and Perrochet, 2003; Perrochet, 2005a, 2005b; Renard, 2005). Some analytical solutions have also been developed for heterogeneous formations (Perrochet and Dematteis, 2007; Yang and Yeh, 2007). These solutions are suitable for systems with layers that are perpendicular to the tunnel so that flow is generally radial. Moreover, they can only be used when the system is relatively unaffected by inflows. Therefore, they cannot be used for assessing large inflows to relatively shallow tunnels because the boundary conditions evolve with time and flow takes place primarily in the aquifer plane rather than radially in the vertical plane perpendicular to the tunnel. Moreover, since the Santa Coloma tunnel is lined, the radial flow towards the tunnel is very small, and most inflows appear at the tunnel face (or in machine-rock contact). The presence of high conductivity fractures that are well connected with permeable boundaries further hinders the use of analytical formulae to compute water inflows. Numerical modeling is required under these conditions.

Careful modeling of flow through fractured formations requires separating the less permeable areas from the dominant fractures, which carry most of the water. This may be accomplished by hybrid models, which combine the main features of equivalent porous media models (EPM) and discrete fracture networks (DFN), i.e. hydraulically dominant fractures are modeled explicitly by means of 1 or 2D elements that are embedded in a 3D continuum model representing minor fractures. The approach is appropriate since it explains scale effects in hydraulic conductivity (Martínez-Landa and Carrera, 2005, 2006). Numerical models have been used to calculate the groundwater flow around the tunnels. In fact, inflows are often used to calibrate the numerical model (Stanfors et al., 1999; Kitterod et al., 2000; Molinero et al., 2002) or find the inflows in a large scale (Yang et al., 2009). By contrast, numerical models have rarely, if ever, been used for forecasting inflows during tunnel excavation (Molinero et al., 2002; Witkke et al., 2006).

The present paper presents a methodology for predicting the location and magnitude of tunnel inflows using a numerical groundwater flow model. The method was applied to the last 700 meters of the Santa Coloma sector of L9 of the Barcelona Subway. To this end, a geological conceptual model and a hydrogeological parametrization were carried out, and a quasi-3D numerical model was constructed. After calibrating this model, the groundwater transient state caused by the TBM was simulated and tunnel water inflows were obtained.

3.2. Geological and geophysical conceptual model

Geological characterization in linear works is commonly restricted to the tunnel course, which creates two sets of problems: a) a 3D picture cannot be obtained because information is restricted to a vertical plane, and b) the connectivity with the most relevant geological features must be obtained beyond the tunnel trace because water may flow laterally towards the tunnel. Geological studies to gain a better understanding of the geology of the Santa Coloma sector of L9 were extended beyond the tunnel trace to include (1) a detailed study of the limited outcrops available in city parks and road cuts; (2) photogrammetry and geological interpretation of old aerial photographs (taken in the 1950s just before urban development); (3) geological field work; (4) borehole re-interpretation; and (5) geophysics.

A new geological map was constructed in the course of this study (Figure 3– 1b), which shows the existence of granodiorite with numerous porphyritic dikes over which Miocene sedimentary rocks lie unconformably. Quaternary alluvial deposits are also present to the west, close to the Besós River. Granodiorite is petrographically homogeneous. The porphyritic dikes, which are kilometers in length and meters thick, run northeast to southwest, sub parallel and vertical. They can be observed and mapped only in outcrops outside the city centre. Subvertical strike-slip faults with a regional Variscan (late Carboniferous) orientation (NNW-SSE) and separated by hundreds of meters, displace the porphyritic dikes. The dikes are more resistant to erosion than granodiorite, which facilitates identification. These faults (north-northwest–south-southeast) also affect Miocene rocks in this area, providing evidence of their reactivation in post-Miocene times. Miocene rocks consist of conglomerates, sandstones, limestones, and some clay layers (Cabrera et al., 2004). The granodiorite-Miocene contact in this zone is a normal fault zone similar to the regional normal faults that generated the Miocene extensional basins related to the formation of the Catalan margin. Cataclastic fault rocks are associated with these normal faults (breccia and fault gauges). The Miocene sedimentary rocks are juxtaposed against the granite across cataclastic rocks (a 15m-wide band mapped at the surface). These granodiorite-Miocene contacts are displaced by the NNW-SSE faulting. Weathering is extensive in the granodiorite rocks. Part of this weathering is of pre-Miocene age, and is evidenced where the unconformity appears.

A geophysical campaign was conducted in the area (Martí et al., 2008) to find the depth and confirm the location of the surface structures. The characterization included 2D and 2.5D

reflection seismic profiles and a 3D tomographic experiment in a football stadium. This dataset showed that the study area is mainly composed of a granitic massif with numerous subvertical porphyric dikes at metric scale. The dikes are high-seismic-velocity features in the tomographic models (Figure 3– 2). NNW-SSE strike-slip faults are common along the tunnel course. A number of east-west brittle faults are also observed in some parts of the study area. These faults are imaged by the tomographic models as low velocity anomalies adjacent to high-velocity zones (low fracture density granite and the porphyritic dikes) (number 115, 245, 210, 110 and 148 in Figure 3– 2 and Figure 3– 3a). The main faults are of Variscan age, were reactivated in the post-Miocene, and displaced the porphyritic dikes at metric scale. The geometry and the depth of the superficial weathered layer, which results from the pre-Miocene alteration of the granites, is controlled by the system of faults and dikes. A relatively sharp velocity gradient indicates the limit between the soft and/or weathered layer and the harder/unaltered granite below. The tomographic models show a steep velocity gradient between the weathered layer and the most competent granite. These changes in the physical properties, clearly imaged with the velocity models, enabled us to constrain the geometry of the mixed face conditions.

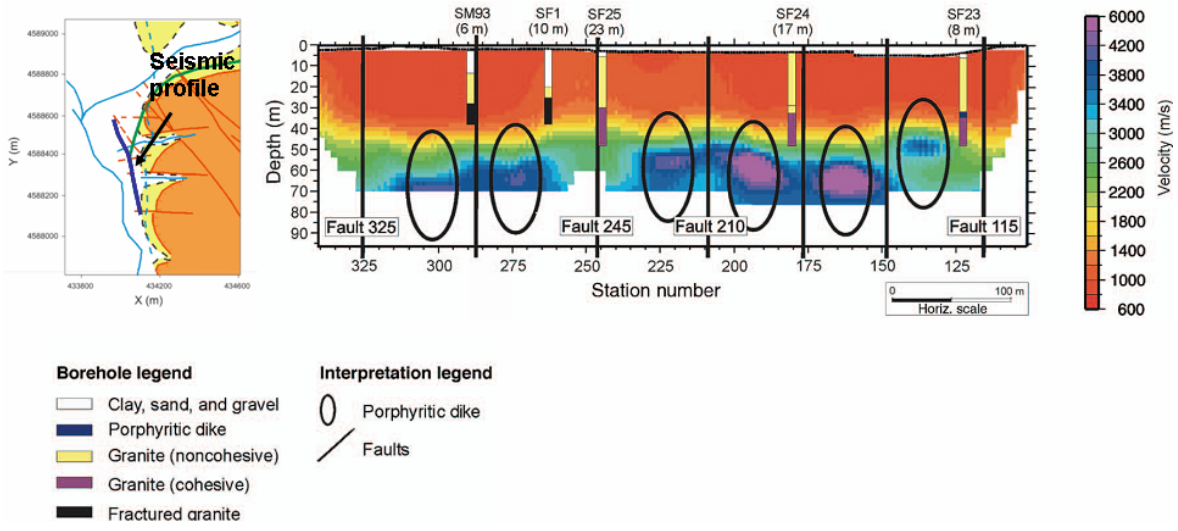

Figure 3– 2. (Extracted from Martí et al., 2008). A 2D seismic cross section and its geological interpretation. The velocity model images a weathered layer of variable thickness characterized by a very low seismic velocity of 600–1200 m/s. The variable thickness of the surface is controlled by several subvertical low- and high-velocity anomalies interpreted as faults (solid black lines) and porphyritic dikes (black ovals) or competent granite, respectively. Faults 115, 210, 245, and 325 coincide with mapped faults at the surface. Superimposed on the tomographic section are the interpreted cores obtained in an earlier study conducted by the construction company. The distance from the geological research boreholes to the seismic section is also included.

The geological model provides constraints on the areas with a high probability of water inflows, and was used to identify the most suitable locations for drilling new boreholes in order to dewater the tunnel surroundings (Figure 3– 3a).

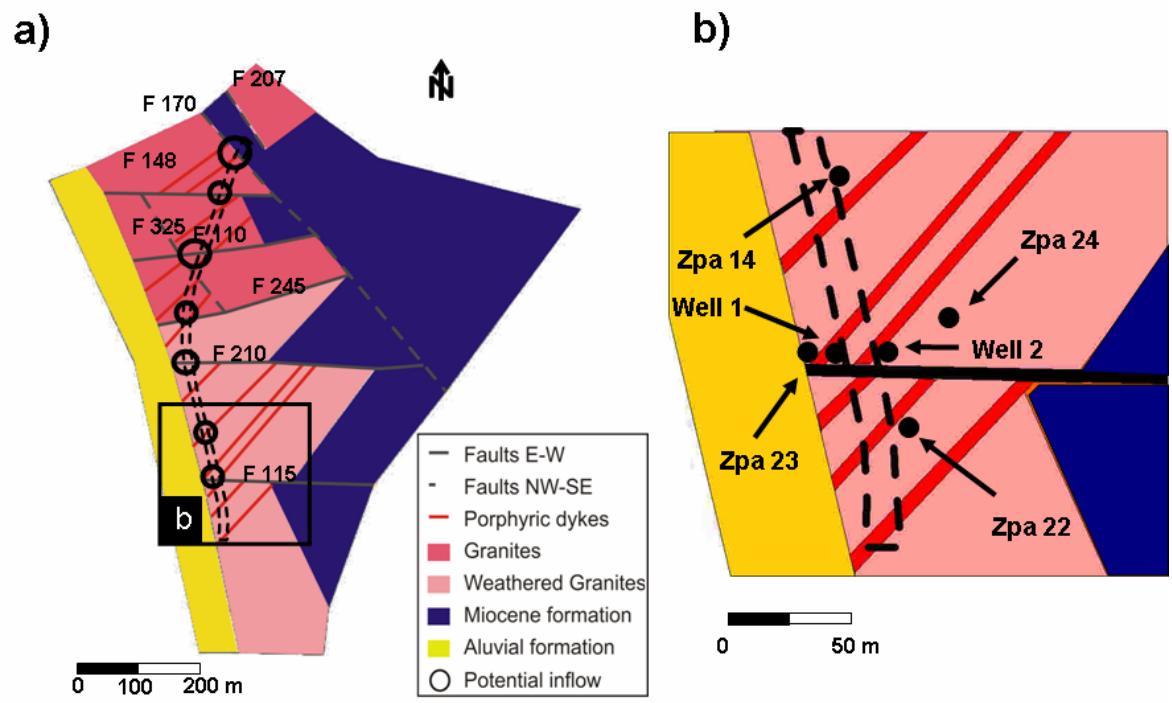

Figure 3– 3. a) Conceptual definition for hydrogeological modeling, including location of the most probable inflow areas. b) Location of pumping test and observation boreholes.

3.3. Hydrogeological investigation

Permeability of the igneous rocks is controlled by permeable faults that are evidenced by lineaments in the surface, and by the degree of rock weathering. The intersections between fractures and dikes are areas of high permeability because the fracturing process produces a greater cataclastic deformation in porphyritic dikes that display a more fragile behavior than in weathered granite (Singhal and Gupta, 1999). Groundwater flows mainly from the granite and the Miocene clay gravels to the Besós alluvial aquifer in the study area. (Figure 3– 1b).

Permeability values were determined by pumping tests performed close to the granite body. The values of the effective transmissivity range between 50 and 600 m^2/day in the B-20 zone (RSE, 2003) and in the Fondo zone (Carrera et al., 2004). Furthermore, hydraulic tests were conditioned by major faults with effective transmissivity of more than 300 m^2/d. Alluvial sediments from the Besós River display transmissivity values between 1500 and 6000 m^2/d (Ondiviela et al., 2005). Very low values of permeability are expected for Miocene clay gravels.

Although these values were obtained in the proximity of the model, they must be regarded as indirect information. Pumping tests are necessary to obtain the local hydraulic parameters as well as anisotropy and connectivity patterns of the main faults and dikes at tunnel scale. A pumping test was carried out using two wells, 26 m deep and fully screened, simultaneously (Figure 3– 3b). The total pumping flow ranged between 1 and 4 L/s. Four piezometers were equipped with head data-logging sensors. They are screened at different depths (ZPA-14; 22-26m, ZPA-22 and ZPA-23; 20-24m, and ZPA-24; 14-17m). The piezometer depth is representative of the tunnel depth (a circle of 12 m diameter with the top located at depths between 14 and 20 m).

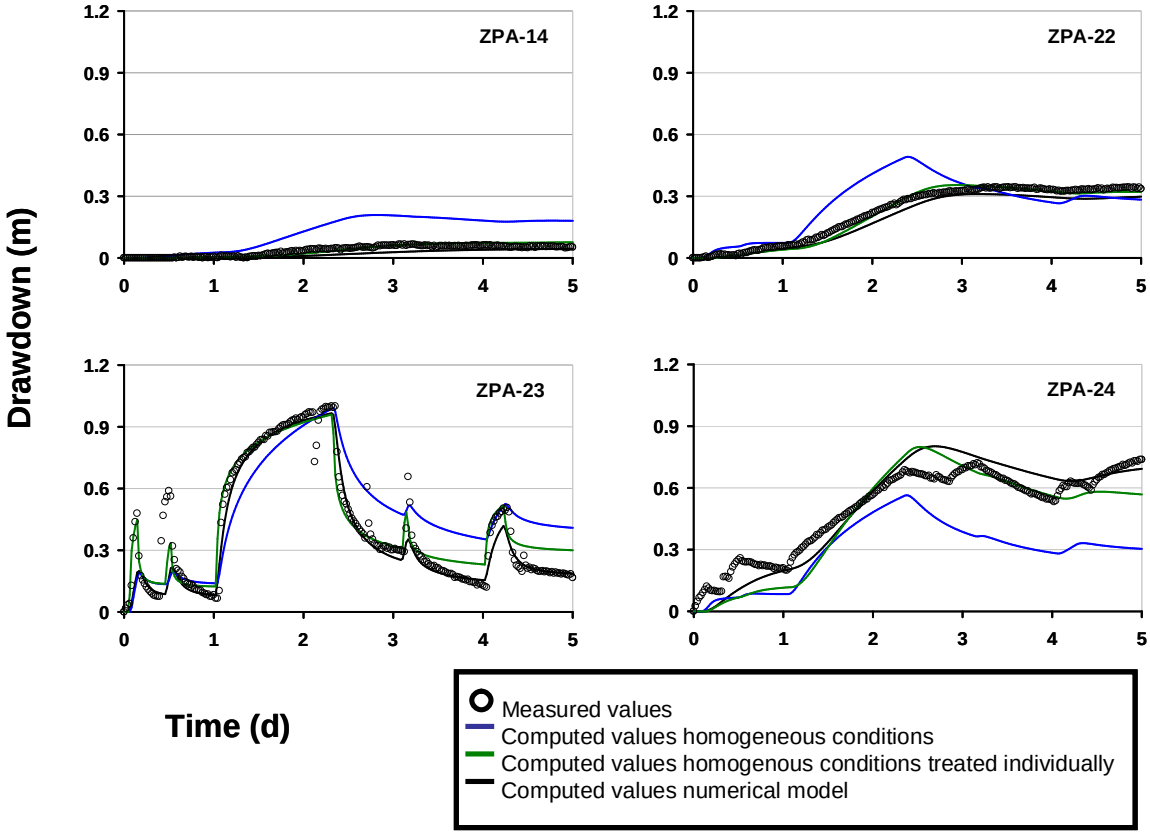

Figure 3– 4. Drawdown calibration of the four tested piezometers also shown is the time evolution of drawdowns: a) measured values (dots), b) computed values homogeneous conditions (blue lines), c) computed values homogenous conditions treated individually (green lines), d) and computed values using the numerical model (black lines).

This pumping test was first interpreted under homogeneous conditions and infinite extent to obtain a preliminary estimate of hydraulic parameters. An interpretation using all piezometers was made with the EPHEBO program (Carbonell et al., 1997), which yielded a transmissivity of 83 m^2/d and a storage coefficient of 0.04. The fit is very poor (Figure 3– 4), which suggests a significant heterogeneity, and demands a different approach. Therefore, each piezometer was analyzed individually. The estimated transmissivity ranged between 30 and 180 m^2/d, and the storativity between 0.001 and 0.1. This large variability in estimated storativity denotes a varying

connectivity between pumping wells and piezometers (Meier et al., 1998; Sanchez-Vila et al., 1999). Low storativity values (0.001) derived from drawdowns in ZPA-23 (E-W direction) imply high connectivity along this direction, which suggest that fractures in this direction display high transmissivity. On the other hand, the high storativity value (0.1) obtained from the response at piezometer ZPA-14 suggests poor connectivity trending N-S.

Given that the drawdown curves could not be fitted with a homogeneous model, a heterogeneous model was set up. A correct definition of heterogeneity was needed to locate and quantify water inflows.

3.4. Numerical model

The aquifer system was simulated with the finite-element numerical model VisualTRANSIN (GHS, 2003; Medina and Carrera, 1996). A mixed model was constructed using the methodology of Martínez-Landa and Carrera (2006). This method requires structural geology understanding to identify the main fractures in addition to geophysics and hydraulic data to characterize them. Hydraulic tests, such as the one described above, are used to identify the fractures that provide hydraulic connection. The transmissivities of these fractures, which must be modeled as discrete features, are derived from calibration. Therefore, the model was built incorporating the main features identified by the geological and geophysical datasets. The igneous rocks (including subvertical dikes and main faults), Miocene rocks and alluvial formations were included in the model (Figure 3– 3).

A quasi-3D model divided into seven four meter thick layers was constructed. These layers were linked to 1D element layers to simulate vertical fluxes. This distribution enabled us to represent the tunnel accurately in its real depth. Faults and dikes were represented in all the layers as narrow bands connected by vertical 1D elements (vertical faults and sub-verticals dikes were projected to depth with a dip of 90º). Borehole and piezometer screens were also located in their corresponding layers. The boreholes that connected more than one layer were represented by highly conductive 1D elements. The eastern limit is a water divide and was defined as a no flow boundary in the model (Figure 3– 5).The model was bounded by the Besós River in the west, and streams in the North and South. All these boundaries were simulated with a leakage boundary condition.

$$q = \alpha_B (h - H_{ext}) \qquad (Equation\ 3-1)$$

Where q represents the boundary flux, α_B is a boundary leakage factor, H_{ext} the head to which the aquifer is connected (e.g., elevation of river water), and h is the head close to the boundary. The finite mesh elements had 36618 elements with sizes ranging between 0.1 and 150 meters.

The aforementioned pumping test was used to calibrate the hydraulic parameters of nearby pumped formations, including granite domain, faults and dike formations. The remaining formations (Miocene, alluvial, distant dikes and faults) were also calibrated, but estimated values were basically identical to those assumed a priori from tests conducted in those formations but outside the model domain. The model was calibrated using the drawdown mode (i.e., only changes in head, rather than absolute heads). The model fit is shown in Figure 3– 4b.

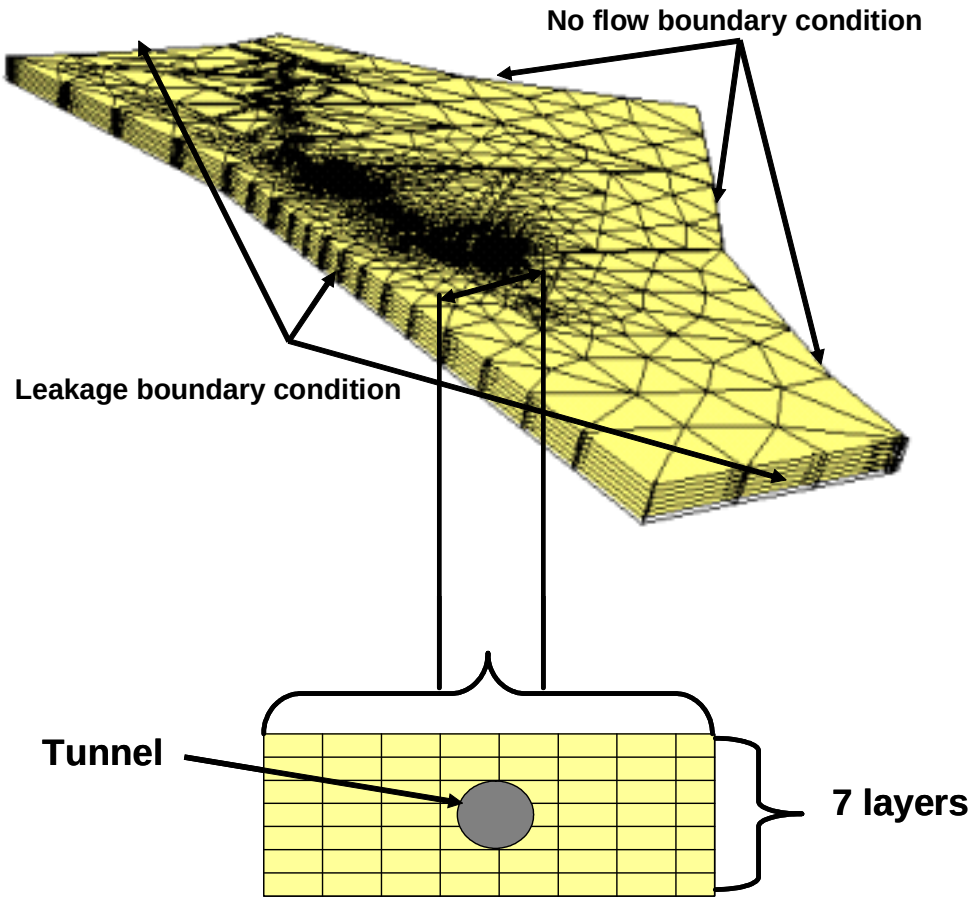

Figure 3– 5. Finite element mesh divided into seven layers (grey and black) connected by 1D elements. Location of boundary conditions; no flow boundary condition and leakage boundary condition on the western and southern and northern sides. (Detail of the tunnel location in the seven layers).

The rest of the model (regional scale) was calibrated under steady-state conditions using 21 observation points with 1 measurement by point. The modeled piezometric surface is shown in Figure 3– 6a, where the residual values of the calibration at each observation point are also included. The best fits are located in the areas close to the tunnel path. The calibrated values of permeability coefficients and specific storage coefficients of the individual geological formations and features are specified in Table 3– 1.

Table 3– 1. Hydraulic parameters of the geological formations, (*) the specific storage of the surface layer includes the whole domain.

Formation	Hydraulic conductivity (m/d)	Hydraulic conductivity (m/s)	specific storage (m^{-1})
Weathered granite	0.5	$5.8 *10^{-6}$	$8.3 *10^{-6}$
Unaltered granite	0.01	$1.2 *10^{-7}$	$4.2 *10^{-6}$
Fault 170	12.5	$1.4 *10^{-4}$	$4.2 *10^{-6}$
Fault 148	9.5	$1.1 *10^{-4}$	$4.2 *10^{-6}$
Fault 325	12.5	$1.4 *10^{-4}$	$4.2 *10^{-6}$
Fault 245	9.5	$1.1 *10^{-4}$	$4.2 *10^{-6}$
Fault 210	10.25	$1.2 *10^{-5}$	$4.2 *10^{-6}$
Fault 115	7.5	$8.7 *10^{-4}$	$4.2 *10^{-6}$
Fault 207	12.5	$1.4 *10^{-4}$	$4.2 *10^{-6}$
Fault 110	9.5	$1.1 *10^{-4}$	$4.2 *10^{-6}$
Dykes	0.02-0.3	$2.3*10^{-7}$ - $2.4*10^{-6}$	$6.3 *10^{-6}$
Aluvial formation	160	$1.9 *10^{-3}$	$6.3 *10^{-6}$
Miocene formatin	0.001-0.01	$1.1*10^{-7}$ - 1.10^{-8}	$4.2 *10^{-7}$
Surface layer	*		$6.0 *10^{-3}$

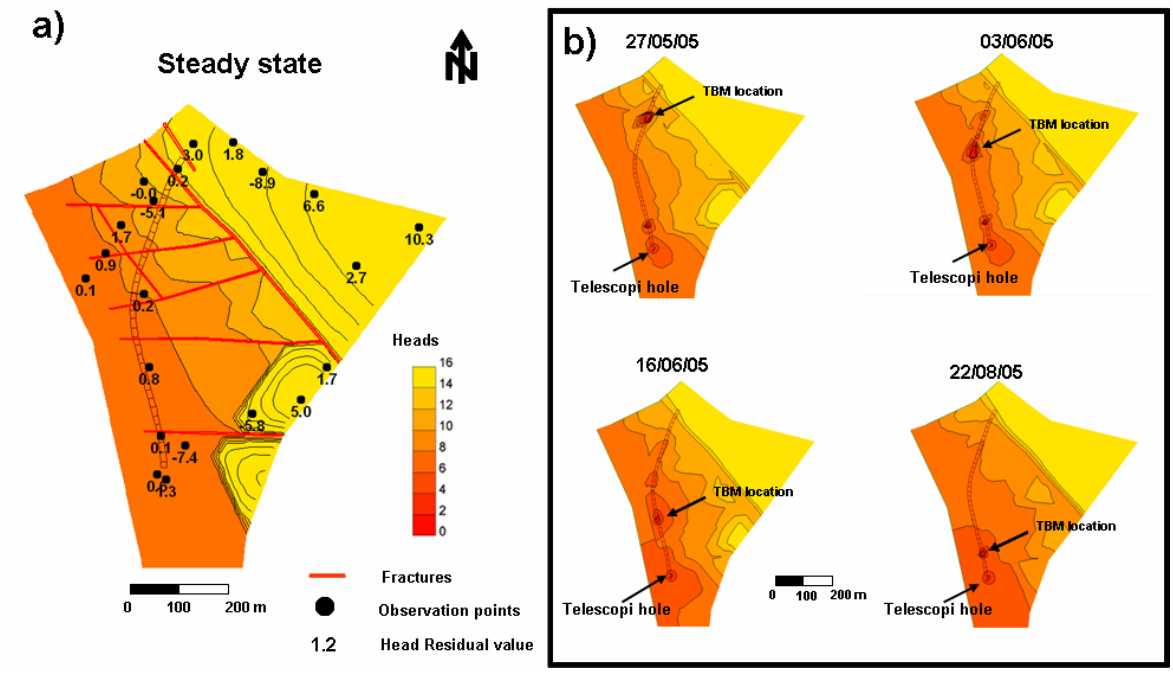

Figure 3– 6. a) Steady state piezometric surface of the modeled area prior to the TBM advance, the observation points and their residual values are also located. b) Transient piezometric surfaces in four different steps with the advance of the TBM. All the piezometric surfaces were carried out at tunnel depth (Layer 4).

The effect of groundwater on the tunnel advance was simulated by dividing the tunnel domain into 36 intervals of 18.5 meters in length (each interval having the length of the machine). Each interval comprised a free tunnel surface before the emplacement of the lining rings (tunnel face and rock-machine contact, Figure 3– 7a). This machine interval coincided with the peak inflow because the tunnel was protected by lining after the TBM advance. The machine offers a water circulation resistance (actual water inflow areas are limited) which was simulated by a leakage function. The actual flow rate drained by each tunnel node, i.e. a node belonging to the tunnel is given by.

$$Q_i = \propto \cdot f_i(t) \cdot A_i \cdot (h_i - z_{tunnel}) \qquad (Equation\ 3-2)$$

Where *i* identifies a tunnel node, Q_i is the inflow rate, α is the leakage factor, which represents an overall conductance of the system comprising the tunnel face and the machine, A_i is the area associated with node *i* and $f_i(t)$ is a time function that enables us to activate this leakage condition when the excavation reaches the tunnel interval that comprises node *i*, i.e. $f_i(t)$ is zero prior to the arrival of TBM to the interval, hi is groundwater head and z_{tunnel} is the level of the bottom of the tunnel. This leakage condition was applied only during the tunneling process. Prior to the arrival of the TBM, these nodes were inactive (i.e., $f_i(t)$=0). The value of α was calibrated by comparing model calculation to observations of the low inflow values during the first 5 intervals, and head variations at the ZPA-12 piezometer. The value of α is 0.007 (1/day).

Groundwater levels did not fully recover after passage of the TBM. This can be attributed to the drainage due to the extraction hole of Telescopi (Figure 3– 6b), which was not present in the steady state, and to water seepage detected in the tunnel, which indicates that the tunnel lining rings were not completely impervious. A residual leakage had to be applied to simulate the lining seepage. The marked reduction of leakage was simulated by adopting a very low value (0.01%) of $f_i(t)$ factor that multiplies α by the time function after passage of the TBM (Figure 3– 7b). This value represents the permeability of the tunnel lining ($3.4 * 10^{-5}$ m/d).

Some dewatering boreholes were drilled at the most favorable locations found in the geological study. These boreholes were designed to diminish the water pressure on the tunnel face so as to reduce tunnel inflows and the risk of sediment drag. The water volume extracted by the boreholes was known at the time of modeling and was incorporated into the model.

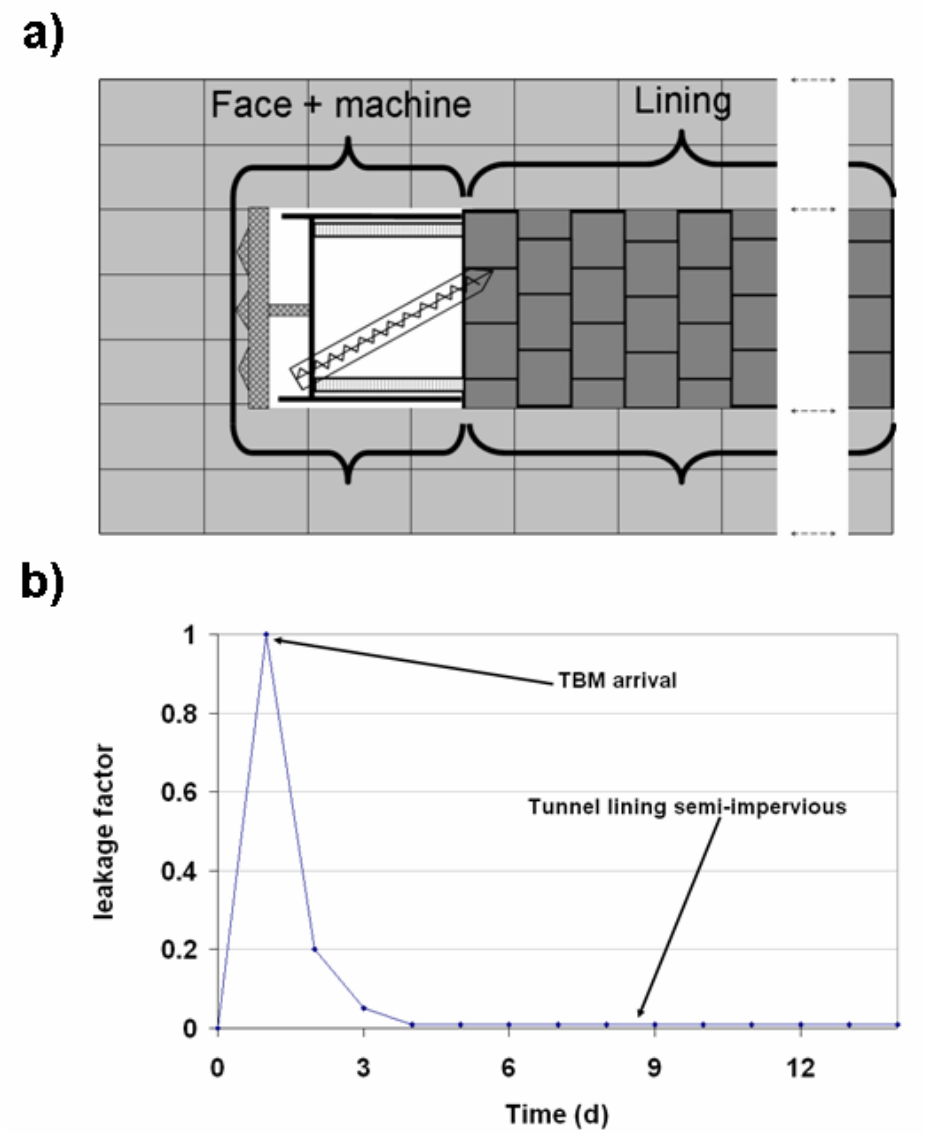

Figure 3– 7. a) Tunnel face and machine scheme profile. b) Transient tunnel leakage function, maximum value when the TBM reaches the tunnel interval (value 1) and decreases to 0.01 after lining construction to simulate residual seepage in the semi-impervious concrete lining.

3.5. Results

Tunnel simulations were validated by the evolution of groundwater heads during tunneling, as shown in Figure 3– 8, where the effect of TBM and the pumping boreholes can be observed. The fit of groundwater heads is good around the tunnel layout. Differences between calculated and measured heads at the ZPA-18 and ZPA-20 piezometers can be attributed to the presence of dewatering boreholes close to the piezometer. The ZPA-22, ZPA-23 and ZPA-24 piezometers are in the pumping test sector. The addition of continuous pumping (not always with a very detailed

time function) and the impact of two months of machine stoppage near this area adversely affected the groundwater fit.

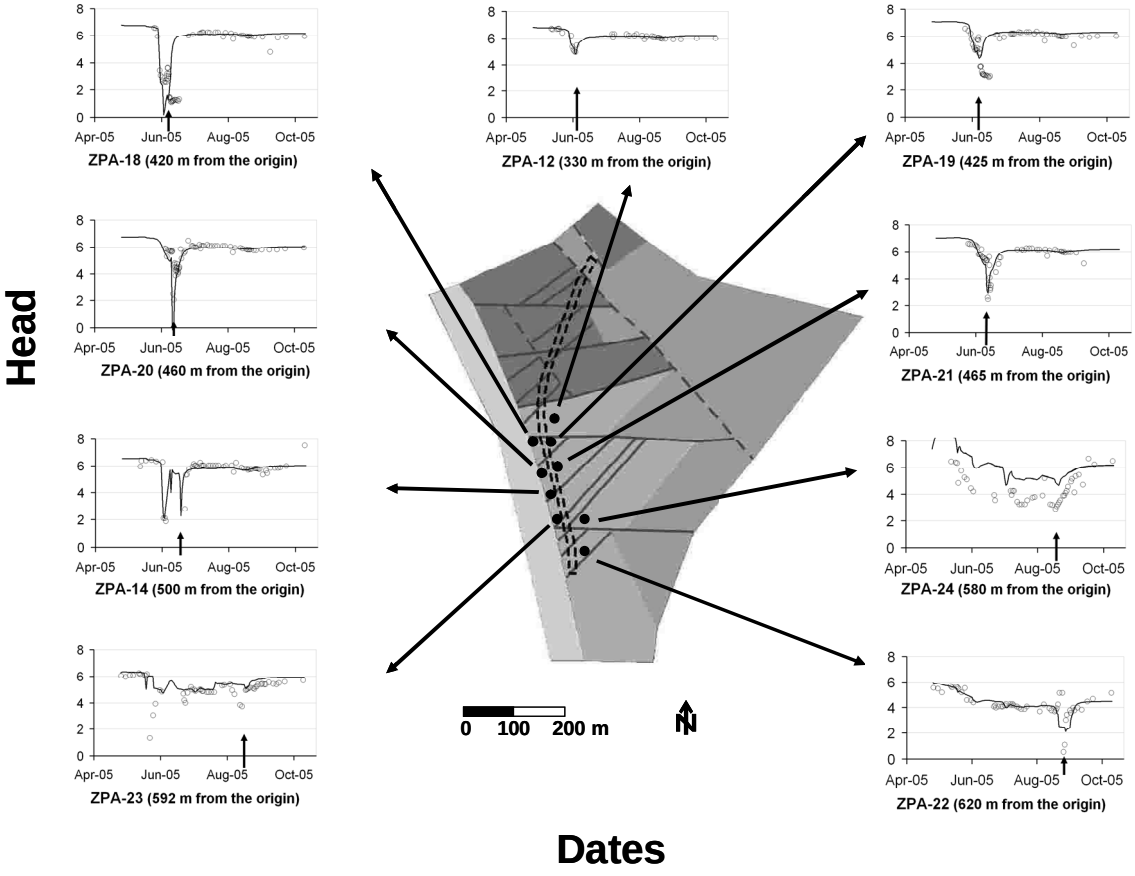

Figure 3– 8. Spatial distribution of piezometers in the transient state of the TBM advance. Also shown is the time evolution of measured (dots) and computed (continuous lines) heads. The TBM location is depicted as a line on the X-axis.

Figure 3– 9 displays the tunnel water inflow and the faults and dikes that correlate water inflow and geology. The largest flow rates were around 2-3 L/s. These values were not measured by the tunneling constructors because they were very low but areas where inflow was qualitatively assessed to be largest coincided with model predictions. The low transmissivity value of the fresh granite accounted for the smaller amounts of water inflow calculated as far as Fault 245. After crossing Fault 245, the TBM drilled the weathered granite with the result that water inflows increased. The largest volumes of water were found in the faults and in the porphyritic dikes. The high values of transmissivity in the faults accounted for the largest volume of water inflows. Higher inflow in dikes than in granite before Fault 245 may be ascribed to their relatively high transmissivity with respect to the granitic rock. Thereafter, the tunnel entered an area of more transmissive weathered granite, where the relative importance of faults and dikes is reduced.

Nevertheless, the geological structures may concentrate the flow or create a barrier effect, which could be attributed to a barrier-conduit behavior of the faults/dikes (Forster and Evans, 1991; Bredehoeft et al., 1992; Ferril et al., 2004; Bense and Person, 2006; Gleeson and Novakowski, 2009). However, it was not possible to verify this because of the scale of the model. Pumping of dewatering boreholes close to the tunnel diminished water inflows in these areas.

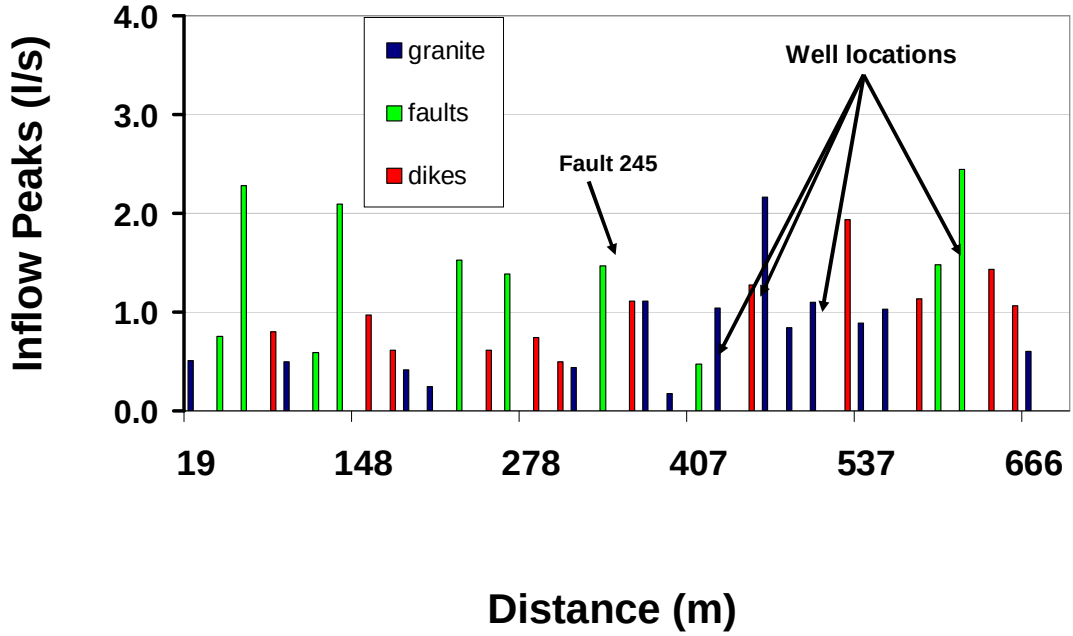

Figure 3– 9. Inflow peaks (L/s) in the 36 intervals of the modeled area. The X-axis shows the distance in meters from the first interval (north of the modeled area). The rock composition of the interval is also indicated, granite (blue), dikes (red) or fractures (green). The location of the dewatering wells is also shown.

3.6. Discussion and conclusions

The methodology presented in this paper enabled us to predict the location and the magnitude of the tunnel inflows (the main inflows are located in the faults and some dikes). Although the drawdown fit due to the TBM correlates well with the piezometers, the value of the modeled inflow was only compared qualitatively with the observations of the constructors.

The use of a numerical model allowed us to connect the geological structures crossed by the tunnel with the external boundary conditions. This connectivity may controls tunnel inflows. The connectivity with a large source of water can provide a considerable and continuous inflow (Stanfors et al., 1999), whereas the absence of this connectivity can bring about a marked drop in water inflow (Moon and Jeong, 2011).

Another important consideration is the determination of the tunnel boundary condition. The method of construction (open face TBM) determines the type of the boundary condition. Two issues were considered: 1) major inflows were concentrated at the face and the rock-machine contact because of the theoretical imperviousness of the tunnel due to the lining installation, which restricted the main entry of water to a "moving interval", and 2) the possibility of some residual seepage in the lining. These two considerations led us to adopt a variable leakage boundary condition in contrast to open tunnels (Molinero et al., 2002), where a transient state without restrictive leakage is applied. A restrictive leakage must be applied when the "moving window" crosses an area. This restrictive leakage represents the resistance of the interaction of the machine and tunnel face to the rock surface. The absence of this leakage would result in unrealistic drawdown and water inflow values. Figure 3– 10a shows a sensitivity analysis using a face-machine without leakage restriction. The fixed head boundary condition at the tunnel level was activated when the TBM reached each tunnel interval (the restrictive leakage remains active when the tunnel is lined). This results in a larger and more continuous drawdown and in unrealistic inflow peaks close to 20 L/s. Moreover, a small residual leakage partially accounts for the absence of a total recovery of the levels after the tunnel construction. The existence of the drained excavation of the Telescopi hole, which represents a decrease in 0.25 m in the regional head, does not wholly account for the decrease in heads. Figure 3– 10b displays a sensitivity analysis to the residual (late time) value of $f_i(t)$, which represents the percentage of diminishing factor leakage. The values with the best fit ranged between 0 and 0.03 %. The value of 0.01 % of this interval was used in the model. Acceptable lining inflow values, ranging between 0.08 and 0.2 L/s *100 m, were obtained for the $f_i(t)$ 0.01-0.03 % (Figure 3– 10c). The permeability of the lining obtained by this approach was 3.4 *10-5 m/d.

Finally, the methodology allows us to locate dewatering wells in the most pervious areas. Knowledge of the areas that have poor rock quality and that are most susceptible to water inflows enabled us to forestall hazards. This would entail dewatering and choosing the most suitable drilling system. Dewatering in tunneling is a controversial issue because it is feared that it may cause surface settlement. Actually, settlements may be due to drawdown caused by the inflows (Shin et al., 2002; Yoo, 2005) or to drawdown directly associated with dewatering (Cashman and Preene, 2002; Forth, 2004). We advocate dewatering in the most hazardous areas in order to prevent the sudden inflow that can drag materials in soft formations in the tunnel face (Barton, 2000). Dewatering usually has a short duration (implying that a small volume of soil is

affected). It is located in pervious materials that have low compressibility, giving rise to small hydraulic gradients and, in consequence, small differential settlements (Carrera and Vazquez-Suñé, 2008). This know-how was acquired in the previous kilometers of L9, where dewatering in the hazard zone of B-20 (after undertaking comprehensive research, Font-Capo et al., 2011) allowed tunneling without problems. The Fondo zone, however, constituted an expensive stoppage of the works owing to the lack a of a groundwater prediction in a hazardous area.

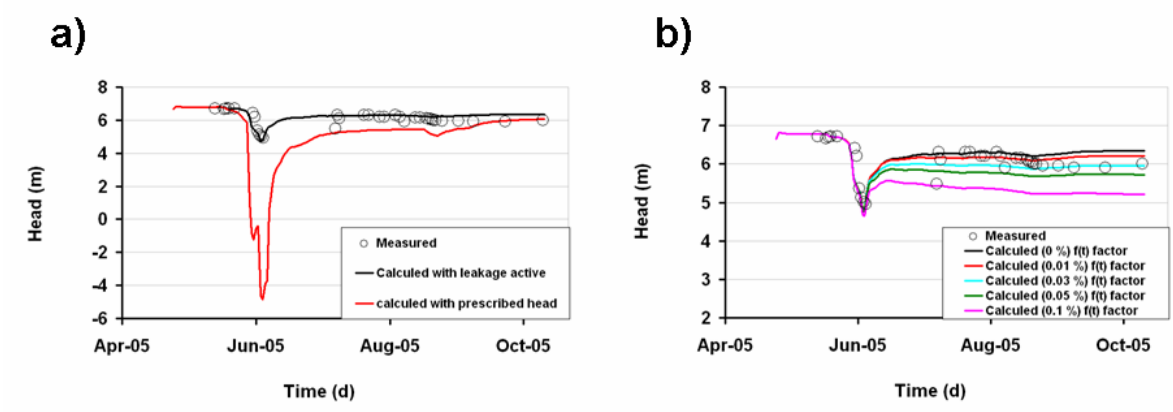

c)

% f(t)	Water inflow (L/s * 100m tunnel)
0	0
0.01	0.08
0.03	0.24
0.05	0.37
0.1	0.67

Figure 3– 10. a) Sensitivity of heads to face-machine boundary condition, ZPA-12 piezometer b) Sensitivity of heads to lining Boundary condition, ZPA-12 piezometer. c) Relationship between the percentage f(t) factors used in the sensitivity analysis with the water inflow (L/s) every 100 m of tunnel.

4. Barrier effect in lined tunnels excavated with Tunnel Boring Machine (TBM)

4.1. Introduction

Most of the underground infrastructures constructed in the metropolitan area of Barcelona in the last decade have been excavated below the water table. The present study arose from the hydrogeological survey during the construction of the subway line L-9 south of Barcelona in the Llobregat Delta (Figure 4– 1). The tunnel, which was excavated with a Tunnel Boring Machine (TBM), cuts a large section of the Llobregat Delta Shallow Aquifer. The potential hydrogeological impacts due to tunnel drainage, barrier effect or others should therefore be quantified.

Tunnel inflows could cause a piezometric drawdown (Cesano and Olofson, 1997; Marechal et al., 1999; Marechal and Etxeberri, 2003; Gargini et al., 2008; Kvaerner and Snilsberg, 2008; Vincenzi et al., 2008; Gisbert et al., 2009; Yang et al., 2009; Raposo et al., 2010). Moreover, tunnels with impermeable lining can be drilled to prevent water inflows that cause drawdowns. Impervious subsurface structures can create a barrier effect by partial or total reduction of the aquifer section (Vázquez-Suñé, et al., 2005, Carrera and Vazquez-Suñe, 2008), decreasing the effective transmissivity and connectivity. Barrier effect leads to an increase in groundwater head on the upgradient side of the tunnel, and to a symmetrical decrease on the downgradient side (Ricci et al., 2007).

Drawdowns caused by tunnel inflows or by barrier effect on the downgradient side could give rise to a number of problems, e.g. a) a settlement caused by the increase in the effective tension and the decrease in the water pressure when the groundwater head diminishes (Zangerl et al., 2003, 2008a, and 2008b; Olivella et al., 2008, Carrera and Vazquez-Suñe, 2008), b) drying of wells and springs (Marechal et al., 1999; Gargini et al., 2008; Vicenzi et al., 2008; Gisbert et al., 2009; Yang et al., 2009; Raposo et al., 2010) or drainage of wetlands (Kvaerner and Snilsberg, 2008), c) seawater intrusion into coastal aquifers and d) swelling due to gypsum precipitation in anhydrite

This chapter is based on the paper Font-Capo, J., Vazquez-Sune, E., Pujades, E., Carrera, J., Velasco, V., Montfort, D., Barrier effect in lined tunnels excavated with Tunnel Boring machine, submitted to Engineering Geology.

rock massifs (Butscher et al.,2011). Head increase on the upgradient side due to the barrier effect could lead to a) floods in surface and ground structures and soil salinization (Vazquez-Suñe et al., 2005; Carrera and Vazquez-Suñe, 2008), b) soil contaminant lixiviation due to piezometric cleaning (Navarro et al., 1992), and to c) changes in the groundwater flow regime that can mobilize contaminants (Chae et al., 2008; Epting et al., 2008).

It is possible to assess the impact caused by tunnel inflows on surface water (Gargini, et al., 2008; Vincenci et al., 2009) and groundwater (Attanayake and Waterman, 2006). Analytical (Bear et al., 1968; Custodio, 1983) and numerical methods (Molinero et al., 2003; Epting et al., 2009; Yang et al., 2009; Raposo et al., 2010; Font-Capó et al., 2011) can be used for inflow quantification. Numerical models (Bonomi and Belleni, 2003; Merrick and Jewell, 2003, Tubau et al., 2004 and Ricci et al., 2007) and also some analytical equations (Marinos and Kavvadas, 1997; Deveughele, et al., 2010 and Pujades et al., 2012) have been designed to quantify head variations in order to assess the barrier effect.

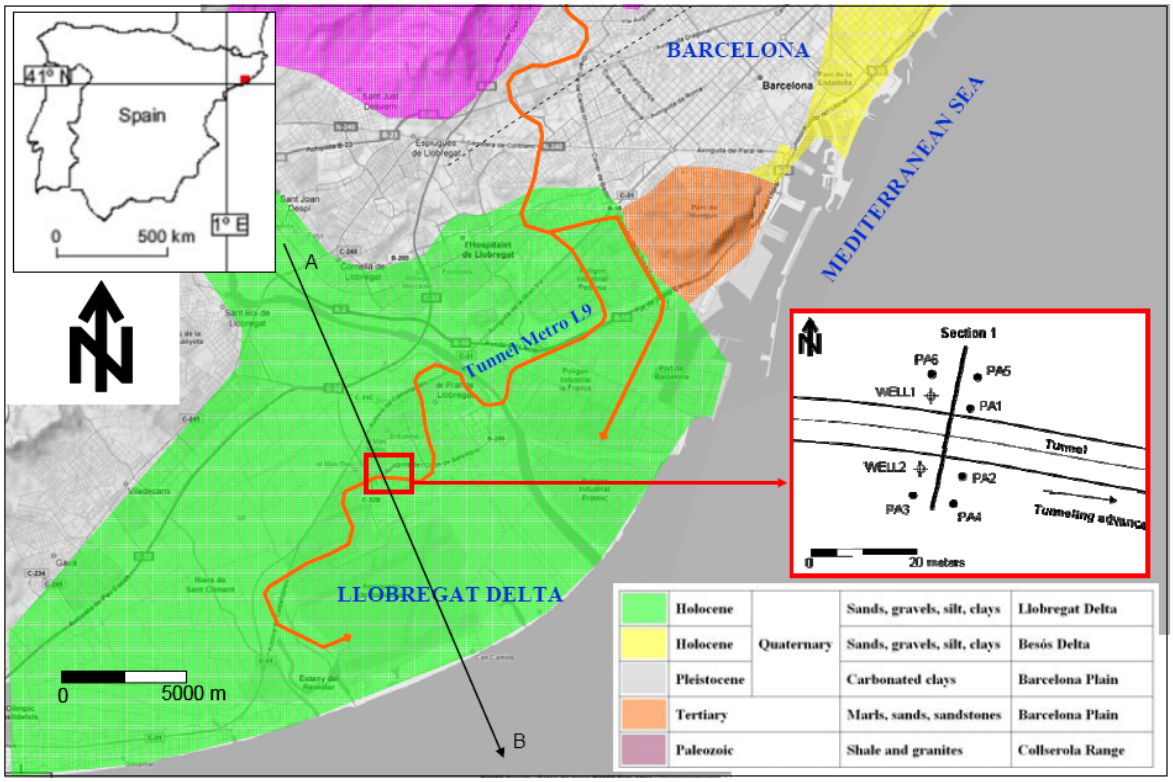

Figure 4– 1. Geographical and geological location of the site area.

The head variation produced by the barrier effect depends on the differences between the undisturbed hydraulic gradient and the hydraulic gradient once the tunnel has been constructed (Pujades et al., 2012). A higher gradient increases head variation and vice versa. Although connectivity and effective transmissivity are considerably reduced by the tunnel construction providing that the undisturbed hydraulic gradient is very low, the barrier effect will be very small. Consequently, the quantification of the head impact and the resulting corrective actions will be very limited.

The reduction in connectivity and effective transmissivity produced by the tunnel can be quantified by pumping tests before and after the construction of the tunnel. However, where the pumping wells are located near the tunnel, their performance (specific yield) may be reduced by the connectivity loss and reduction of the overall effective transmissivity.

This paper seeks 1) to quantify the impact of an impermeable tunnel constructed with the TBM on the steady state heads, and 2) to quantify the impact of the tunnel on the connectivity by using pumping tests.

4.2. Methods

4.2.1. Basic concepts

Pujades et al., (2012) define the barrier effect (S_B) as the increase in head loss along flow lines caused by the reduction in conductance associated with an underground construction. Therefore, the barrier effect (S_B) can be defined mathematically as

$$s_B = \Delta h_B - \Delta h_N \qquad \text{(Equation 4–1)}$$

Where Δh_B is the head drop across the barrier and Δh_N is the head drop between the same observation points in natural conditions (prior to construction). Its magnitude depends on the situation of the observation points with regard to the barrier. The maximum rise or drop of the head is measured close to the barrier further from the aperture. For this reason, local (S_{BL}) and regional (S_{BR}) barrier effects are distinguished. See Pujades et al., (2012) for details.

The use of analytical methods and numerical modeling enables the quantification of the tunnel barrier effect under permanent flow conditions. Numerical models can also be used to quantify the barrier effect (Deveughele et al., 2010; Pujades et al., 2012).

The use of a synthetic model allows us to determine the effect created by a tunnel on a homogeneous aquifer. A model of finite elements was constructed with the code VISUALTRANSIN (Medina and Carrera, 1996; GHS, 2003). We used a square model (2000 X 2000 m). A north-south natural flow was imposed with leakage boundary conditions on the northern and southern sides with the result that the gradient was 1/200. Transmissivity of $1 m^2/d$ and a storativity of 10^{-4} were used. A 10 m tunnel that separated the northern side from the southern side of the modeled domain was inserted (Figure 4– 2a). Two piezometers were placed 5 m apart on each side of the tunnel, PZ1 (downgradient side) and PZ2 (upgradient side, Figure 4– 2b). Different T effective (T_{eff}) values for the aquifer area occupied by the tunnel were used. This allowed us to simulate the partial occupation of the aquifer by the tunnel. T_{eff} values were 0.5, 0.1 and 0.01 m^2/d and were employed to achieve the transmissivity decrease due to aquifer obstruction.

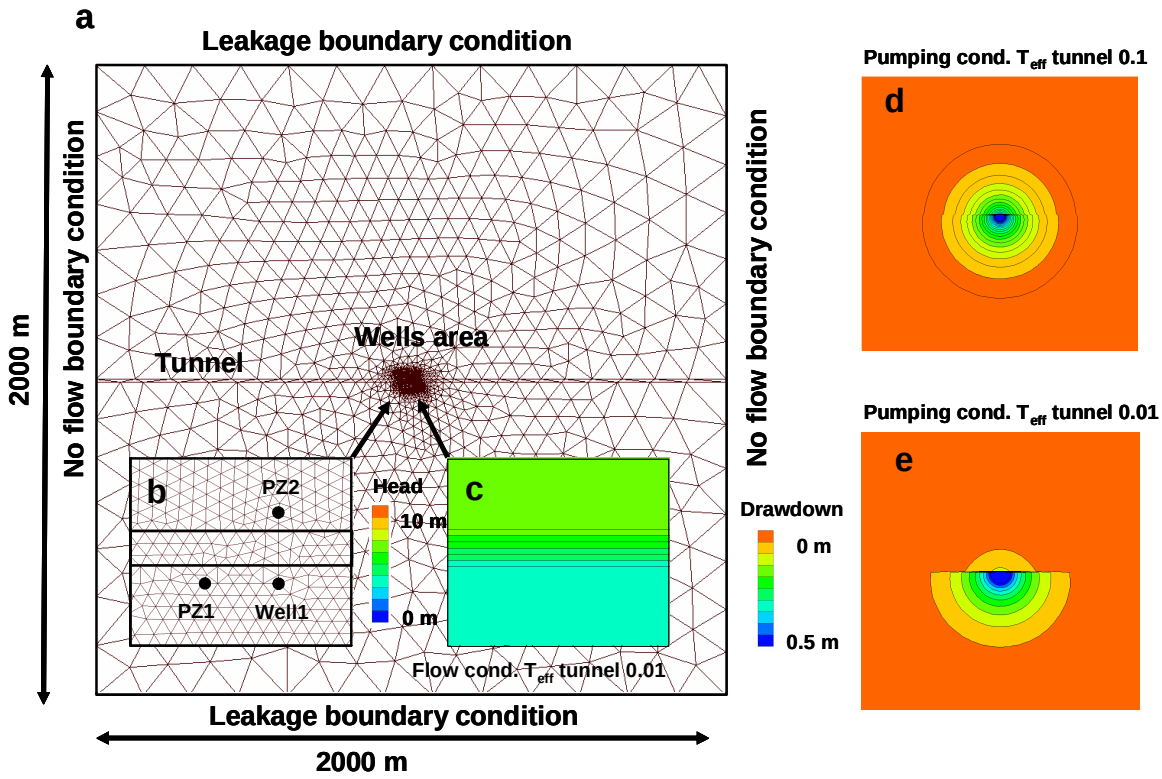

Figure 4– 2. a) Synthetic model mesh. b) Tunnel, well and piezometers details. c) Piezometric head around tunnel area (T_{eff} = 0.01). d) Drawdown around the tunnel (T_{eff}= 0.1). e) Drawdown around the tunnel (T_{eff}= 0.01).

Some simulations were made to assess the barrier effect on natural flow. The whole simulation period lasted 50 days and the tunnel effect was introduced into the model on the 10th day. Heads on the upgradient and downgradient sides of the tunnel show a symmetrical behavior (Figure 4– 3a). The barrier effect increases as T_{eff} decreases. There is an increase in the gradient in the tunnel area, especially when T_{eff} is low (Figure 4– 2c).

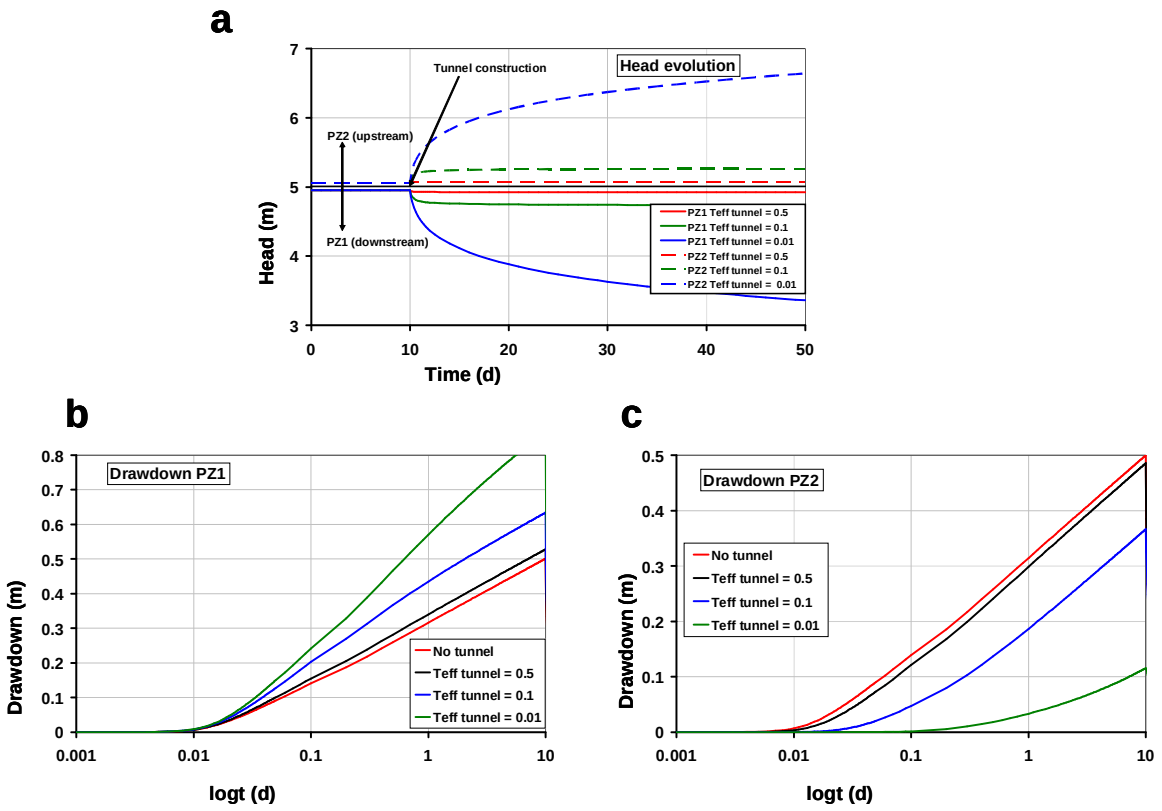

Figure 4– 3. a) Piezometric head in PZ1 and PZ2 for different T_{eff} possibilities. b) Drawdown in PZ1 for different T_{eff} possibilities. c) Drawdown in PZ2 for different T_{eff} possibilities.

Moreover, some simulations were made to assess the barrier effect on perturbed flow. Pumping tests before and after the tunneling were undertaken to evaluate the effect of the tunneling on the local connectivity. Comparison of the drawdown magnitude and the time response enabled us to quantify the connectivity variation. Pumping tests were simulated by numerical modeling in order to determine the local effect of the tunnel on groundwater connectivity. In our case, a pumping well was placed on the southern side of the tunnel at a distance of 5 m from it and 20 m from each piezometer (Figure 4– 2b) The well was used to simulate pumping with a volume rate of $1m^3/d$ for 10 days. As expected, the different behavior of the piezometer drawdowns depends on their relative position between the tunnel and the pumping well. Drawdown on the tunnel side where the pumping well was placed (PZ1) increases when T_{eff} decreases (Figure 4– 3b). On

the opposite side of the tunnel (PZ2) T_{eff} decreases, causing a drawdown reduction (PZ2) (Figure 4– 2d, Figure 4– 2e and Figure 4– 3c). The Drawdown response in time is also affected by T_{eff}. Lower values of T_{eff} create a delay in the drawdown response, leading to an increase in t_0 (Jacob equation), i.e. high values of t_0 and storativity indicate low connectivity between two points (Meier et al., 1998; Sanchez Vila et al., 1999).

4.2.2. Governing equations

Some authors propose analytical solutions to quantify the barrier effect (Carrera and Vazquez-Suñe, 2008; Lopez, 2009; Deveughele, et al., 2010). Pujades, et al., (2012) study the local and regional barrier effect on natural flow (not perturbed). They study the barrier effect in dimensionless form, S_{BLOD} and S_{BROD} respectively:

$$s_{BRD} = \frac{s_{BR}}{i_N b} = \begin{cases} 0 & if \quad b_{bD} \le 0.1 \\ \dfrac{2}{3\pi} \ln\left(\dfrac{1}{5\pi b_{bD} \left(1 - b_{bD}\right)^6} \right) & if \quad b_{bD} > 0.1 \end{cases} \qquad \text{(Equation 4–2)}$$

$$s_{BLD} = \frac{s_{BL}}{i_N b} = \begin{cases} 2b_{bD} & if \quad b_{bD} < 0.28 \\ \sqrt{\dfrac{3}{8}} \ln\left(\dfrac{2{b_{bD}}^{0.29}}{{b_{aD}}^2} \right) & if \quad b_{bD} \ge 0.28 \end{cases} \qquad \text{(Equation 4–3)}$$

Where i_N is the natural head gradient perpendicular to the barrier, b is the aquifer thickness and b_{bD} and b_{aD} are the dimensionless lengths of the barrier and the aperture, respectively. Assuming that b is the characteristic length, $b_b = b_{bD} i_N b$ and $b_a = b_{aD} i_N b$, where b_b and b_a are the lengths of the barrier and the aperture, respectively.

Moreover, the barrier effect caused by flux below the structure is given by the semipermeable barrier solution (Pujades et al., 2012)

$$S_{BID\,(L,L+L_B)} = \frac{S_{BI}}{i_N L_B} = \frac{b}{b_a} - 1 \qquad (Equation\ 4-4)$$

where S_{BID} is the dimensionless barrier effect generated below the barrier and L_B is the width of the barrier. This value, which may be negligible when $b>>L_B$, must be added to the barrier effect.

Note that the dimensionless barrier effect (Equations 4–2 and 4–3) only depends on the barrier geometry and on the natural gradient perpendicular to the barrier.

Pujades et al., (2012) describe the relationship between S_B, the aquifer effective permeability (k) and the reduction of the aquifer effective permeability considering the barrier (k_B) as

$$S_{BD} = \frac{S_B - i_N L_B}{i_N L_B} = \frac{k}{k_B} - 1 \qquad (Equation\ 4-5)$$

To compute S_B it is assumed that the flow through the aquifer remains unchanged. If local flow is perturbed by additional factors (i.e., recharge or pumping) S_B cannot be computed by these methods. When groundwater gradients are very low, the difference in the levels are small and may be subject to inaccuracies in the altimetry of piezometers, in measurements, and in head fluctuations due to natural or anthropogenic causes.

4.3. Application

The study area consists of a section of Line 9 of the Subway of Barcelona at El Prat del Llobregat (Figure 4– 1). The area was ideal for the application of our study. It is an area without surface infrastructures (i.e. it is easy to drill boreholes and carry out pumping tests). The geological and hydrogeological conditions were well known and there was sufficient time to drill boreholes and undertake pumping tests before tunneling.

The tunnel was drilled with a 9.4 m diameter Earth Pressure Balance (EPB) tunnel boring machine. This machine was adapted to drill in soft deltaic materials below the ground water level (Di Mariano et al., 2009). The tunnel was located at a depth of 15 m.

4.3.1. Geological Settings

The study area (Pilot Site) is located in El Prat de Llobregat which forms part of the metropolitan area of Barcelona (NE Spain) (Figure 4– 1). This is a very densely populated area located in the Llobregat Delta in the western Mediterranean. This Delta River is a quaternary formation and is considered to be a classic example of a Mediterranean Delta controlled by fluvial and coastal processes. It is a Holocene depositional system that was also active during the Pleistocene and rests unconformably on Paleozoic to Pliocene deposits (Gamez, 2007). The sedimentation of the Llobregat Delta was mainly controlled by glacio-eustatic sea level changes (Manzano et al., 1986; Gámez et al., 2009; Custodio, 2010). Earlier geological studies (Marques, 1984; Simó et al., 2005) considered the delta to have been formed by two detritical complexes: a Pleistocene Detritical Complex (Q3, Q2, and Q1 in Figure 4– 4) and a Holocene Upper Detritical Complex (Q4 in Figure 4– 4).

The Lower Detritical Complex consists of fluvial gravels interbedded with yellow and red clays and ranges between 10-100 m in thickness. This detritical complex contains 4 incisive fluvial systems separated by marginal marine strata and is associated with three paleodeltas currently located seawards of the present shoreline.

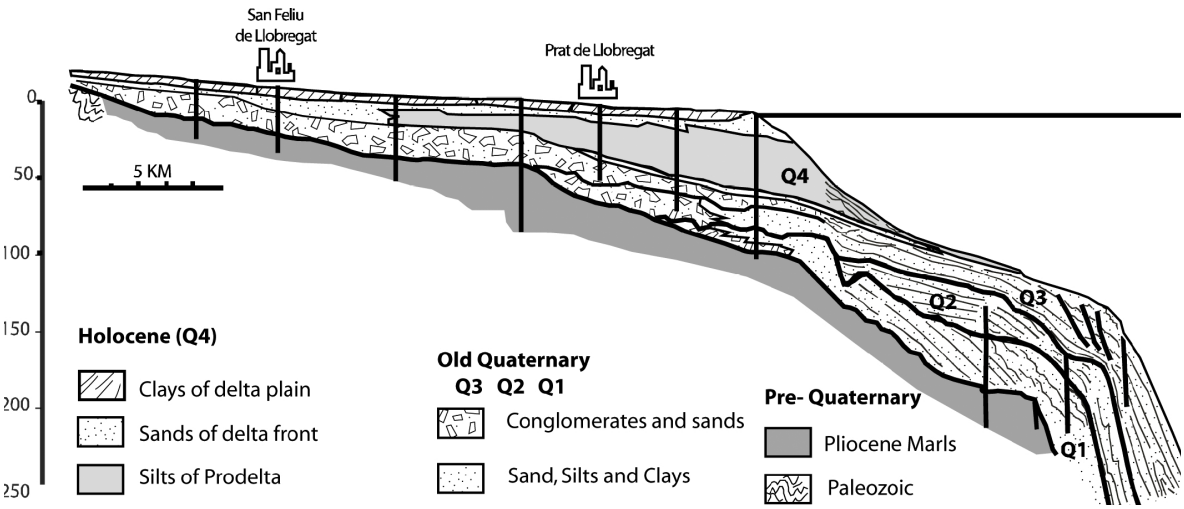

Figure 4– 4. General geological cross section (original from Gamez et al., 2005).

The Upper Detritical Complex consists of the typical stratigraphic delta sequence and is composed of four lithofacies, from bottom to top, transgressive sands, prodelta silts, delta front sands and silts and an uppermost unit made up of delta plain gravels and sands, floodplains fine sands, silts and red clay (Gamez, 2007).

Extensive geological investigations (Figure 4– 5) were performed in the study area. Geological core research (three pairs of piezometers with 15, 20 and 30 of depth, respectively), 2 logs (natural gamma) and surface geophysical measurements were undertaken.

The whole range of facies belts of the Holocene Deltaic Complex (subaerial to submarine) are identified and described:

- Delta Plain: this facies belt consists of grey and brown clay with intercalations of very fine sand and attains 2-3 meters in thickness.
- Delta Front: this is constituted by different lithofacies that grade from silty fine sands to coarser sand with intercalations of gravels in a silty matrix. It ranges from 14 to 15 m in thickness.
- Prodelta: this is made up of gray clays and silts with intercalations of fine sands and stretches of fine sand with intercalations of silt.

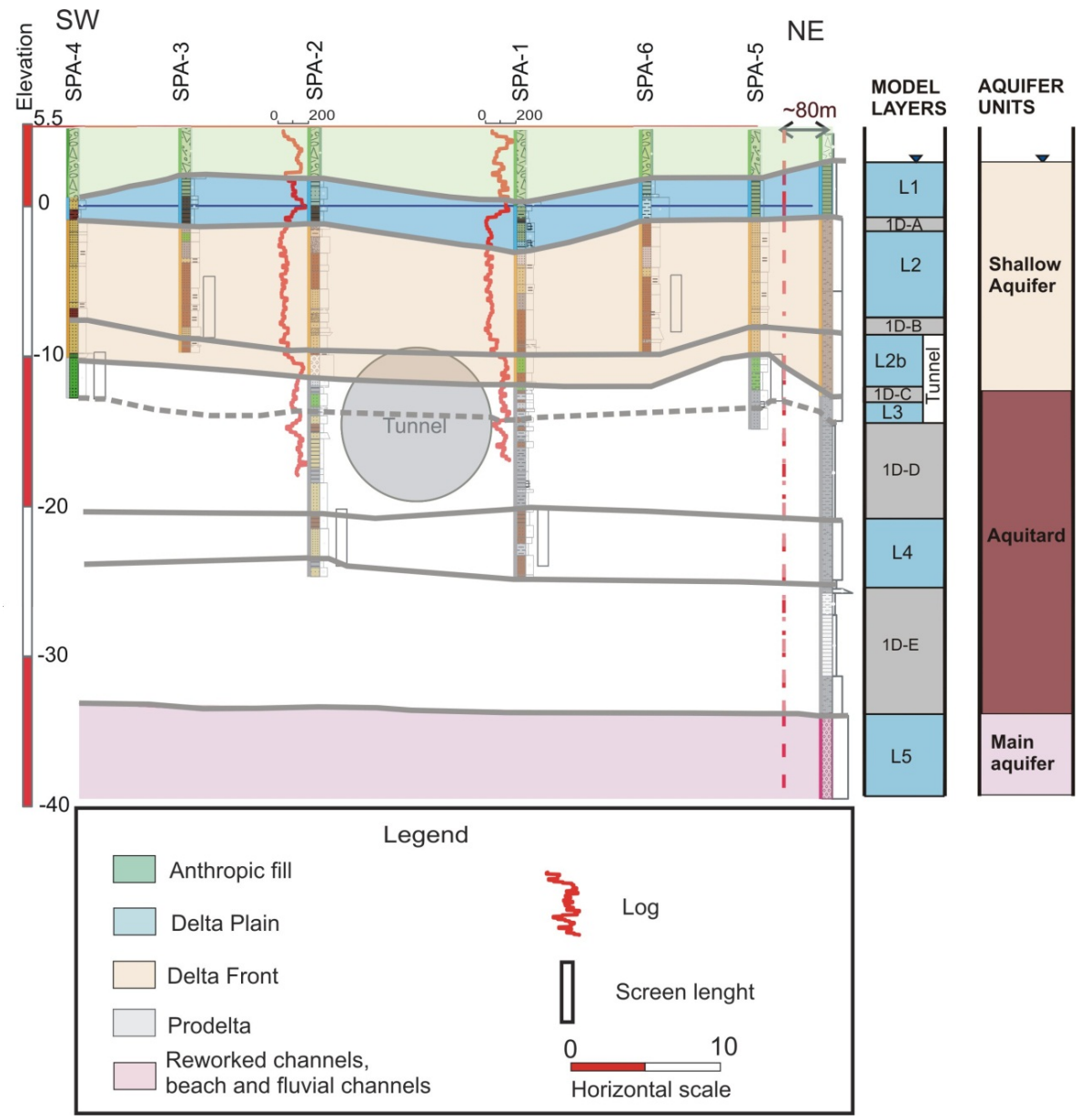

Figure 4– 5. Geological cross section of the site area. Geological description of the exploration boreholes and geophysical research are included.

Deeper boreholes near the pilot site and surface geophysical measurements were employed in the lower part of the prodelta, which is formed by deposits mainly composed of sands and gravels. This formation was interpreted as a reworking of alluvial deposits by marine processes in a beach setting and as beach deposits (Gamez et al., 2009).

4.3.2. Hydrogeological settings

The Llobregat Delta is formed by two main aquifers separated by an aquitard layer. The prodelta silts of Q4 act as a confining unit separating the impervious upper units (shallow aquifer) from the Main aquifer of the Llobregat delta. This aquifer is formed by a very thin and very permeable basin layer of reworked gravels and beach sands and the upper gravels of Q3. The aquifer is an essentially horizontal aquifer (about 100 km^2) and is 15–20 m thick. High transmissivity zones are associated with the paleochannel systems of Q3 (Abarca et al., 2006).

To this end, we differentiated between aquifer and aquitard units at the pilot site. Thus, the coarser deposits from the delta plain and the sediments from the delta front constitute an aquifer unit that corresponds to the shallowest aquifer in the delta complex. In addition, the finer deposits of the prodelta are less permeable and act as an aquitard, although thin grained layers may enhance the horizontal flow at a small scale. Finally, the sediments from the reworked channels, beach sands and fluvial channel constitute the main aquifer of the system.

Different piezometers were used in the quantification of the barrier effect. Piezometers were located at a different depths and each piezometer had its equivalent on the other side of the tunnel: top level (PA6 upgradient side and and PA3 downgradient side), intermediate or tunnel level (PA5 upgradient side and PA4 downgradient side), and bottom level (PA1 upgradient side and PA2 downgradient side). The screened intervals were located taking into account their relative position with respect to the tunnel. They were located in the upper part at the same level and the below the tunnel (Figure 4– 5). The upper piezometers (top level; PA3 and PA6) were screened between depths of 10 and 14 m correspond to the high permeability delta front materials. The tunnel level piezometers (PA4 and PA5) were screened between depths of 15 and 19 m that correspond to the delta front-prodelta limit, and finally the lower piezometers (PA1 and PA2) were screened between depths of 25 and 29 meters that correspond to the low permeability materials from the prodelta. The hydrogeological characterization included a slug test campaign to obtain punctual values of parameters of the tested levels. The piezometers were filled with water and the recovery to the initial level was measured manually and with pressure transducers. The interpretation was done with the Theis and Horner methods using the EPHEBO code (Carbonell et al., 1997). The permeability ranged between 0.2 and 4 m/d in the upper

piezometers (PA3 and PA6), between 0.06 and 0.1 m/d in the tunnel layer piezometers (PA4 and PA5) and finally the lower layer (PA1 and PA2) yielded a lower permeability value 0.04-0.05 m/d.

To complete the hydrogeological research two 30 m deep fully screened pumping wells were drilled (Figure 4– 1): pumping Well 1 was located on the northern side of the tunnel pathway (upgradient side) and pumping Well 2 was situated on the southern side (downgradient side) of the tunnel pathway.

Pumping Tests started at Well 1 and when the levels had almost recovered pumping commenced at Well 2. These two pumping tests were used to calculate the hydraulic parameters of the aquifer (Table 4– 1). The tests were repeated under the same conditions after tunneling to calculate the barrier effect. Drawdown response was measured with a dipper in all the piezometers and pumping wells and pressure data loggers were also used in the piezometers. The head variations were measured in a period of 105 days. This period included the four pumping tests and the tunneling. A double piezometer with two separate screen depths was instrumented. It was located 150 m from the wells area. The first screen was located in the Shallow Aquifer (15 m) and the second screen was placed at a depth of 60 m in the Main Aquifer of the Llobregat Delta to obtain the piezometric variations outside the testing area. The flow rates from pumping Wells 1 and 2 ranged between 3.5-4.5 L/s. These were measured both manually and automatically, using a calibrated barrel, and an axial turbine flow meter. Flow rate measurements are very similar by both methods.

4.4. Results

4.4.1. Barrier effect in natural flow

As discussed above, the permanent effect caused by the undrained tunnel implies an increase in heads on the upgradient side of the tunnel and a decrease in heads on the downgradient side of the tunnel. In the study area, the piezometric gradient variation due to tunneling was obtained with these pairs of piezometers.

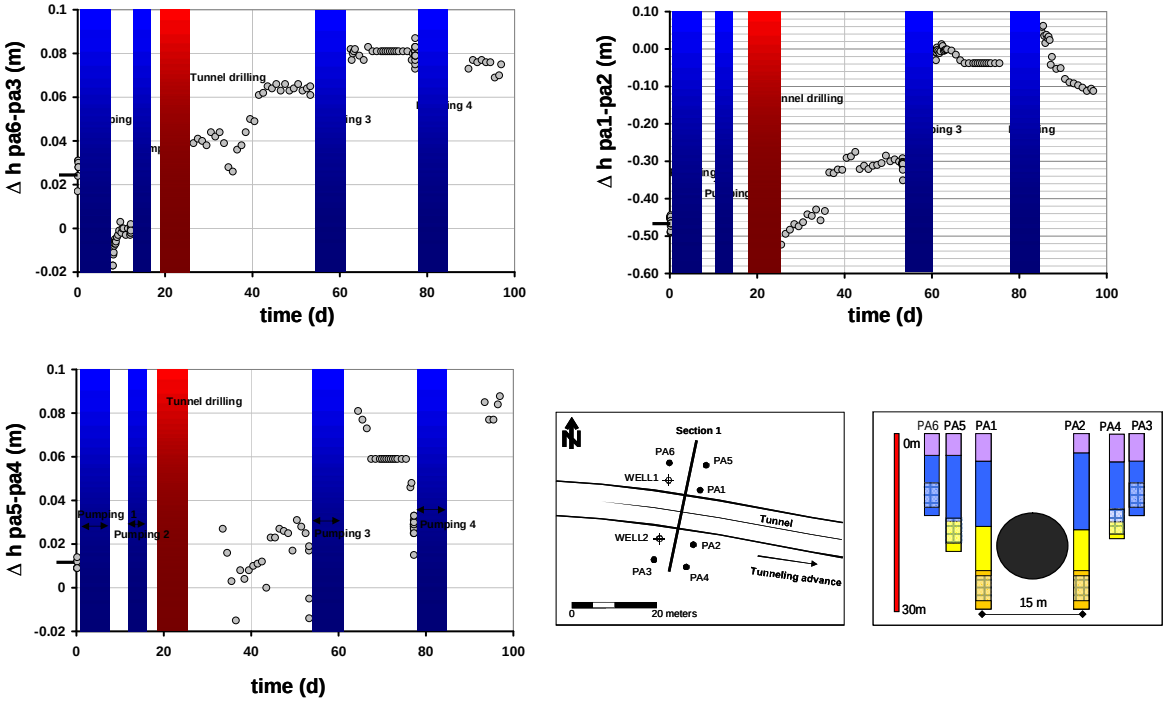

Figure 4– 6. Barrier effect, piezometric head variation between pairs of piezometers located in the three levels (top, tunnel and bottom).

The gradient variation between the different pairs of piezometers is shown in Figure 4– 6. The values during the pumping tests are not given because they do not represent the variation at steady state. After tunnel construction, a gradient variation of 5-6 cm was measured in the upper and tunnel level piezometers. The measured head variations show a great deal of noise due to natural variations (recharge by rain, etc.) or anthropogenic activities (pumping or nearby drainage works, etc.). Levels between piezometers cannot be compared with accuracy when the hydraulic gradient is very small. Furthermore, this variation was not immediate after tunneling. It was faster in the upper level than at tunnel level. A high variation in gradient heads can be observed in the lower level, but an inconsistent response is observed. The upgradient piezometer (PA1) had a lower initial piezometric head than the downgradient side (PA2).

The barrier effect was calculated by using the equations proposed in the basic concepts section. It is only possible to calculate the local barrier effect because the piezometers are close to the structure. Moreover, a long time is necessary to reach the steady state regional barrier effect.

The barrier effects between the barrier and the aquifer boundary (s_{BLO}) and below the barrier (s_{BI}) are calculated and added. Given that the barrier effect is produced in layers 2b to 3 of the model and given that the tunnel diameter is 10 meters, the lengths b, b_b and b_a are 14, 5 and 10 m, respectively $b_{bD} > 0.28$ and applying Equation (3), we obtain

$$S_{BLOD} = \sqrt{\frac{3}{8}} ln\left(\frac{2{b_{bD}}^{0.29}}{{b_{aD}}^{2}}\right) = 0.78$$

And applying Equation (4–4), we obtain

$$S_{BID} = \frac{b}{b_a} - 1 = 0.006$$

The characteristic length of the vertical barrier effect is the aquifer thickness (b), which must be corrected for anisotropy. Computing the anisotropy ratio (α= (kv/kh) 0.5) requires knowledge of the hydraulic conductivity distribution. k_V and k_H are calculated using the data of a pumping test, as the harmonic and arithmetic averages, respectively, of the hydraulic conductivities of the layers. i.e.

$$k_V = 1.75\frac{m}{d} \qquad \text{and} \qquad k_H = 5.16\frac{m}{d}$$

Then,

$$a = \sqrt{\frac{k_H}{k_V}} = 1.72$$

Thus

$$b_C = b \cdot a = 15m \cdot 1.72 = 25.8\, m$$

where b_C is the corrected thickness of the aquifer. Using i_N=0.001 which was obtained with the head observations measured at the piezometers before the tunnel construction

$$S_{BLO} = S_{BLOD}\, i_N\, b_C = 0.02m$$

Similarly, S_{BI} is obtained from S_{BID} as

$$S_{BI} = S_{BID} i_N L_B = 0.006 \text{ m}$$

and

$$S_{BL} = S_{BLO} + S_{BI} = 0.026\ m$$

This value is close to that of S_{BL} observed at the piezometers PA4 and PA5 as a result of the tunnel construction (Figure 4– 6). The presence of low hydraulic conductivity layers no identified would rise the anisotropy factor and the value of the local effect.

The tunnel is regarded as an area with a low hydraulic conductivity in the model. Therefore, the effective hydraulic conductivity is calculated to compare the results of the non-perturbed flow with the results obtained from the numerical model when the pumping tests are simulated. Given that the S_{BL} calculated is 0.085 m and applying equation 5

$$S_{BL} = \frac{k}{\frac{S_B - i_N L_B}{i_N L_B}} = 2.12\ m$$

This is the effective hydraulic conductivity of the area where the tunnel is constructed.

4.4.2. Barrier effect due to pumping test

Changes in the local connectivity (due to the construction of the tunnel that partially obstructed the aquifer) were studied using a series of pumping tests before and after tunneling. The tests enabled us to compare and quantify the drawdown variation and the connectivity reduction due to the tunnel construction.

As in the synthetic model discussed above, the presence of an “object” that partially obstructs the pathway between a pumping well and a piezometer can cause a decrease in the drawdown due to pumping. On the other hand, if the piezometer is located on the same side as the pumping well with respect to the obstacle, the drawdown could increase because the barrier acts as an impermeable boundary condition that diminishes the flow to the tested area.

An analysis of the drawdown before and after the tunnel excavation was performed. The response effect because of the distance between the pumping wells and the piezometers was eliminated by dividing the time by the square of the distance (Martínez-Landa and Carrera, 2005; Font-Capó et al., 2012). The drawdowns were also divided by the flow rate because the pumping test did not have a constant rate.

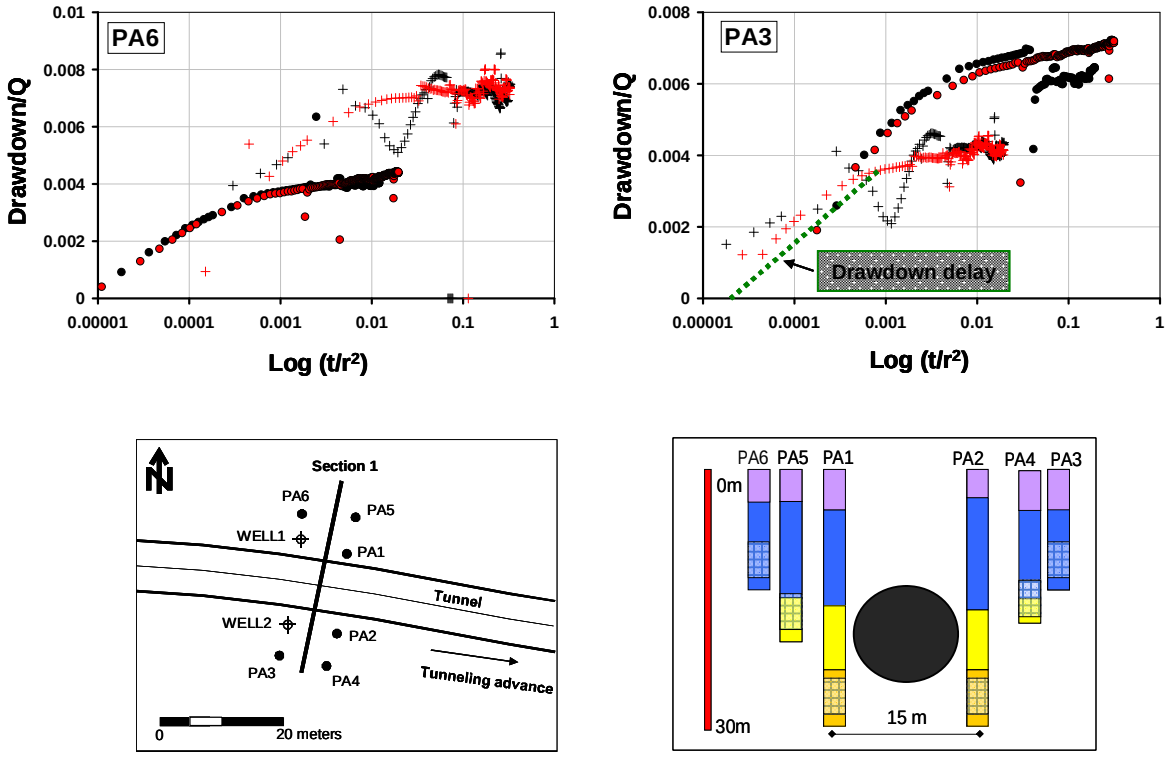

Figure 4– 7. Corrected drawdown (s/Q) versus corrected time (t/r^2) of the top piezometers. The four pumping tests are plotted, 2 pretunneling (black crosses for pumping 1 and black points for pumping 2) and 2 post tunneling tests (red crosses for pumping 3 and red points for pumping 4).

These data are plotted in Figure 4– 7, Figure 4– 8 and Figure 4– 9. Each piezometer is drawn separately and the four pumping tests are represented in each figure (the two pumping pre-tunnel tests and the two post-tunnel tests). The distance effect was not correctly eliminated when the piezometer was placed on the same side of the tunnel as the pumping well. This implied that the drawdown was too marked in these cases. The piezometers of the upper and tunnel levels behaved in a similar manner (Figure 4– 7; Figure 4– 8). The drawdown slope of these four piezometers decreased, which suggests the location of a recharge boundary or a more transmissive area 130-150 m above the well area.

The theoretical drawdown behavior due to tunnel interruption described in section 2 can only be observed in some cases. The drawdowns located on the same side of the pumping well behaved in a similar way after tunneling with respect to the drawdowns in the initial tests. The poor quality of the data on the drawdowns located on the same side of the tunnel as the pumping well does not allow us to observe variations after tunneling.

The drawdowns on the other side of the tunnel from the pumping well confirmed the theoretical behavior predicted in section 2. Drawdown after tunneling in the piezometers located at tunnel level (Figure 4– 8) shows an increase in drawdown with respect to the results obtained before tunneling. The drawdown variation was about 25% in terms of s/Q. The theoretical phenomena that would imply a delay in the drawdown response due to tunneling can be observed (section 2). The piezometers on the same level of the tunnel were located in more permeable layers that did not delay the response. A permanent effect in the drawdown was caused in the tunnel level piezometers because of aquifer obstruction. The vertical heterogeneity did not allow calculating the T_{eff}.of tunnel area using the average of drawdown reduction used in the synthetic model.

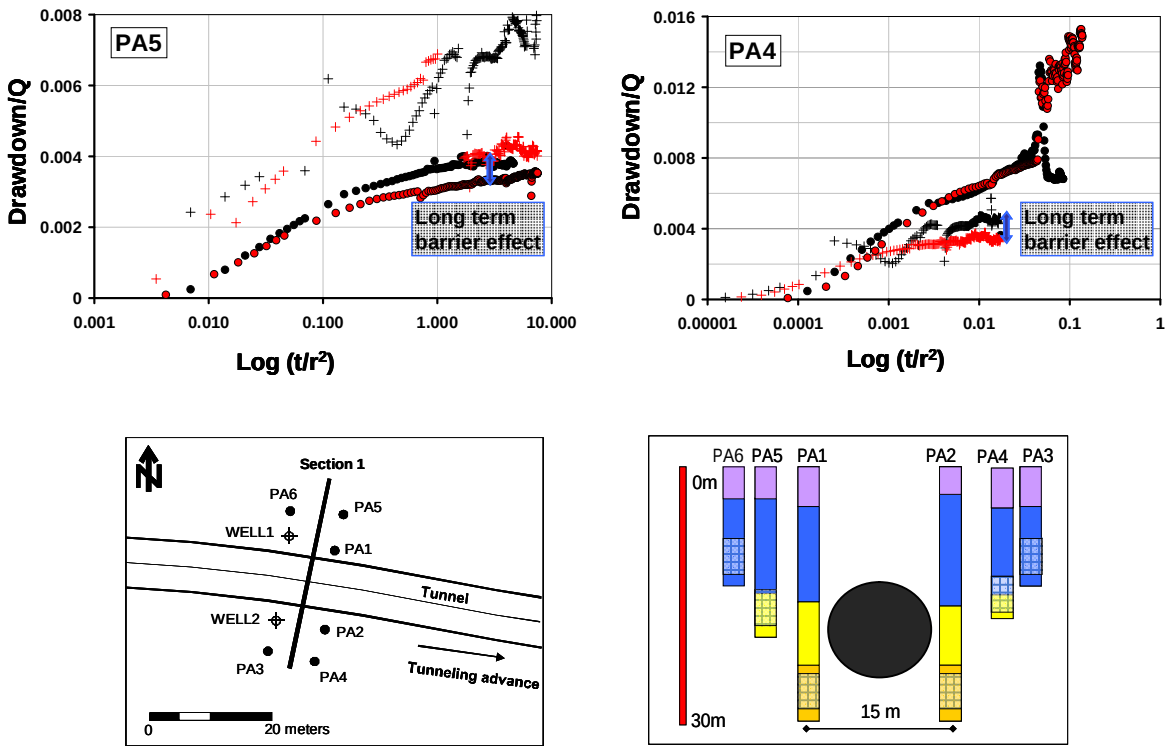

Figure 4– 8. Corrected drawdown (s/Q) versus corrected time (t/r^2) of the tunnel piezometers. The four pumping tests are plotted, 2 pretunneling (black crosses for pumping 1 and black points for pumping 2) and 2 post tunneling tests (red crosses for pumping 3 and red points for pumping 4).

The lower piezometers (PA1 and PA2, Figure 4– 9) and the upper piezometer PA3 (Figure 4– 7) registered a delay in the drawdown response after tunneling. The different response in the piezometers located on the other side of the tunnel from the pumping wells can be partially attributed to connectivity variations between the piezometers and the pumping well. Low piezometers PA1 and PA2 registered a delay after tunneling in pumping on the other side of the tunnel but recovered the drawdowns normally. These piezometers were located in low permeability formations under the tunnel layers. The fast response in the drawdowns can be attributed to drawdowns of the more permeable layers located under the piezometers. The connectivity between the low piezometers and the pumping well decreased when these layers were obstructed by the tunnel.

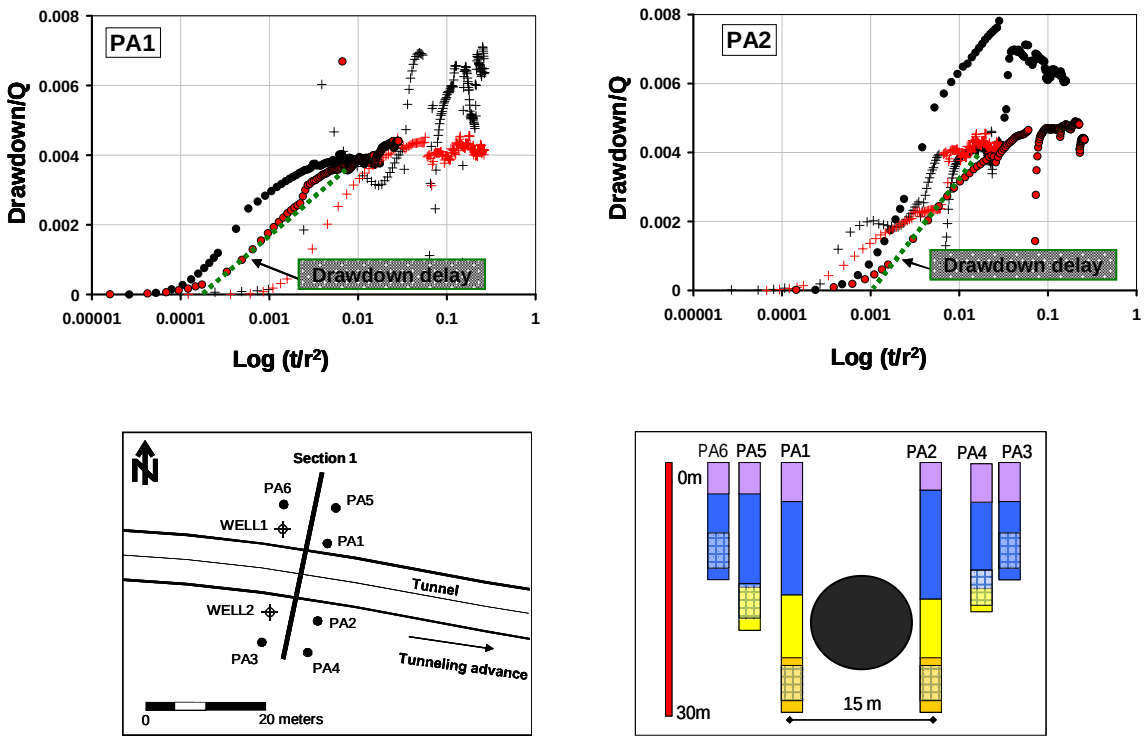

Figure 4– 9. Corrected drawdown (s/Q) versus corrected time (t/r^2) of the bottom piezometers. The four pumping tests are plotted, 2 pretunneling (black crosses for pumping 1 and black points for pumping 2) and 2 post tunneling tests (red crosses for pumping 3 and red points for pumping 4)

4.4.3. Modeling

The construction of a numerical model enabled us to calibrate the conceptual model and the hydraulical parameters with the two pumping tests before tunneling. Subsequently, the different response of the two post-tunneling pumping tests was simulated using the numerical model. The location of the tunnel geometry in the numerical model was tested as a methodology to forecast the response after tunneling.

The numerical model used was the finite elements code VISUALTRANSIN (Medina and Carrera, 1996; GHS, 2003). The model had different layers in order to be consistent with the conceptual model, and to correctly locate each piezometer at its real depth in the tunnel. The numerical model had 6 layers (five hydrogeological layers and an additional layer to correctly locate the tunnel) separated by 1 Dimension element layers (which only allow the vertical flow). The 1D elements allowed us to simulate the aquitards or the vertical permeability layers (Figure 4– 5). The different modeled layers are detailed below:

- Layer 1 (L1): This layer has a thickness of approximately 1.5 m. It is constituted by the coarser deposits from the Delta Plain (fine sand with some clay).
- Layer 2 (L2): This comprises the shallow aquifer which is formed mainly by the coarser fraction of the delta front (sand and intercalations of gravels). It is approximately 10.5 m thick. L2b is not a hydrogeological layer located under Layer 2, but corresponds to Layer 2 occupied by the tunnel.
- Layer 3 (L3): This consists of the finer part of the aforementioned delta front and is constituted by sand with intercalations of clay. This layer is 3 m thick and comprises the lower part of the shallow aquifer.
- Layer 4 (L4): This consists of the coarser part of the Prodelta and its permeability is very low.
- Layer 5 (L5): This is formed by the main aquifer of the deltaic complex of the Llobregat.
- Aquitard1 (1D-D): This aquitard separates layers 3 and 4. It is made up of the low permeability clay materials from the prodelta.
- Aquitard 2 (1-D-E): This aquitard consists of the low permeability aquitard from the Llobregat Delta.

The external boundary conditions of the model were located at 1000 m from the wells in order to minimize the influence of these boundaries. A 1/1000 gradient existed in the shallow aquifer in the pilot area. The gradient was achieved by locating a constant rate boundary condition on the northern side to simulate the water volume entrance. A prescribed head boundary condition was located on the southern side to simulate the water exit (Figure 4– 10). The vertical permeabilities of the 1D element areas were calibrated in order to obtain the vertical gradient. The real head of the shallow aquifer and the head of the Delta del Llobregat Aquifer (obtained using the head time function of the 60 m depth piezometer) were used in this calibration. Tunnel layout was implemented in its geographical position and its real depth (layers 2b and 3), and only was activated with the tunneling

The high permeability area detected previously in the drawdown study was regarded as a north-south high transmissivity area in the upper layer. The vertical gradient was reduced by the presence of fully penetrating wells that enhance the water flow because of gravel filter. These wells and their associated skin areas were also calibrated. The wells were introduced into the model as very small transmissive areas that connected all the layers (including the 1D layers) to simulate the pipe effect created by the wells.

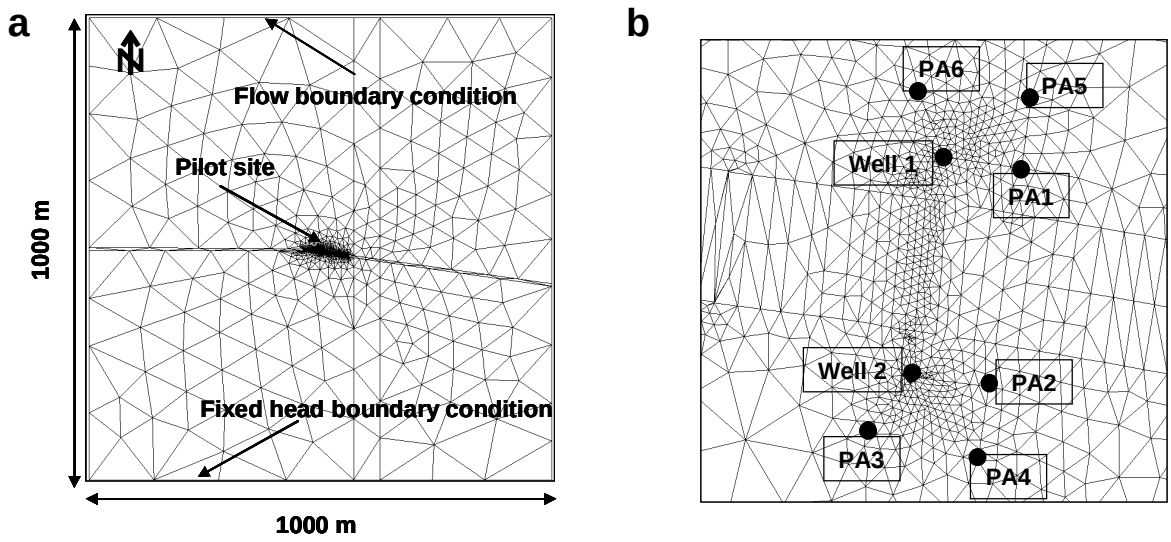

Figure 4– 10. a) Modeled area with the mesh finite elements and boundary conditions, b) Detail of pilot site.

4.4.4. Modeling results

The measured heads of the intermediate layers allowed us to correct the calibration of the vertical permeabilities. The calibration of the two first pumping tests (pre-tunnel conditions) enabled us to determine the permeability of detritic layers covered by the piezometer and the well stretches (Figure 4– 11) and (Table 4– 1). The effective transmissivity of the aquifer crossed by the tunnel is $80m^2/d$.

The barrier effect can be simulated after the calibration of the model. The simulation included two scenarios; 1) simulation after tunneling without the introduction of the tunnel layout into the model and 2) simulation after tunneling with the introduction of the tunnel layout into the model. The temporal series that included the tunneling and the repetition of the pumping tests were added to the model in the latter case.

Fits of scenario 1 in the upper piezometers (PA3 and PA6 in Figure 4– 12) did not show large differences between the pre and post tunneling periods. The tunnel layer piezometers (PA4 and PA5 in Figure 4– 12) show a bad fit in the simulation undertaken without the introduction of the tunnel into the model. The calculated head in piezometers located on the other side of the tunnel from the pumping well (pumping test 3 in PA4, and pumping test 4 in PA5) were lower than the observed head. On the other hand, the simulation in scenario 2 had a good fit. This simulation allowed us to reproduce the permanent tunnel impact caused by aquifer obstruction.

The lower piezometers show a puzzling behavior during tunneling (PA1 and PA2 in Figure 4– 12). The surface and intermediate piezometers increased in the head when the TBM was close to them, whereas the lower piezometers underwent a permanent decrease in the head after tunneling, recovering the initial low head that was changed by the pumping tests.

Table 4– 1. Hydraulic parameters of the model layers.

Layer	Permeability (m/d)	Storativity (1/m)
1	0.5	0.01
2	7.5	6*10-5
3	1.4	2*10-4
4	0.02	1*10-6
5	100	1*10-6
1D-1	0.0004	–
1D-2	0.01	–
1D-3	2*10-7	–
1D-4	2*10-7	–

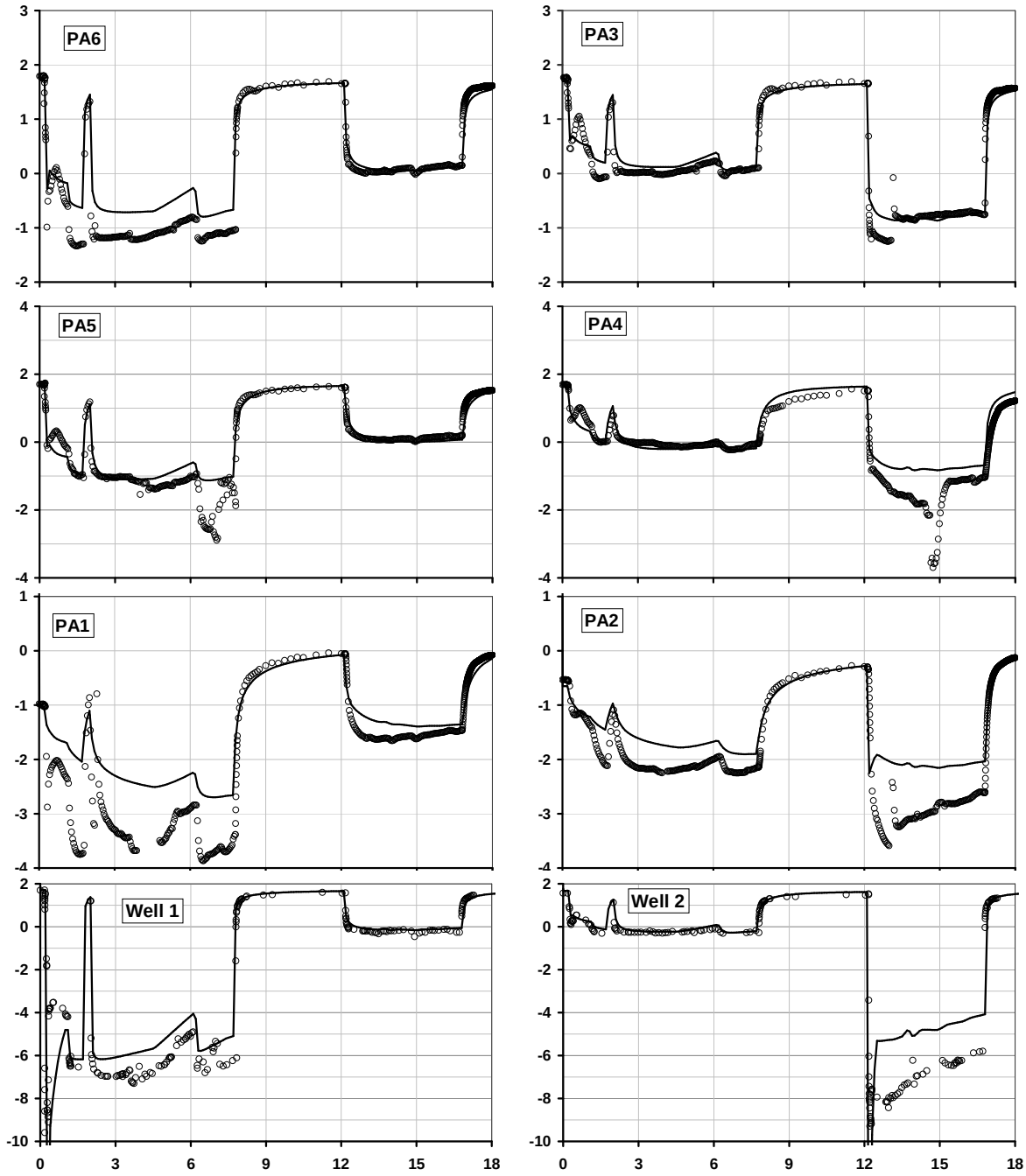

Figure 4– 11. Calibration heads in the two pretunneling pumping tests in wells and piezometers (reds points for the measured heads and red continuous line for calibrated heads).

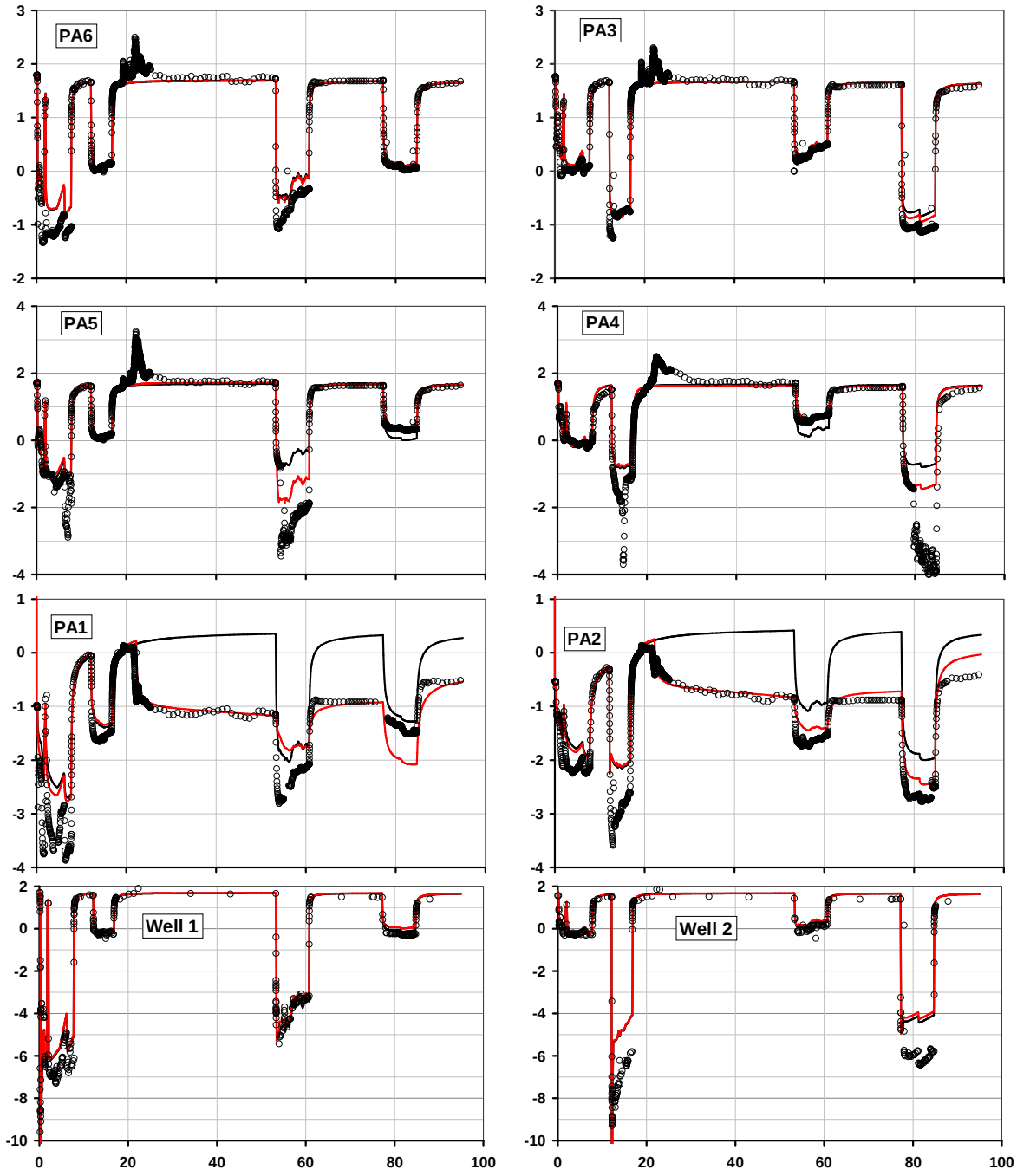

Figure 4– 12. Simulated heads of all pumping tests in wells and piezometers (reds points for measured heads and red continuous line for simulation without tunnel introduction, and Red continuous line for simulation with tunnel introduced into the model).

4.5. Discussion and Conclusions

Barrier effect of the lined tunneling under natural flow conditions can be forecasted by analytical methods. Results obtained with the equations (Pujades et al., 2012) in the Sant Cosme case were similar to the measured results. The value of the S_b is quite similar and the differences can be attributed at the very low value of the hydraulic gradient. When the gradients are very low the level difference is also small and therefore its value may be subject to errors due to inaccuracies in the piezometers references altimetry, in the making measurements, by head fluctuations by natural or anthropogenic causes. Analytical methods allowed us to determine the effective transmissivity of the portion of aquifer where the tunnel was located. The K_B effective calculated by the analytical methods is 2.12 m/d that results in a transmissivity of 29.7 m^2/d. This transmissivity value differs from the obtained with pumping tests 75 m^2/d before the pumping tests. This result implies a big reduction of the transmissivity of the aquifer where the tunnel is located, the new T_{eff} is a 40% of the initial transmissivity.

Pumping test in the tunnel area allowed study the barrier effect minimizing the gradient effect. The repetition of two pumping tests before and after the tunneling permitted to observe the different responses due to tunneling. Drawdown in the piezometers located on the same side of the tunnel as the pumping well do not permitted to observe drawdown effects associated to tunneling due to local perturbations. Drawdown differences can be observed in the piezometers located on the other side of the tunnel as the pumping well. The two theoretical behaviors (permanent drawdown decrease and response delay) described in section 2 can be observed. Permanent decrease drawdown due to tunneling (considering as permanent the period of the pumping test) can be observed in the piezometers located on the same depth of the tunnel. Delay response behavior is difficult to observe in the piezometers located in the aquifer affected by tunnel, elevate diffusivity of the formations avoided the delay. Piezometers located under the tunnel presented a small delay in the drawdown response in the post tunnel pumping event. The behavior can be attributed at their location in low permeable materials. The tunnel crossed high permeable materials located above these piezometers, these formations can transmit easily the drawdown and its interruption created a small delay in post-tunnel drawdown. Pumping test enabled us to detect the layers affected by the barrier effect created by the tunnel.

Numerical model enabled us simulate the groundwater changes due to the tunneling. The tunnel introduction into the model allowed simulating the barrier effect taking into account the hydrogeological heterogeneity. The introduction the tunnel into the model enabled us to compare the groundwater changes due to tunneling. The S_b value under permanent conditions is very low in Sant Cosme and it is difficult to calculate with numerical methods due to the low gradient of the aquifer. The use of pumping tests enabled us to calculate the permanent drawdown and the connectivity changes due to tunneling. The drawdown effect due to tunneling can be modeled by the introduction of the tunnel into the numerical model. The use of numerical methods allowed us to confirm the validity of the use of the pumping test for the determination of the barrier effect.

Numerical methods may be useful methods to forecast the barrier effect under natural flow and the barrier effect in the connectivity (changes in drawdown responses due to tunneling). The difficulty to calculate the barrier effect under natural flow can be solved by using numerical methods where the horizontal and vertical heterogeneity can be introduced correctly.

5. Conclusions

Chapter 5 includes the main contributions of this thesis. The major findings respond to the main aim of gaining a better understanding of the relationships of groundwater and tunnels excavated with a TBM. This concerns the problems arising from groundwater in the tunnel excavation (Inflows), and the impact of tunneling on groundwater flow.

Our methodology allowed us to forecast the main areas where tunneling may encounter problems due to groundwater. Exhaustive geological and hydrogeological studies (including pumping tests) were necessary to develop the conceptual model. Discrete numerical modeling enabled us to consider the connectivity with the rest of the massif and the hydraulic behavior of fractures and geological units (conduit or barrier), which was instrumental in defining the tunneling method and other excavation works (dewatering…).

In order to include the tunnel in the model (conceptual and numerical), it is necessary to specify the problems of construction due to groundwater and the tunneling impact. Tunnels excavated with a TBM usually focus on construction problems at the tunnel face. Analytical methods cannot detect inflows into the tunnel face in shallow tunnels where boundary conditions can be very close to the tunnel. The possibility that the machine offers resistance to the entry of water also invalidates this method. The introduction of the tunnel into the model in real time activated a tunnel boundary condition that simulated the tunnel-face water restriction as leakage. Leakage disappeared when the tunnel was completely impermeable, but some seepage occurred in the tunnel and consequently some residual leakage had to be applied to the model. As a result, inflows at the tunnel face can be correctly calculated.

Drainage which is the most common impact due to tunnel inflows, is minimized in TBM tunnels, which have impermeable lining and hence restrict the inflows to the tunnel face. The barrier effect is the main impact produced by lined tunnels. Impacts under permanent conditions can be calculated by analytical methods or by numerical modeling. Furthermore, connectivity variations

due to tunneling using pumping tests also enabled us to determine the barrier effect under other conditions. The barrier effect is very sensitive to aquifer obstruction due to tunneling and the hydraulic gradient. In addition, vertical anisotropy and the degree heterogeneity have been shown to have adverse consequences for the barrier effect determination. The use of the pumping tests allowed us to determine the barrier effect more effectively than the analytical methods and better locate which portions of the aquifer are more affected by the tunnel.

6. References

Abarca, E., Vazquez-Sune, E., Carrera, J., Capino, B., Gamez, D., Batlle, F., 2006. Optimal design of measures to correct seawater intrusion. Water Resources Research 42 (9).

Anderson, E. I, Bakker, M., 2008. Groundwater flow through anisotropic fault zones in multiaquifer systems. Water Resources Research 44 (11).

Attanayake, P.M., Waterman, M. K., 2006. Identifying environmental impacts of underground construction Hydrogeology Journal 14 (7), 1160-1170.

Babendererde, S., Hoek, E., Marinos, P., Cardoso, A.S., 2004. Geological risk in the use of TBMs in heterogeneous rock masses – The case of "Metro do Porto" and the measures adopted. Presented at the Course on Geotechnical Risks in Rock Tunnels, University of Aveiro, Portugal.

Babiker, M., Gudmundsson, A., 2004. The effects of dykes and faults on groundwater flow in an arid land: the Red Sea Hills, Sudan. Journal of Hydrology 297 (1-4), 256-273.

Banks, D., Rohr-Torp, E., Skarphagen, H., 1994. Groundwater resources in hard rock; Experiences from the Hyvaler study, southeastern Norway. Applied Hydrogeolgy 2/94.

Banks, D., Solbjorg, M., Rohrtorp, E., 1992. Permeability of fracture-zones in a precambrian granite. Quarterly Journal of Engineering Geology 25 (4), 377-388.

Barton, N., 2000. TBM tunnelling in jointed and faulted rock. Rotterdam. Brookfield, VT: Balkema, cop.

Benedek, K., Bothi, Z., Mezo., G., Molnar, P., 2009. Compartmented flow at the Bataapati site in Hungary. Hydrogeology Journal 17(5), 1219-1232.

Bense, V., Van Balen, R., 2004. The effect of fault relay and clay smearing on groundwater flow patterns in the lower Rhine Embayment. Basin Research 16 (3), 397-411.

Bense, V., Van Balen, R., & de Vries, J., 2003. The impact of faults on the hydrogeological conditions in the Roer Valley rift system: an overview. Netherlands Journal of Geosciences-Geologie en Mijnbouw 82 (1), 41-54.

Bense, V., Person, M., 2006. Faults as conduit-barrier systems to fluid flow in siliciclastic sedimentary aquifers. Water Resources Research 42 (5).

Berg, S., Skar, T., 2005. Controls on damage zone asymmetry of a normal fault zone: outcrop analyses of a segment of the Moab fault, SE Utah. Journal of Structural Geology 27 (10), 1803-1822.

Bonomi, T., Bellini, R., 2003. The tunnel impact on the groundwater level in an urban area: a modelling approach to forecast it. Materials and Geoenvironment 50, 45-48.

Bredehoeft, J., Belitz, K., Sharphansen, S., 1992. The hydrodynamics of the big horn basin - a study of the role of faults. AAPG Bulletin-American Association of Petroleum Geologists 76(4), 530-546.

Bruhn, R., Parry, W., Yonkee, W., Thompson, T., 1994. Fracturing and hydrothermal alteration in normal-fault zones. Pure and Applied Geophysics 142 (3-4), 609-644.

Butscher, C., Huggenberger, P.., Zechner, E., 2011. Impact of tunneling on regional groundwater flow and implications for swelling of clay-sulfate rocks. Engineering Geology 117 (3-4), 198-206.

Cabrera, L., Roca, E., Garcés, M., de Porta, J., 2004. Estratigrafía y evolución tectonosedimentaria oligocena superior-neógena del sector central del margen catalán Cadena Costero-Catalana , in J. A. Vera, ed., Geología de España: Sociedad Geológica de España. Instituto Geológico y Minero de España 569–573.

Caine, J., Evans, J., Forster, C., 1996. Fault zone architecture and permeability structure. Geology 24 (11), 1025-1028.

Caine, J., Forster, C., 1999. Fault zone architecture and fluid flow: Insights from field data and numerical modeling, in Mozley P.S. Moore J.C. in Haneberg, W.C. Goodwin, L.B. ed.,'faults and subsurface fluid flow in the shallow crust. American Geophysical Union geophysical monograph 101-127.

Caine, J., Tomusiak, S., 2003. Brittle structures and their role in controlling porosity and permeability in a complex Precambrian crystalline-rock aquifer system in the Colorado Rocky Mountain Front Range. Geological Society of America 115 (11), 1410-1424.

Carrera, J., Vázquez-Suñé, E., Font-Capó, J., Jordan, J., 2004. Ensayo de bombeo en Fondo, L9. UPC. Department of Geotechnical Engineering & Geosciences. Internal Report.

Carrera, J., Vazquez-Suñe, E., 2009. Sobre la interacción entre acuíferos y aguas subterráneas. AIH-GE (ed.) Proceedings: Jornadas sobre el agua y las infraestructuras en el medio subterráneo.

Carbonell, J.A, Pérez-Paricio, A., Carrera, J., 1997. MARIAJ-IV: Programa de calibración automática de ensayos de bombeo. Modelos analíticos y numéricos. ETSECCPB, UPC, Barcelona.

Chae, G.-T., Yun, S.-T., Choi, B.-Y., Yu, S.-Y., Jo, H.-Y., Mayer, B., Kim, Y.-J., Lee, J.-Y., 2008. Hydrochemistry of urban groundwater, Seoul, Korea: The impact of subway tunnels on groundwater quality. Journal of Contaminant Hydrology 101 (1-4), 42-52.

Cembrano, J., Gonzalez, G., Arancibia, G., Ahumada, I., Olivares, V.,Herrera, V., 2005. Fault zone development and strain partitioning in an extensional strike-slip duplex: A case study from the Mesozoic Atacama fault system, Northern Chile. Tectonophysics 400 (1-4), 105-125.

Cashman, P., Preene, M., 2002. Groundwater Lowering in Construction a practical guide. Spon Press, London and New York.

Cesano, D., Olofsson, B., 1997. Impact on groundwater level when tunnelling in urban areas Conference: XXVII International-Association-of-Hydrogeologists Congress E Midlands Conf

ctr, Nottingham, England, Groundwater in the Urban Environment - vol I: Problems, processes and management 219-224.

Cesano, D., Olofsson, B., Bagtzoglou, C., 2000. Parameters Regulating Groundwater Inflows into Hard Rock Tunnels-a Statistical Study of the Bolmen Tunnel in Sothern Sweden. Tunneling and Underground Space Technology 15 (2), 153-165.

Cesano, D., .Amvrossios, C., Bagtzoglou, C., Olofsson. B., 2003. Quantifying fractured rock hydraulic heterogeneity and groundwater inflow prediction in underground excavations: the heterogeneity index. Tunneling and Underground Space Technology 18 (1), 19-34.

Chester, F., Logan, J., 1986. Implications for mechanical-properties of brittle faults from observations of the punchbowl fault zone, California. Pure and Applied Geophysics 124 (1-2), 79-106.

Chester, F., Evans, J., Biegel, R., 1993. Internal structure and weakening mechanisms of the san-andreas fault. Journal Of Geophysical Research-Solid Earth 98 (B1), 771-786.

Chisyaki, T, 1984. A study on confined flow of groundwater through a tunnel. Ground Water 22 (2), 162-167.

Cook, J.E., Dunne, W.M., Onasch, C.A., 2006. Development of a dilatant damage zone along a thrust relay in a low-porosity quartz arenite. Journal Of Structural Geology 28 (5), 776-792.

Custodio, E., 2010. Coastal aquifers of Europe: an overview. Hydrogeology Journal 18 (1) 269-280.

Dalgic, S, 2003. Tunneling in fault zones, Tuzla tunnel, Turkey. Tunnelling and Underground Space Technology 18 (5), 453-465.

Day, M.J, 2004. Karstic problems in the construction of Milwaukee's Deep Tunnels. Environmental Geology 45 (6), 859-863.

Day-Lewis, F., Hsieh, P., Gorelick, S., 2000. Identifying fracture-zone geometry using simulated annealing and hydraulic-connection data. Water Resources Research 36 (7), 1707-1721.

Denny, S.C., Allen, D. M., Journeay, J. M., 2007. DRASTIC-FM: a modified vulnerability mapping method for structurally controlled aquifers in the southern gulf Islands, British Columbia, Canada. Hydrogeology Journal 15(3), 483-493.

Deva, Y, Dayal, H.M, Mehrotra, A., 1994. Artesian blowout in a TBM driven water conductor tunnel in Nortwest Himalaya, India. In Oliveira et al. (eds), Proc 7th IAEG congress Lisbon. Rotterdam, Balkelma 4347-4354.

Deveughele, M., Zokimila, P., Cojean, R., 2010. Impact of an impervious shallow gallery on groundwater flow. Bulletin of Engineering Geology and the Environment 69 (1), 143-152.

Di Mariano A., Persio, R., Gens, A., Castellanza, R., Arroyo, M., 2009. Influence of some EPB Operation Parameters on Ground Movements. 2nd International conference on computational methods in tunnelling. Ruhr University Bochum 2009, 43-50.

El Tani, M., 2003. Circular tunnel in a semi-infinite aquifer. Tunnelling and Underground Space Technology 18 (1), 49-55.

Epting, J., Huggenberger, P., Rauber, M., 2008. Integrated methods and scenario development for urban groundwater management and protection during tunnel road construction: a case

study of urban hydrogeology in the city of Basel, Switzerland. Hydrogeology Journal 16 (3), 575-591.

Evans, J., 1988. Deformation mechanisms in granitic-rocks at shallow crustal levels. Journal of Structural Geology 10 (5), 437-443.

Evans, J., Chester, F., 1995. Fluid-rock interaction in faults of the San-Andreas system - inferences from San-Gabriel fault rock geochemistry and microstructures. Journal Of Geophysical Research-Solid Earth 100 (B7), 13007-13020.

Evans, J., Forster, C., Goddard, J., 1997. Permeability of fault-related rocks and implications for hydraulic structure of fault zones. Journal of Structural Geology 19 (11), 1393-1404.

Ferrill, D., Sims, D., waiting, D., Morris, A., Franklin, N., Schultz, A., 2004. Structural framework of the Edwards aquifer recharge zone in south-central Texas. Geological Society of America Bulletin 116 (3-4), 407-418.

Faulkner, D., Lewis, A., Rutter, E., 2003. On the internal structure and mechanics of large strike-slip fault zones: field observations of the Carboneras fault in southeastem Spain. Tectonophysics 367 (3-4), 235-251.

Faulkner, D., Rutter, E., 2001. Can the maintenance of overpressured fluids in large strike-slip fault zones explain their apparent weakness?. Geology 29 (6), 503-506.

Faulkner, D.R., Jackson, C.A.L., Lunn, R.J., Schlische, R.W., Shipton, Z.K., Wibberley, C.A.J., Withjack, M.O., 2010. A review of recent developments concerning the structure, mechanics and fluid flow properties of fault zones. Journal of Structural Geology 32 (11), 1557-1575.

Flint, A., Flint, L., Kwicklis, E., Bodvarsson, G., Fabryka-Martin, J., 2001. Hydrology of Yucca Mountain, Nevada, Reviews of Geophysics 39 (4), 447-470.

Folch, A., Mas-Pla, J., 2008. Hydrogeological interactions between fault zones and alluvial aquifers in regional flow systems. Hydrological Processes 22 (17), 3476-3487.

Font-Capo, J., Vazquez-Sune, E., Carrera, J., Marti, D.; Carbonell, R., Perez-Estaun, A., 2011. Groundwater inflow prediction in urban tunneling with a tunnel boring machine (TBM). Engineering Geology 121, 46-54.

Font-Capo, J., Vazquez-Suñe, E., Carrera., Herms, I., 2012. Groundwater characterization of a heteorogeneous granitic rock massif for shallow tunnelling. Geologica Acta, published online. DOI: 10.1344/105.000001773

Forster, C., Evans, J., 1991. Hydrogeology of thrust faults and crystalline thrust sheets - results of combined field and modeling studies. Geophysical Research Letters 18 (5), 979-982.

Forth, R., 2004. Groundwater and geotechnical aspects of deep excavations in Hong Kong. Engineering Geology 72 (3-4), 253-260.

Gamez, D., 2007. Sequence Stratigraphy as a tool forwater resources management in alluvial coastal aquifers: application to the Llobregat delta (Barcelona, Spain). Ph'D Thesis, Technical University of Catalonia, Barcelona, 177. (http://www.tdx.cesca.es/).

Gamez, D., Simo, J.A., Lobo, F.J., Barnolas, A., Carrera, J. Vazquez-Sune, E., 2009. Onshore-offshore correlation of the Llobregat deltaic system, Spain: Development of deltaic

geometries under different relative sea-level and growth fault influences. Sedimentary Geology 217 (1-4), 65-84.

Gargini, A., Vincenzi, V., Piccinini, L., Zuppi, G.M., Canuti, P., 2008. Groundwater flow systems in turbidites of the Northern Apennines (Italy): natural discharge and high speed railway tunnel drainage. Hydrogeology Journal 16 (8), 1577-1599.

Gisbert J., Vallejos A., Gonzalez A., Pulido-Bosch, A., 2009. Environmental and hydrogeological problems in karstic terrains crossed by tunnels: a case study. Environmental Geology 58 (2), 347-357.

Gleeson, T., Novakowski, K., 2009. Identifying watershed-scale barriers to groundwater flow: lineaments in the canadian shield. Geological Society of America Bulletin 121 (3-4), 333-347.

Goddard, J., Evans, J., 1995. Chemical-changes and fluid-rock interaction in faults of crystalline thrust sheets, northwestern Wyoming, USA. Journal of Structural Geology 17 (4), 533-547.

Goodman, R.F., Moye, D.G, Van Schaikwyk, A., Javandel, I., 1965. Groundwater inflows during tunnel driving. Bulletin of International Association of Engineering Geologists 2 (1), 39–56.

Grupo de Hidrología Subterránea (GHS). 2003. Visual Transin Code. GHS—Universitat Politècnica de Catalunya. http:// www.h2ogeo.upc.es (accessed July 2006).

Gudmundsson, A., 2000, Fracture dimensions, displacements and fluid transport. Journal of Structural Geology 22 (9), 1221-1231.

Guimera, J., Vives, L., Carrera, J., 1995, A discussion of scale effects on hydraulic conductivity at a granitic site (el Berrocal, Spain). Geophysical Research Letters 22(11), 1449-1452.

Hsieh, P., 1998. Scale effects in fluid flow through fractured geological media, scale dependence and scale invariance in hydrology. Cambridge University press.

Illman, W.A., Neuman, S., 2001. Type curve interpretation of a cross-hole pneumatic injection test in unsaturated fractured tuff. Water Resources Research 37(3), 583-603.

Illman, W.A., Neuman, S., 2003. Steady-state analysis of cross-hole pneumatic injection tests in unsaturated fractured tuff. Journal of Hydrology 281(1-2), 36-54.

Illman, W.A., Tartakovsky, D.M., 2006. Asymptotic analysis of cross-hole hydraulic tests in fractured granite. Ground Water 44 (4), 555-563.

Illman, W., 2006. Strong field evidence of directional permeability scale effect in fractured rock. Journal of Hydrology 319 (1-4), 227-236.

Illman, W.A., Liu, X., Takeuchi, S., Yeh, T.-C.J., Ando, K., Saegusa, H., 2009, Hydraulic tomography in fractured granite: Mizunami underground research site, Japan. Water Resources Research 45 (W01406).

Kim, Y., Peacock, D., Sanderson, D., 2004. Fault damage zones. Journal Of Structural Geology 26 (3), 503-517.

Kitterod, NO., Colleuille, H., Wong, W.K., Pedersen, T.S., 2000. Simulation of groundwater drainage into a tunnel in fractured rock and numerical analysis of leakage remediation, Romeriksporten tunnel, Norway. Hydrogeology Journal 8 (5), 480-493.

Kolymbas, D., Wagner, P., 2007. Groundwater ingress to tunnels - The exact analytical solution. Tunnelling and Underground Space Technology 22 (1), 23-27.

Knudby, C., Carrera, J., 2005. On the relationship between indicators of geostatistical, flow and transport connectivity. Advances in Water Resources 28 (4), 405-421.

Knudby, C., Carrera, J., 2006. On the use of apparent hydraulic diffusivity as an indicator of connectivity. Journal of Hydrology 329 (3-4), 377-389.

Krishnamurthy, J., Mani, A., Jayaraman, V., Manivel, M., 2000, Groundwater resources development in hardrock terrain. International Journal of Applied Earth Observation and Geoinformation 2 (3-4), 204-215.

Kvaerner, J., Snilsberg, P., 2008. The Romeriksporten railway tunnel - Drainage effects on peatlands in the lake Northern Puttjern area. Engineering Geology 101 (3-4), 75-88.

Le Borgne, T., Bour, O., Paillet, F.L., Caudal, J.P., 2006. Assessment of preferential flow path connectivity, and hydraulic properties at single-borehole and cross-borehole scales in a fractured aquifer. Journal of Hydrology 328 (1-2), 347-359.

Lei, S.Z., 1999. An analytical solution for steady flow into a tunnel. Ground Water 37 (1), 23-26.

Lipponen, A., Airo, M., 2006. Linking regional-scale lineaments to local-scale fracturing and groundwater inflow into the Paijanne water-conveyance tunnel, Finland, Near Surface. Geophysics 4 (2), 97-111.

Lipponen, A., 2007. Applying GIS to assess the vulnerability of the Paijanne water-conveyance tunnel in Finland. Environmental Geology 53 (3), 493-499.

López, A., 2009. Estudio analítico del efecto barrera: Definición, tipología, soluciones y aplicación a caso real. Msc thesis. Universitat Politecnica de Catalunya (UPC).

Lunn, R.J., Willson, J.P., Shipton, Z.K., Moir, H., 2008. Simulating brittle fault growth from linkage of preexisting structures. Journal Of Geophysical Research-Solid Earth 113 (B7).

Mabee, S.B., 1999. Factors Influencing Well Productivity in glacied metamorphic rocks. Ground water 37 (1), 88-97.

Mabee, S.B., Curry, P., Hardcastle, K., 2002. Correlation of Lineaments to Ground Water Inflows in Bedrock Tunnel. Ground Water 40 (1), 37-43.

Manzano, M., Pelaez, M.D., Serra, J., 1986–1987. Sedimentos prodeltaicos en el Delta emergido del Llobregat. Acta Geologica Hispánica 21–22, 205–211.

Maréchal, J.C., Perrochet, P., 2003. New analytical solution for the study of hydraulic interaction between Alpine tunnels and ground water. Bulletin de la Société Geólogique de France 174 (5), 441–448.

Marechal, J., Etcheverry, D., 2003. The use of H-3 and O-18 tracers to characterize water inflows in Alpine tunnels. Applied Geochemistry 18 (3), 339-351.

Marechal, J., Perrochet, P., Tacher, L., 1999. Long-term simulations of thermal and hydraulic characteristics in a mountain massif: The Mont Blanc case study, French and Italian Alps. Hydrogeology Journal, 7 (4), 341-354.

Marinos, P., Kavvadas, M., 1997. Rise of the groundwater table when flow is obstructed by shallow tunnels, in: Chilton, J. (Eds.), Groundwater in the urban environment: Problems, processes and management. Rótterdam, Balkema 49-54.

Marques, M.A., 1984. Las formaciones cuaternarias del delta del Llobregat LXXI. Institut d'Estudis Catalans, Barcelona, 1–280.

Marti, D., Carbonell, R., Flecha, I., Palomeras, I., Font-Capo, J., Vazquez-Sune, E., Perez-Estaun, A., 2008. High-resolution seismic characterization in an urban area: Subway tunnel construction in Barcelona, Spain. Geophysics 73 (2), B41-B50.

Martínez-Landa, L., Carrera, J., 2005. An analysis of hydraulic conductivity scale effects in granite (Full-scale Engineered Barrier Experiment (FEBEX), Grimsel, Switzerland). Water Resources Research 41 (3), W03006.

Martínez-Landa, L., Carrera, J., 2006. Methodology to interpret cross-hole tests in a granite block. Journal of Hydrology 325 (1-4), 222-240.

Mayer, A., May, W., Lukkarila, C., Diehl, J., 2007. Estimation of fault-zone conductance by calibration of a regional groundwater flow model: desert hot springs, California. Hydrogeology Journal 15 (6), 1093-1106.

Mcgrath, A., Davison, I., 1995. Damage zone geometry around fault tips. Journal of Structural Geology 17 (7), 1011-1024.

Medina, A., and J. Carrera. 1996. Coupled estimation of flow and solute transport parameters. Water Resources Research 32, no. 10: 3063–3076.

Meier, P.M., Carrera, J., Sanchez-Vila, X., 1998. An evaluation of Jacob's method for the interpretation of pumping tests in heterogeneous formations. Water Resources Research 34 (5), 1011-1025.

Molinero, J., Samper, J., Juanes, R., 2002. Numerical modeling of the transient hydrological response produced by tunnel construction in fractured bedrocks. Engineering Geology 64 (4), 364-386.

Merrick, N., Jewell, M., 2003. Modelling of the groundwater impact of a sunken urban motorway in Sydney, Australia. Materials and Geoenvironment 50, 229-232.

Moon, J., Jeong, S., 2011. Effects of highly pervious geological features on ground-water flow into a tunnel. Engineering Geology 117 (3-4), 207-216.

Navarro, A., Carrera, J., Sánchez-Vila, X., 1992. Contaminación por lavado piezometrico a partir de vertederos enterrados. Aplicación a un acuifero real. Hidrogeologia y recursos hidraulicos XVI, 371-387.

Olivella, S., Mokni, N., Carrera, J., 2008. Surface movements in a rock massif induced by drainage associated to tunnel excavation. UPC, CSIC, Barcelona.

Ondiviela, M., Vázquez-Suñé, E., Nilsson, J., Carrera, J., Sanchez-Vila, X., 2005. Effect of intensive pumping of infiltrated water in the Plaça de la Vila parking lot in Sant Adrià del Besòs (Barcelona, Spain). In: Groundwater intensive use: IAH selected papers on hydrogeology 7. Balkema 2005, 261-267.

Park, B.Y., Kim, K.S., Kwon, S., Kim, C., Bae, D.S., Hartley, L.J, Lee, H.K., 2002. Determination of the hydraulic conductivity components using a three-dimensional fracture network model in volcanic rock. Engineering Geology 66 (1-2), 127–141.

Park, K.H., Owatsiriwong, A., Lee J.G., 2008. Analytical solution for steady-state groundwater inflow into a drained circular tunnel in a semi-infinite aquifer: A revisit. Tunnelling and Underground Space Technology 23 (2), 206-209.

Perrochet, P., 2005a. A simple solution to tunnel or well discharge under constant drawdown. Hydrogeology Journal 13 (5–6), 886–888.

Perrochet, P., 2005b. Confined flow into a tunnel during progressive drilling: An analytical solution. Ground Water 43 (6), 943–946.

Perrochet, P., Dematteis, A., 2007. Modeling Transient Discharge into a Tunnel Drilled in a Heterogeneous Formation. Ground Water 45 (6), 786–790.

Pujades, E., López, A., Carrera, J., Vazquez-Suñe, E., Jurado, A., 2012. Barrier effect of underground structures on aquifers, submitted to Engineering Geology.

Renard, P., 2005. Approximate discharge for constant head test with recharging boundary. Ground Water 43 (3), 439–442.

Raposo, R., Molinero, J., Dafonte, J., 2010. Quantitative evaluation of hydrogeological impact produced by tunnel construction using water balance models. Engineering Geology 116 (3-4), 323-332.

Rhen, I., Thunehed, H., Triumf, C., Follin, S., Hartley, L., Hermansson, J., Wahlgren, C., 2007. Development of hydrogeological model description of intrusive rock at different investigation scales: an example from south-eastern Sweden. Hydrogeology Journal 15 (1), 47-69.

Roca, E., Sans, L., Cabrera, L., Marzo, M., 1999. Oligocene to Middle Miocene evolution of the Central Catalan margin, North-western Mediterranean. Tectonophysics 315, 209–229.

Ricci, G., Enrione, R., Eusebio, A., 2007. Numerical modelling of the interference between underground structures and aquifers in urban environment. The Turin subway Line 1, in: Barták, Hrdine, Romancov and Zlámal (Eds.), Underground Space. Taylor and Francis Group, London, pp. 1323-1329.

RSE 2003. Linia 9 del tram 4t. (B20) Informe tecnic. Estudi geològic, geotecnic i hidrogeològic. GISA, Gestor d'infraestructures S.A.

Sanchez-Vila, X., Meier, P., Carrera, J., 1999. Pumping tests in heterogeneous aquifers: An analytical study of what can be obtained from their interpretation using Jacob's method. Water Resources Research 35 (4), 943-952.

Schwarz, L., Reichl, I., Kirschner, H., Robl. K.P., 2006. Risks and hazards caused by groundwater during tunnelling: geotechnical solutions used as demonstrated by recent examples from Tyrol, Austria. Environmental Geology 49 (6), 858-864.

Selroos, J.O., Walker, D.D., Strom, A., Gylling, B., Follin, S., 2002. Comparison of alternative modelling approaches for groundwater flow in fractured rock. Journal of Hydrology 257 (1-4), 174-188.

Sener, E., Davraz, A., Ozcelik, M., 2005. An integration of GIS and remote sensing in groundwater investigations: a case study in Burdur, Turkey. Hydrogeology Journal 13(5-6), 826-834.

Shaban, A., El-Baz, F., Khawlie, M., 2007. The relation between water-wells productivity and lineaments morphometry: selected zones from Lebanon. Nordic Hydrology 38(2), 187-201.

Shang, Y.J., Xue, J.H., Wang, S.J., Yang, Z., Yang, J., 2004. A case history of Tunnel Boring Machine jamming in an inter-layer shear zone at the Yellow River Diversion Project in China. Engineering Geology 71 (3-4), 199-211.

Shapiro, A.M., Hsieh, P.A., 1991. Research in fractured-rock hydrogeology: characterizing fluid movement and Chemicals transport in fractured rock at the Mirror Lake drainage basin. In: Mallard, G.E., Aronson, D.A., (Eds). Proceedings of the Technical Meeting of US Geological Survey Toxic Substances Hydrology Program, Monterey, CA, March 11–15, Reston, VA (also, Water Resources Investigation Report 91-4034, US Geological Survey).

Shapiro, A., 2003. The effect of scale on the magnitude of formation properties governing fluid movement and chemical transport in fractured rock. In Groundwater in fractured rocks. Proceedings of the international conference, september 15–19, 2003. Prague, Czech Republic.

Shin, J., Addenbrooke, T., Potts, D., 2002. A numerical study of the effect of groundwater movement on long-term tunnel behaviour. Geotechnique 52 (6), 391-403.

Simó, J.A., Gàmez, D., Salvany, J.M., Vàzquez-Suñé, E., Carrera, J., Barnolas, A., Alcalà, F.J., 2005. Arquitectura de facies de los deltas cuaternarios del río Llobregat, Barcelona, España. Geogaceta 38, 171–174.

Smith, L., Schwartz, F., 1984. An analysis of the influence of fracture geometry on mass-transport in fractured media. Water Resources Research 20(9), 1241-1252.

Sultan, M., Wagdy, A., Manocha, N., Sauck, W., Gelil, K.A., Youssef, A.F., Becker, R., Milewski, A., El Alfy, Z., Jones, C., 2008. An integrated approach for identifying aquifers in transcurrent fault systems: The Najd shear system of the Arabian Nubian shield. Journal Of Hydrology 349 (3-4), 475-488.

Stanfors, R., Rhen, I., Tullborg, E., Wikberg P., 1999. Overview of geological and hydrogeological conditions of the Aspo hard rock laboratory site. Applied Geochemistry 14, 819-834.

Tubau, I., 2004. Estudio Hidrogeológico y propuesta de proceso constructivo para la excavación de un túnel entre pantallas en el delta del Llobregat. Minor thesis. Universitat Politecnica de Catalunya (UPC).

Tseng, D.J., Tsai, B.R., Chang, L.C., 2001. A case study on ground treatment for a rock tunnel with high groundwater ingression in Taiwan. Tunnelling and Underground Space Technology 16 (3), 175-183.

Varol, A., Dalgic, S., 2006. Grouting applications in the Istanbul metro, Turkey. Tunnelling and Underground Space Technology 21 (6), 602-612.

Vazquez-Sune, E., Sanchez-Vila, X., Carrera, J., 2005. Introductory review of specific factors influencing urban groundwater, an emerging branch of hydrogeology, with reference to Barcelona, Spain. Hydrogeology Journal 13 (3), 522-533.

Wittke, W., Druffel, R., Erichsen, C., Gattermann, J., Kiehl, J., Schmitt, D., Tegelkamp, M., Wittke, M., Wittke-Gattermann, P., Wittke-Schmitt, B., 2007. Stability Analysis and Design for Mechanized Tunneling. Foundation Engineering, P. D.-I. W. W. C. E. & in Rock Ltd. (WBI), C. (ed.).

Yang, S.Y., Yeh, H.D., 2007. A closed-form solution for a confined flow into a tunnel during progressive drilling in a multi-layer groundwater flow system. Geophysical Research Letters 34 (7), L07405.

Yang, F.R., Lee, C.H., Kung, W.J., Yeh, H.F., 2009. The impact of tunneling construction on the hydrogeological environment of "Tseng-Wen Reservoir Transbasin Diversion Project" in Taiwan. Engineering Geology 103 (1-2), 39-58.

Yechieli, Y., Kafri, U., Wollman, S., Lyakhovsky, V., Weinberger, R., 2007. On the relation between steep monoclinal flexure zones and steep hydraulic gradients. Ground Water 45 (5), 616-626.

Yoo, C., 2005. Interaction between tunneling and groundwater - Numerical investigation using three dimensional stress-pore pressure coupled analysis. Journal of Geotechnical and Geoenvironmental Engineering. 131 (2), 240-250.

Zangerl, C., Eberhardt, E. Loew, S., 2003. Ground settlements above tunnels in fractured crystalline rock: numerical analysis of coupled hydromechanical mechanisms. Hydrogeology Journal 2003, 11 (1), 162-173.

Zangerl, C., Evans, K.F., Eberhardt, E. Loew, S., 2008. Consolidation settlements above deep tunnels in fractured crystalline rock: Part 1-Investigations above the Gotthard highway tunnel. International Journal of Rock Mechanics and Mining Sciences 45 (8), 1211-1225.

Zangerl, C., Eberhardt, E., Evans, K.F., Loew, S., 2008. Consolidation settlements above deep tunnels in fractured crystalline rock: Part 2-Numerical analysis of the Gotthard highway tunnel case study. International Journal of Rock Mechanics and Mining Sciences 45 (8), 1211-1225.